ANKARA YILDIRIM BEYAZIT UNIVERSITY

GRADUATE SCHOOL OF NATURAL AND APPLIED SCIENCES



Ni-B-Co COATING ON MEDIUM-CARBON STEELS BY ELECTRODEPOSITION

M.Sc. Thesis by

Uğur BARUT

Department of Material Engineering

July, 2018

ANKARA

Ni-B-Co COATING ON MEDIUM-CARBON STEELS BY ELECTRODEPOSITION

A Thesis Submitted to

The Graduate School of Natural and Applied Sciences of

Ankara Yıldırım Beyazıt University

In Partial Fulfillment of the Requirements for the Degree of Master of Science in Material Engineering, Department of Material Engineering

by

Uğur BARUT

July, 2018

ANKARA

M.Sc. THESIS EXAMINATION RESULT FORM

We have read the thesis entitled **"Ni-B-Co COATING ON MEDIUM-CARBON STEELS BY ELECTRODEPOSITION"** completed by **UĞUR BARUT** under the supervision of **Asst. Prof. Dr. RAMAZAN KARSLIOĞLU** and we certify that in our opinion it is fully adequate, in scope and in quality, as a thesis for the degree of Master of Science.

Asst. Prof. Dr. Ramazan KARSLIOĞLU

Supervisor

Prof. Dr. Hasan OKUYUCU

Jury Member

Asst. Prof. Dr. Hanifi ÇİNİCİ

Jury Member

Prof. Dr. Ergün ERASLAN

Director

Graduate School of Natural and Applied Sciences

ETHICAL DECLARATION

I hereby declare that, in this thesis which has been prepared in accordance with the Thesis Writing Manual of Graduate School of Natural and Applied Sciences,

- All data, information and documents are obtained in the framework of academic and ethical rules,
- All information, documents and assessments are presented in accordance with scientific ethics and morals,
- All the materials that have been utilized are fully cited and referenced,
- No change has been made on the utilized materials,
- All the works presented are original,

and in any contrary case of above statements, I accept to renounce all my legal rights.

2018, 19 July **Uğur BARUT**

ACKNOWLEDGMENTS

Firstly, I would like to express my sincere gratitude to my advisor, Asst. Prof. Dr. Ramazan KARSLIOĞLU, for his tremendous scientific and humanitarian support, experience and advices during my study.

I must also express my profound appreciations to my family for providing me endless support throughout my life. The completion of this study would not have been possible without their prays.

2018, 19 July **Uğur BARUT**

Ni-B-Co COATING ON MEDIUM-CARBON STEELS BY ELECTRODEPOSITION

ABSTRACT

The nickel-boron alloy coating has been improved in several engineering fields in recent years due to their high hardness, good corrosion resistance, long durability and suitable solderability as an alternative to hard chrome plating.

Due to its superior properties nickel-cobalt based coatings have wide application areas in industrial and technological fields. Coating layers which are used in Micro Electro Mechanical Systems (MEMS) and Nano Electro Magnetic Systems (NEMS) and whose thickness starts from nm level and reaches to mm level according to usage area is needed. The coatings to be produced for these applications require superior mechanical, high abrasion and corrosion resistance, low internal stress and high thermal stability. nickel-cobalt based coatings are good candidates for such applications.

In this study, nickel-boron coatings containing trimethylamine borane in different amounts were produced by direct current by using a watt bath on medium-carbon steels, nickel-boron-cobalt alloy coatings containing in fixed amounts of trimethylamine borane and in different amounts of cobalt sulphate were produced by direct current by using a watt bath on medium-carbon steels and also, nickel-boron-cobalt alloy coatings containing in fixed amounts trimethylamine borane and cobalt sulphate were produced by direct current, pulse current and pulse reverse current by using a watts on medium-carbon steels. The resulting coatings are characterized using scanning electron microscope and X-ray diffraction methods. The effect of amount of the trimethylamine borane and cobalt sulphate and current type on the mechanical, tribological and corrosion properties was investigated. The best results for Ni-B alloys as a result of the investigations were obtained with addition of 1.5 g/L trimethylamine borane and the best results for Ni-B-Co alloys were obtained with 1 g/L addition cobalt sulphate and direct current.

Keywords: Electrodeposition, Nickel electrodeposition, Ni-B coating, Ni-B-Co alloys

ELEKTRODEPOZİSYON İLE ORTA KARBONLU ÇELİKLERDE Ni-B-Co KAPLAMA

ÖZ

Nikel-bor alaşım kaplama, yüksek sertlik, iyi korozyon direnci, uzun dayanıklılık ve uygun lehim kabiliyetlerinden dolayı son yıllarda sert krom kaplamaya alternatif olarak çeşitli mühendislik alanlarında geliştirilmiştir.

Nikel-kobalt esaslı kaplamalar üstün özelliklerinden dolayı endüstriyel ve teknolojik alanlarda geniş uygulama alanlarına sahiptir. Mikro Elektro Mekanik Sistemlerde ve Nano Elektro Manyetik Sistemlerde kullanılan ve kullanım alanına göre kalınlığı nm seviyesinden başlayan ve mm seviyesine kadar kalınlığa ulaşan kaplama tabakalarına ihtiyaç duyulmaktadır. Bahsi geçen uygulamalar için üretilecek kaplamalardan üstün mekanik, yüksek aşınma ve korozyon direnci düşük iç gerilim, yüksek termal stabilite gibi özellikler istenmektedir. Nikel-kobalt alaşım kaplamaları bu tür uygulamalar için iyi bir adaydır.

Bu çalışmada, orta karbonlu çelikler üzerine farklı miktarlarda trimethylamine borane içeren nikel-bor alaşım kaplamaları ile sabit miktarda trimethylamine borane ve farklı miktarlarda kobalt sülfat içeren nikel-bor-kobalt alaşım kaplamaları doğru akım yöntemi ile ve sabit miktarda trimethylamine borane ve kobalt sülfat içeren nikel-bor-kobalt alaşım kaplamaları ise doğru akım, pulse akım ve pulse reverse akım yöntemleri ile watts tipi banyo kullanılarak üretilmiştir. Üretilen kaplamalar taramalı elektron mikroskobu ve X-ışınları difraksiyonu metodu kullanılarak karakterize edilmiştir. Trimethylamine borane ile kobalt sülfat miktarının ve akım türünün mekanik, tribolojik ve korozyon özelliklerine etkisi incelenmiştir. Yapılan incelemeler sonucunda nikel-bor alaşımları için en iyi sonuçlar 1.5 g/L trimethylamine borane ilavesinde, nikel-bor-kobalt alaşımları için en iyi sonuçlar 1 g/L kobalt sülfat ilavesi ve doğru akım türünde elde edilmiştir.

Anahtar Kelimeler: Elektrodepozisyon, Nikel elektrodepozisyon, Ni-B kaplama, Ni-B-Co alaşımları

CONTENTS

M.Sc. THESIS EXAMINATION RESULT FORM ii
ETHICAL DECLARATION iii
ACKNOWLEDGMENTS iv
ABSTRACT v
ÖZ vi
CONTENTS vii
LIST OF TABLES xi
LIST OF FIGURES xii
CHAPTER 1 - INTRODUCTION 1
CHAPTER 2 - LITERATURE REVIEW 3
2.1 The Elements 3
2.1.1 Nickel 3
2.1.2 Cobalt 4
2.1.3 Boron 5
2.2 Nickel Coatings 7
2.2.1 Decorative Nickel Coating 7
2.2.2 Engineering Nickel Coating 7
2.2.3 Nickel Electroforming Process 8
2.2.4 Production Methods of Nickel Based Coatings 9
2.2.4.1 Electrolytic Coating 9
2.2.4.1.1 Electroless Plating 10
2.2.4.1.2 Electroplating 12
2.2.4.2 Parameters Affecting Quality of Coating 14
2.2.4.3 Influence of Bath Types on Electroplating 17
2.2.4.3.1 Nickel Watts Bath 17
2.2.4.3.2 Nickel Sulphamate Bath 18
2.2.4.3.3 Other Nickel Plating Baths 19
2.2.4.3.4 Comparison of Nickel Watts and Nickel Sulphamate baths 20
2.2.4.4 Influence of Current Types on Electroplating 22
2.3 Review of Related Works 25
CHAPTER 3 - EXPERIMENTAL PROCEDURE 36
3.1 Preparation of Experimental Setup and Testing 36

3.1.1 Preparation of Substrates 36
3.1.2 Preparation of Coating Bath 37
3.1.3 Electrodeposition Processes of Pure Ni coating and All Alloy Coatings 37
3.2 Characterization of Deposited Layers 41
3.2.1 Scanning Electron Microscope Analysis 41
3.2.2 XRD Analysis 41
3.2.3 Microhardness Measurements 42
3.2.4 Coating Thickness Measurements 43
3.2.5 Wear Tests 44
3.2.6 Corrosion Measurements 44
CHAPTER 4 - RESULTS AND DISCUSSION 46
4.1 Structural Analysis 46
4.1.1 Microstructural Analysis 46
4.1.2 Energy Dispersive Spectrometer (EDS) analysis 52
4.1.3 X-Ray Diffraction Analysis 55
4.2 Hardness of Coatings 61
4.3 Coating Thicknesses 64
4.4 Tribological Properties 64
4.4.1 Wear Behavior 64
4.4.2 Wear Mechanisms 68
4.5 Evaluation of Corrosion Resistance 72
CHAPTER 5 - CONCLUSIONS AND FUTURE WORK 78
5.1 Conclusions 78
5.2 Future Work 81
REFERENCES 83
CURRICULUM VITAE 91

NOMENCLATURE

Abbreviations

µA	Microampere
µm	Micrometer
Å	Angstrom
Al_2O_3	Aluminum oxide
B	Boron
C	Carbon
cm^2	Square centimeter
cm^3	Cubic centimeter
Co	Cobalt
$CoSO_4$	Cobalt sulphate
$CoSO_4.7H_2O$	Cobalt sulphate heptahydrate
dm^2	Square decimeter
F	Faraday constant
°F	Fahrenheit
g	Gram
GPa	Gigapascal
h	Hour
H_3BO_3	Boric acid
HV	Hardness vickers
K	Kelvin
kV	Kilovolt
m	Meter
mΩ	Milliohm
mA	Milliampere
ml	Milliliter
Mo	Molybdenum
mV	Millivolt
Ni	Nickel
$NiCl_2.6H_2O$	Nickel Chloride
$NiSO_4$	Nickel sulphate
$NiSO_4.6H_2O$	Nickel sulphate hexahydrate

$Ni(NH_2SO_3)_2.4H_2O$	Nickel sulphamate
nm	Nanometer
rpm	Round per minute
s	Second
S	Siemens
SiC	Silicon carbide
V	Voltage
W	Tungsten

Acronyms

CNT	Carbon nanotube
DMAB	Dimethylamine borane
DC	Direct current
EDS	Energy dispersive spectroscope
FCC	Face-centered cubic
FWHM	Full widths at half maximum
HCP	Hexagonal close-packed
JCPDS	Joint committee on powder diffraction standards
MEMS	Microelectromechanical system
NEMS	Nanoelectromechanical systems
PC	Pulse current
pH	Power of Hydrogen
PRC	Pulse reverse current
SEM	Scanning electron microscope
TEM	Transmission electron microscope
TMAB	Trimethylamine borane
XRD	X-ray diffractometer

LIST OF TABLES

Table 2.1 Elemental properties of nickel. 3

Table 2.2 Elemental properties of cobalt. 4

Table 2.3 Elemental properties of boron. 6

Table 2.4 Compound and operating conditions for nickel watts electroplating baths 17

Table 2.5 Compound and operating conditions for nickel sulphamate electroplating baths. 19

Table 2.6 Compound and operating conditions for nickel sulphamate electroplating baths. 20

Table 2.7 Comparison of nickel watts and nickel sulphamate solutions. 21

Table 2.8 Possible effects of current type on deposit structures. 23

Table 3.1 Bath composition and electrodeposition conditions of the coating bath. .. 38

Table 3.2 Bath parameters are given for pure nickel coating, Ni-B and Ni-B-Co alloy coatings. 39

LIST OF FIGURES

Figure 2.1 Application areas of nickel. 4

Figure 2.2 Application areas of cobalt. 5

Figure 2.3 Application areas of boron. 6

Figure 2.4 Electroformed nickel mould for reinforced plastic automotive body component. 9

Figure 2.5 Schematic view of the electroless plating bath. 11

Figure 2.6 Comparison of deposit uniformity for electroless plating and Electroplating. 12

Figure 2.7 Schematic view of electrodeposition method. 13

Figure 2.8 Topographic image of the Ni coating layer produced by using a) DC, b) PC, c) PRC electrodeposition method. 24

Figure 2.9 Types of current: a) DC, b) PC, c) PRC. 24

Figure 2.10 Surface morphology of Ni–B coatings electrodeposited at different current densities: (a) 1, (b) 3, (c) 5, and (d) 10 A/dm^2 26

Figure 2.11 SEM surface micrographs of Co-Ni coatings at different current densities: a) A/dm^2 , b) 2 A/dm^2 , c) 3 A/dm^2 , d) 4 A/dm^2 27

Figure 2.12 Ni–Co alloy coatings at 50°C for 30 min at 5 A/dm^2 current density; a) DC, b) PC and c) PRC methods. 29

Figure 2.13 The micrographs of samples produced from coating bath with addition of a) 30 g/L, b) 20 g/L, c) 10 g/L, d) 0 g/L $Ni_2Cl.6H_2O$ for 30 min. at 50 °C by DC during optimization of bath parameters. 31

Figure 2.14 The SEM images of effect of $NiSO_4.6H_2O$ / $CoSO4.7H_2O$ (g/L) ratios on the coating layer 250/50, b) 200/100, c) 100/200 and d) 5/25. 32

Figure 2.15 Electroless Ni-B coatings (a) as-deposited; and heat treated at (b) 350°C; (c) 400°C; (d) 450°C. 33

Figure 2.16 Electroless Ni-B-W coatings (a) as-deposited; and heat treated at (b) 350°C; (c) 400°C; (d) 450°C. 34

Figure 2.17 The change of surface morphology of Ni–B coatings with boron content. Scanning electron micrographs of (a) Pure Ni, (b) Ni-2 at.% B, (c) Ni-6 at.% B, (d) Ni-9 at.% B. 35

Figure 3.1 HITACHI TM4000Plus Tabletop Microscope. 41

Figure 3.2 Rigaku-MiniFlex 600 X-ray diffractometer. 42

Figure 3.3 Shimadzu-HMV-G 21S Vickers microhardness test device. 43

Figure 3.4 Coating thickness gauge. 43

Figure 3.5 CH Instruments potentiodynamic polarization test device. 45

Figure 4.1 SEM surface images of pure nickel coating and Ni-B alloy coatings produced by DC according to amount of TMAB added to electrolytic bath (g/L) : a) pure nickel, b) 0.25, c) 0.5, d) 1, e) 1.5, f) 2.5, g) 5. 47

Figure 4.2 SEM surface images of Ni-B-Co alloy coatings containing fixed amount of TMAB (g/L) and different amount of $CoSO_4$ (g/L) in electrolytic bath produced by DC: a) 0.5, b) 1, c) 2.5, d) 5, e) 50. 49

Figure 4.3 SEM surface images of Ni-B-Co alloy coatings produced by different current : a) DC, b) PC, c) PRC. 50

Figure 4.4 EDS Map Sum spectrum of pure nickel coating produced by DC. 52

Figure 4.5 Atomic percentage of boron element in Ni-B alloy coatings containing different amount TMAB in electrolytic bath produced by DC according to result of EDS analysis. 53

Figure 4.6 Atomic percentage of boron and cobalt element in Ni-B-Co coating layer containing constant amount of TMAB and different amount of $CoSO_4$ in electrolytic bath produced by DC according to result of EDS analysis. 54

Figure 4.7 Atomic percentage of boron and cobalt element in Ni-B-Co alloy coatings produced by DC, PC and PRC type according to result of EDS analysis. 54

Figure 4.8 XRD patterns of pure nickel coating. 55

Figure 4.9 (a) Influence of amount of TMAB added to electrolytic bath on phase structure in electrodeposited Ni-B coatings prepared by DC, (b) detailed analysis of XRD patterns of the Ni-B alloy coatings deposited at different amount of TMAB added to electrolytic bath. 56

Figure 4.10 (a) Influence of amount of $CoSO_4$ added to electrolytic bath on phase structure in electrodeposited Ni-B-Co coatings prepared by DC, (b) detailed analysis of XRD patterns of the Ni-B-Co alloy coatings deposited at different amount of TMAB added to electrolytic bath. 58

Figure 4.11 (a) Effect of current type on phase structure in Ni-B-Co alloy coatings, (b)detailed analysis of XRD patterns of the Ni-B-Co alloy coatings deposited by different current types. 60

Figure 4.12 The microhardness of Ni-B alloy coatings produced by DC according to amount of TMAB added to electrolytic bath. 62

Figure 4.13 The microhardness of Ni-B-Co alloy coatings containing fixed amount of TMAB (g/L) and different amount of $CoSO_4$ (g/L) in electrolytic bath produced by DC. 63

Figure 4.14 The microhardness of Ni-B-Co alloy coatings produced by DC. 64

Figure 4.15 Wear trace width of pure nickel coating (a), Ni-B alloy coating which contains 1.5 g/L TMAB (b) and Ni-B-Co alloy coating which contains 1 g/L $CoSO_4$ in the electrolytic bath. 65

Figure 4.16 Specific wear rate of pure nickel coating and Ni-B alloy coatings coatings produced by DC according to amount of TMAB added to electrolytic bath. 66

Figure 4.17 Specific wear rate of Ni-B-Co alloy coatings containing fixed amount of TMAB (g/L) and different amount of $CoSO_4$ (g/L) in electrolytic bath produced by DC. 67

Figure 4.18 Specific wear rate of Ni-B-Co alloy coatings produced by DC,PC and PRC. 68

Figure 4.19 SEM images of wear traces of Ni-B alloy coatings produced by DC ; (a) pure Ni coating, addition of (b) 0.25, (c) 0.5, (d) 1, (e) 1.5, (f) 2.5, (g) 5 g/L TMAB to electrolytic bath. 70

Figure 4.20 SEM images of wear traces of Ni-B-Co alloy coatings produced by DC; addition of (a) 0.5 (b) 1, (c) 2.5, (d) 5, (e) 50 g/L $CoSO_4$ to electrolytic bath. 71

Figure 4.21 SEM images of wear traces of Ni-B-Co alloy coatings produced by (a) DC, (b) PC, (c) PRC. 72

Figure 4.22 Polarization curves of Ni-B alloy coatings produced by different amount of TMAB that obtained with scan rate of 0.5 mV/s in 3% aqueous solution. 73

Figure 4.23 Polarization curves of Ni-B-Co alloy coatings produced by different amount of $CoSO_4$ that obtained with scan rate of 0.5 mV/s in 3% aqueous solution. 73

Figure 4.24 Polarization curves of Ni-B-Co alloy coatings produced by different current types that obtained with scan rate of 0.5 mV/s in 3% aqueous solution. 74

Figure 4.25 Corrosion current and grain size of Ni-B alloy coatings prepared with different amount of TMAB added to electrolytic bath. 75

Figure 4.26 Corrosion current and grain size of Ni-B-Co alloy coatings prepared with different amount of $CoSO_4$ added to electrolytic bath. 76

Figure 4.27 Corrosion current and grain size of Ni-B-Co alloy coatings prepared with different current type. 76

CHAPTER 1

INTRODUCTION

The coating technology has for the last few years been largely carried out in several engineering fields, comprising automobiles, electronics, aviation, defense industry, daily necessities, etc. Especially, in these areas, hard chrome platings is widely used. They have various advantages, such as its great corrosion resistance, high stiffness and surface smoothness, but they are dangerous against the environment and human body because of containing hexavalent chromium(Cr^{+6}) [1–3]. So, alternative coatings for hexavalent chrome platings should be available. Ni platings provide a proper alternative and have been largely used in engineering applications for the last five decades due to their unique properties that enhance wear, abrasion and corrosion resistance [4]. But, when compared to hard chrome plating, Ni coatings are inferior in durability and stiffness. In order to obtain better mechanical characteristics, some Ni-based alloy coatings, such as Ni-B, Ni-Co, Ni-W, Ni-P, have been improved [5,6].

Ni-B alloy coatings have been improved in various industrial applications, because of good corrosion resistance, long durability, high hardness and proper solderability, with electro- and electroless nickel coating methods [7]. In particular, for hard chrome replacement, Ni electroless platings have been regarded as a potential candidate, but some mechanical properties of these platings such as wear resistance so far has not quite equaled that of hard chrome [4]. Electroless coating of Ni–B from boron hydride coating bath is carried out at high pH conditions, at 80–90 °C. The nickel coating is occurred via the reduction of nickel ions by the boron hydride. In these circumstances, metallic nickel which is not tightly connected to the film can precipitate owing to spontaneous decomposition of the reducing agent [8]. Electroplating is well-known as a typical plating method of alloy thin films or metal. For this method, it is easy to check growth rate and also it is low cost and simple method [9,10]. In order to produce Ni–B alloy coatings, electroplating is alternative method and it is typically come true at lower temperatures, around 50 °C, and is conventionally used boron hydrides, boric acid [11,12]. The Ni-B alloy coatings are prepared with the electrodeposition method

from Ni bath solution in the presence of a reducing agent, such as triethylamine borane (TMAB) [11,13], dimethylamine borane (DMAB) [14].

Nickel-cobalt alloys are important engineering materials that are widely used in the industry due to their properties such as high strength, good wear resistance, high thermal and conductivity and electrocatalytic activity [15]. In recent years, Nickel-Cobalt magnetic films have begun to be used in different thicknesses ranging from nanometer level to millimeter levels due to their application in Micro Electro Mechanical Systems (MEMS) due to their good adhesion, high corrosion resistance, low internal stresses and high thermal stability [16]. Among the various production methods for producing Ni-Co films, electrolytic coating has proven to be a simple and economical method since it does not require high temperature and pressure. Electrolytic coating has attracted considerable interest in recent years due to the control of the change of coating parameters. Many metallic coatings such as Zn-Mn, Zn-Co, Zn-Ni and Fe-Cr-P have been produced in the electrolytic coating in recent years. There are many studies on Ni-Co alloy film production by electrolytic coating [15].

From this point of view, it is aimed to produce Ni-B-Co alloy coatings by electrodeposition method which can be easily coated on complex geometries, low cost, easy to apply and can be successfully applied at room temperature and atmospheric conditions. The production of Ni-B-Co alloy coatings by the electrodeposition coating method is not currently available in the literature. Microstructural analysis was performed by X-ray diffractometer (XRD) and scanning electron microscopy (SEM). In addition to micro-structural analysis, it is aimed to investigate optimum parameters by examining mechanical properties such as hardness, abrasion and corrosion resistance. The main objective of this master thesis work is to produce coatings with mechanical properties such as high hardness, good wear resistance for micro electromechanical systems (MEMS) and nano electromechanical systems (NEMS) which have increased in importance in recent years. Although there are literature reports on the production of such coatings under DC, PC and PRC currents, there is no study to optimize tribological properties and corrosion properties by using three different methods. It is aimed to contribute to the universal literature from this point of view.

CHAPTER 2

LITERATURE REVIEW

2.1 The Elements

2.1.1 Nickel

Nickel is one of the most abundant elements on Earth. Nickel is not chemically active. Elemental characteristic for nickel are given in Table 2.1. Nickel is a metal which has corrosion resistance, particularly it has alkali corrosion resistance. It has ferromagnetic property at room temperature. Also, it is a soft metal and weldable. It can be tailored at low and high temperatures. Cold working increases its stiffness. Nickel is one of the most valuable and important metals for industrial applications. Nowadays, nickel has nearly become the most used element after iron. As shown in Figure 2.1, it is used in many industrial areas such as stainless steels, special-purpose, low-alloy steels, cast irons materials like magnetic alloys and controlled-expansion alloys and also, it can be used as the basic element for many corrosion and heat resistance alloys [17].

Table 2.1 Elemental properties of nickel [18].

Atomic number	**28**
Atomic weight	**58.6934 g/mol**
Crystal structure	**FCC**
Lattice constant	**0.35167 nm**
Density	**8.902 g/cm^3**
Melting point	**1453 °C (2647 °F)**
Linear thermal expansion coefficient	**0.0000134 K^{-1}**
Electrical conductivity	**1.4×10^7 S/m**
Young modulus	**200 GPa**
Hardness	**195 HV**

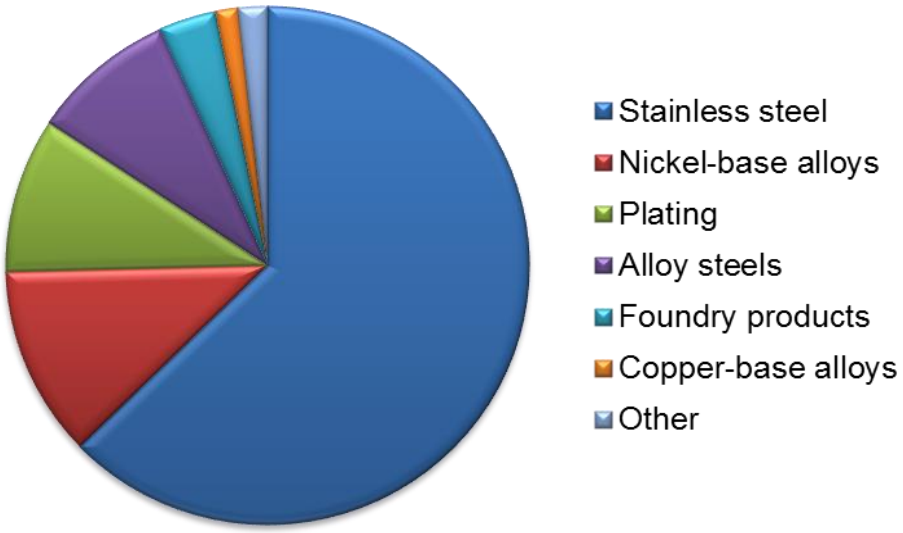


Figure 2.1 Application areas of nickel [18].

2.1.2 Cobalt

Cobalt has ferromagnetic properties at room temperature. Therefore, it is usually used for magnetic alloy applications. It is generally used together with nickel and aluminium as powerful magnetic materials. Furthermore, it has high heat resistance, so it can be used safely where high temperature strength is needed. It has high corrosion resistance but it is influenced by precipitation and alloying elements. As shown in Figure 2.2 shows, cobalt is used in various areas like portable electronic devices, rechargeable batteries, mobile phones and computers. Some cobalt alloys can be used as orthopedic implants. Also, cobalt has non-etallurgical applications such as drying agents for paints, inks, varnishes, porcelain enamels and batteries enamels [18] Elemental properties of cobalt is shown in the Table 2.2.

Table 2.2 Elemental properties of cobalt [19].

Atomic number		27
Atomic weight		58,93 g/mol
Crystal structure		HCP (Below 417 ºC)
Lattice constant of the fcc form		0.25071, 0.25071, 0.40695 nm
Density		8.85 g/cm^3 (similar to nickel)

Table 2.2 Elemental properties of cobalt [19] (continue).

The electrical resistivity	6×10^{-8} mΩ
Electrical conductivity	1.7×10^{7} S/m
Curie temperature	1131º C (1394 ºK)
Young modulus	209 GPa
Hardness	320-330 HV

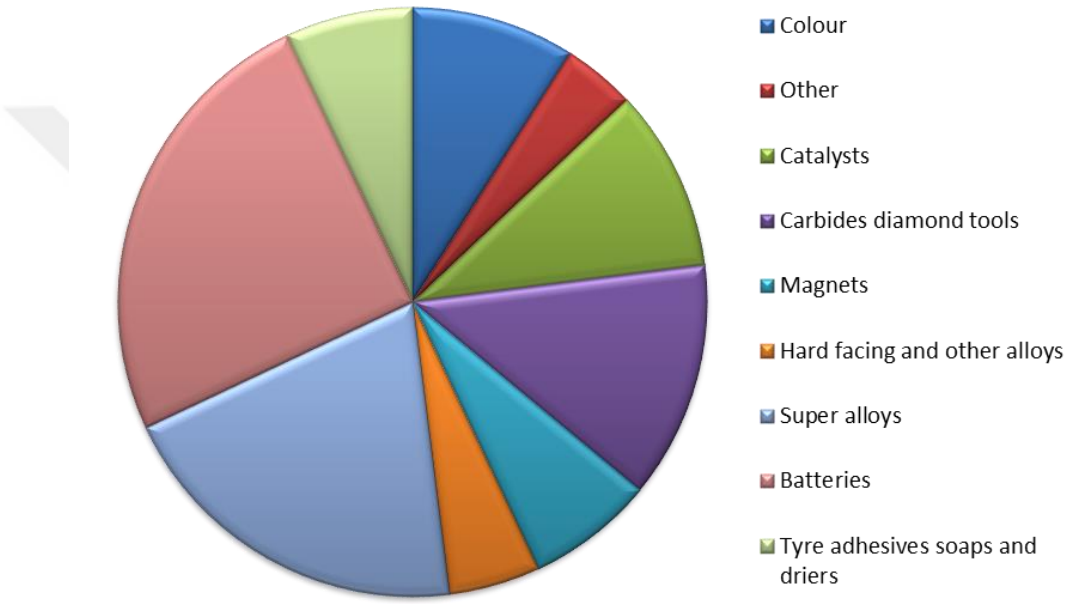


Figure 2.2 Application areas of cobalt [20].

2.1.3 Boron

Boron is a highly rigid element and heat-resistant semi-metal that can be found in different types and is widely used in compounds to produce everything from glass and bleaches to agricultural fertilizers and semiconductors. Boron has low electric conductivity at low temperatures, however this situation modifies as temperatures increase. Whereas crystalline boron is very constant and not reactive with acids, the amorphous form slowly oxidizes in air and it may react heavily in acid [21]. Elemental properties of boron is shown in Table 2.3 and application areas of boron is shown in Figure 2.3

Table 2.3 Elemental properties of boron [22].

Atomic number	5
Atomic weight	10.81
Crystal structure	Simple Trigonal
Lattice constant	506, 506, 506 pm
Density	2.46 g/cm^3
Melting Point	2075 º C
Boiling Point	4000 º C
Linear thermal expansion coefficient	6×10^{-6} K^{-1}
The electrical resistivity	10000 mΩ
Electrical conductivity	0.0001 S/m
Hardness (Vickers)	49000 MPa

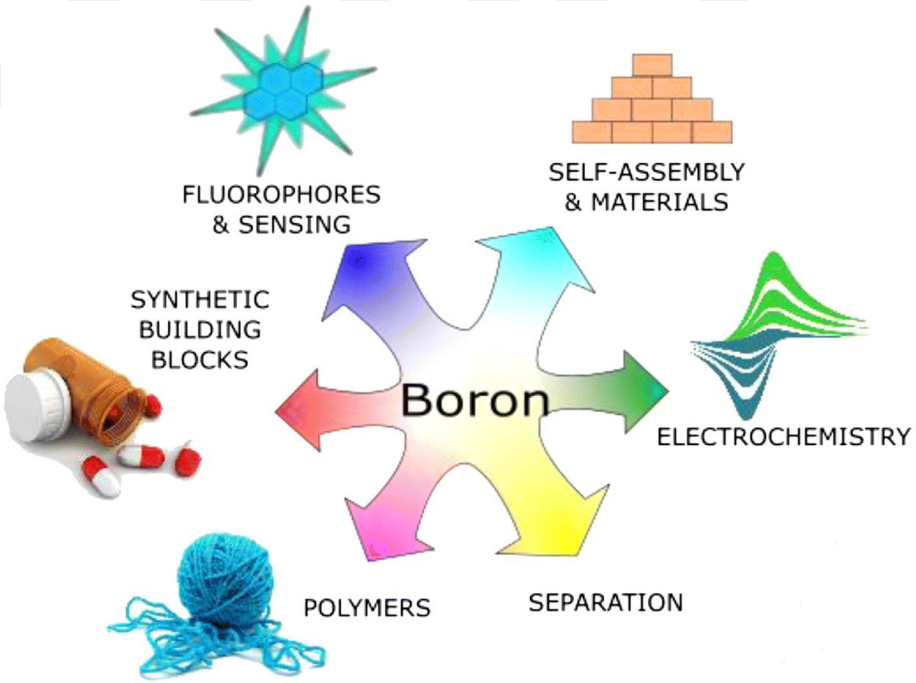


Figure 2.3 Application areas of boron [23].

2.2 Nickel Coatings

The nickel coating method is utilized comprehensively for decorative, engineering, and electroforming applications since the appearance and other characteristics of electrodeposited nickel may be modified over wide ranges by arranging the operating parameters and the composition of the coating bath. Decorative area of usage involve about 80% of the nickel used up in coating; 20% is employed for electroforming and engineering applications. Also, electroless nickel coating method is commercially substantial. The annual worldwide consumption of nickel in electrocoating process is approximately 180 million pounds (81,700 metric tons) and it involves 11 to 12% of world nickel consumption [24].

2.2.1 Decorative Nickel Coating

Modern decorative nickel platings include organic additives that modify the electro crystallization method in order that highly-leveled, mirror-bright nickel platings are coated directly from bath. Before the introduction of "organic" baths, decorative nickel platings were generated by polishing parts coated nickel mechanically [24].

Nickel coating is comprehensively utilized in a variety of ornamental areas of usage. These contain parts for the automotive, bicycle and marine industries, household devices, jewelry, door furnishing, hardware items and a large variety of consumer items. The basic aim of decorative coating is to increase the decorative appeal and appearance of the articles, but the platings can also be needed to meet strict performance criteria. The criteria can involve ductility, corrosion resistance, adhesion etc. depending upon the application and service conditions [25]

2.2.2 Engineering Nickel Coating

The area of engineering use of nickel coating involve those where a fully bright aspect is not needed. Nickel coatings for engineering applications are generally sulfur-free and matte in appearance. These deposits can be indicated to develop corrosion and wear resistance, to salvage or strengthen worn or undersized components, to develop magnetic properties, to arrange surfaces for organic coating or for enameling, to

operate as diffusion barriers in electronic area of use and for alternative objectives [24,26].

2.2.3 Nickel Electroforming Process

Electroforming is the process by which components are produced through generating metal by electroplating onto a suitable mandrel, which is afterwards removed.

Electroforming process has some properties, which make it a applicable manufacturing method for exclusive applications. These involve:

• accurate reproduction of fine surface detail

(e.g. the electroforming of stampers for the manufacturing of compact discs)

• duplicate of surface features

(e.g. moulds to remanufacture leather patterns or wood grain)

• high degree of dimensional accuracy (e.g. accurate components)

• capability to electroform shapes that are hard and expensive to manufacture by another process of production (e.g. rotary printing screens)

Owing to its great mechanics characteristics, good corrosion resistance and fine grain structure, nickel is the most metal used for electroforming. These features make it especially practical for the electroforming of moulds and dies for casting and moulding [27]. Figure 2.4 shows electroformed nickel mould for reinforced plastic automotive body component.

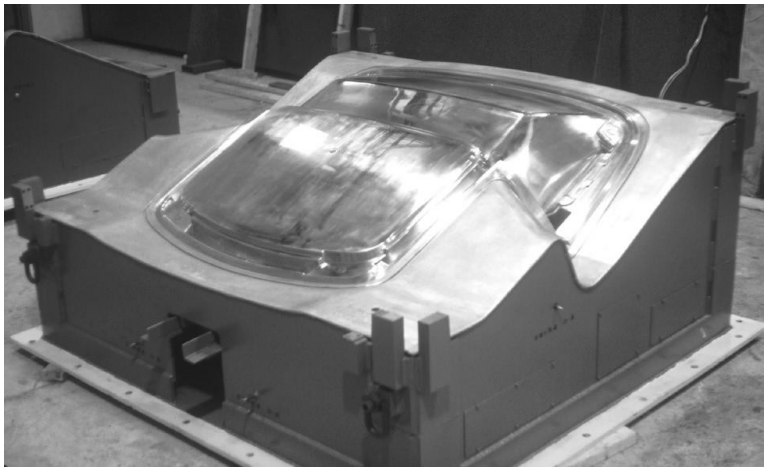


Figure 2.4 Electroformed nickel mould for reinforced plastic automotive body component [25].

2.2.4 Production Methods of Nickel Based Coatings

2.2.4.1 Electrolytic Coating

The electrodeposition method is a popular method for obtaining alloy coatings and nanocrystalline metal matrix composite materials. The method has the advantages of producing dense material, low size and shape limitation, high production speed. The properties of the material to be produced during the process (grain size etc.) can be controlled by coating parameters such as bath composition, pH, temperature and current density. An important advantage of the method is that it is easy to transfer to technology [28].

Since the surface properties of bulk materials can be easily changed by using the electrodeposition method, it has a very common technological usage area. Designers and researchers are able to satisfy a variety of needs using this method. Especially it is possible to economically improve the surface properties of materials with irregular surface geometries. It is not always possible to produce bulk material in desired properties such as economy and combination of various properties. Using the electrodeposition method, desired surface properties can be met economically. For this, the basic process parameters must be carefully should be selected. Most scientific disciplines such as surface science, solid state physics, metallurgy and materials science, electronics, electrochemistry and electrochemical engineering deal with

electrolytic coating. Electrolytic coated materials are used in applications involving both physical and mechanical properties. Physical properties; electrical and thermal conductivity, magnetic behavior, thermoelectric effects, density, melting point and lattice structure. The mechanical properties are; elastic modulus, hardness, ductility and strength [28,29].

In recent years, the electrodeposition method has found wide use in the microelectronic industry. Examples include electronic bridges, connectors, magnetic recording heads, optics, optoelectronic systems, sensors and many other applications. It is possible to produce many micro-devices with three-dimensional structure with electrolytic coating, including corrosion protection, high abrasion resistance, thermal and magnetic properties. The use of iron group alloys produced by electrolytic plating in computer data storage and sensing is based on the interest of researchers [30–33].

In particular, the coating of nickel and iron binary alloys provides suitable properties for recording, memory and storage devices. Nickel, cobalt and iron triple alloys are used in high density recordings because they have a higher magnetic flux density and lower coercivity properties than Permalloy (Ni80Fe20). Multilayer alloys, which are nanometer-sized, containing nickel, iron and cobalt together with copper are noteworthy because of their high degree of magnetic resistance. For other application areas; microwave guides and micro-electro-mechanical system technologies [30]. The electrons required for the reduction process can be obtained from different sources. There are two basic methods for this: electroplating and electroless plating [34,35].

2.2.4.1.1 Electroless Plating

There is no need for an external electron source in electroless coatings. The electrons required to reduce metal ions are released as a result of the chemical reaction that occurs in the solution. The coating system with the electroless plating method is schematically shown in Figure 2.5. The electroless coating is usually are divided into two groups.

1- Deposition by ion or charge exchange

2 - Metal deposits containing reducible materials [33]

The deposition by ion or charge exchange occurs when the second metal is submerged in the metal salt bath and spontaneously deposits the second metal by partial ion attack on the surface of the first metal. Since the reaction contains the atoms of the sample and the ions of the solution, the process stops when the surface of the sample metal is coated with the solution metal. Due to these reasons, the coating thickness is low [35]. This kind of deposit can be used in limited applications due to the accumulation quality and limited thickness. In recent years, especially copper and processes containing nickel have gained great importance and can also be used in situations where current coating cannot be applied. Coatings with excellent chemical and physical properties suitable for practical applications are possible [36–38].

Coatings with a more homogeneous and less porous surface can be produced by means of the electroless coating. The concentration difference due to current density in the electroplating makes it difficult to obtain the coating surface in these properties. Furthermore, the surface of nonconductive materials such as ceramics and plastics can also be coated with electroless plating. However, this method has some disadvantages. It has a more complex solution bath than the electroplating bath and new materials should be added as this bath is used [39,40]. Figure 2.5 shows Schematic view of the electroless plating bath and comparison of deposit uniformity for electroless plating and electroplating is shown in Figure 2.6.

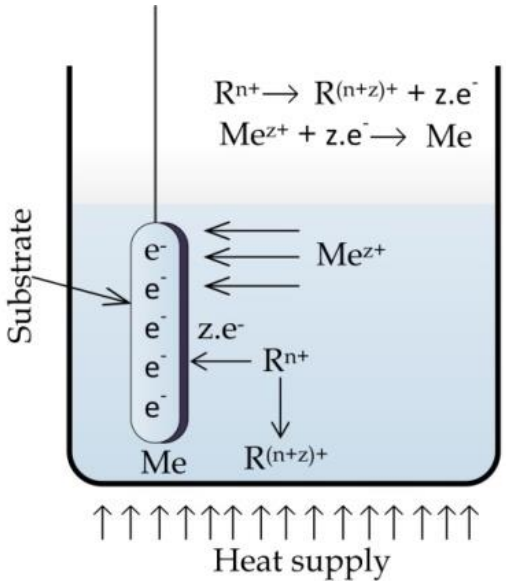


Figure 2.5 Schematic view of the electroless plating bath [40].

Some advantages of electroless plating:

- Does not use electric power.
- Even plating on parts surface could also be obtained.
- There isn’t any refined jigs or racks are required.
- There is flexibility in coating volume and thickness.
- The method will sheet recesses and blind holes with constant thickness.
- Chemical renewal are monitored automatically.
- Complex filtration technique isn't required.

Some disadvantages of electroless plating:

- Lifetime of chemicals is limited.
- Waste treatment cost is high owing to the rapid chemical renewal.
- Porous microstructure of electroless coating results in poor material structure as compared to electrolytic methods [29].

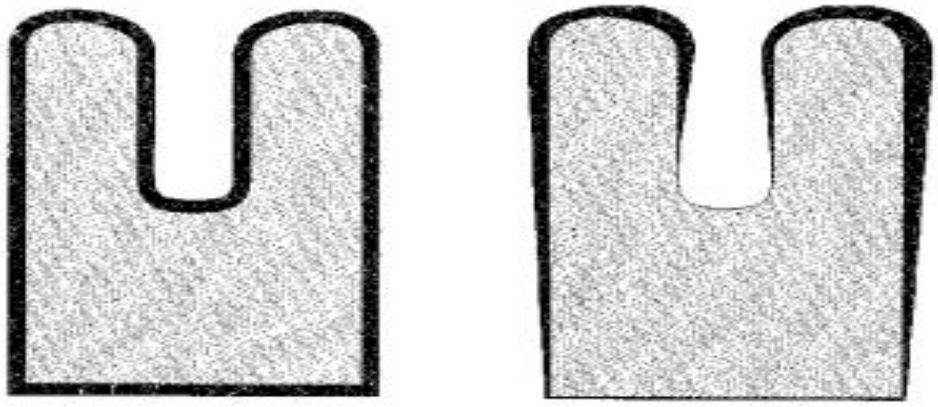


Figure 2.6 Comparison of deposit uniformity for electroless plating(left) and Electroplating (right) [41].

2.2.4.1.2 Electroplating

Electroplating is an electrolytic process for depositing a layer of metal upon a conductive substrate to increase the properties or appearance of the component. Electroplating is a method which is a form of electrodeposition.

Electrodeposition is based on cathodically releasing metal ions. During the electrolysis of the metal salt solution, ions are reduced to the metal used as the base in the cathode. As a cathode electron source, the anode acts as a receiver for electrons. The required electrons are derived from the external current source. In the event of cathodic metal deposition from an aqueous solution, the metal is preferably present as an anionic complex, not as simple hydrate (an aqueous solution, composition that crystallizes with one or more water molecules) ions. The hydrate metal ion follows many steps while being neutral. As the metal ion passes through the diffusion layer, the water molecules surrounding the ion are redirected. When metal ions pass into the Helmholtz layer, the potential change required to separate water molecules from the metal ion is quite high. For this, when the actual neutralization process occurs on the cathode surface, it contains only a simple dehydration ion. The metal ion is first attracted to the cathode surface (absorbed). It then moves toward the point where it will develop along the surface and is incorporated into the metal lattice [36] . Schematic view of electrodeposition method is shown in Figure 2.7.

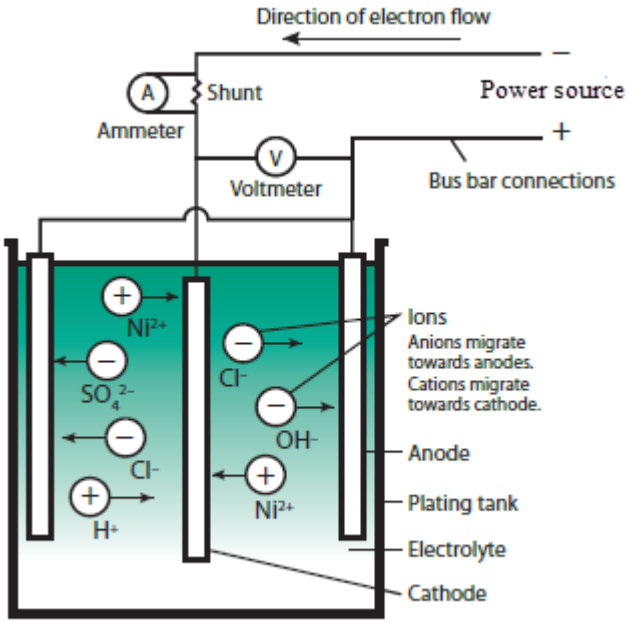


Figure 2.7 Schematic view of electrodeposition method [25].

General reaction for electroplating process is given by Eq. 2.1.

$$(A_x B_y)\, z + mxe \rightarrow xA^0 + yB \quad (2.1)$$

B can be ion or molecule, such as Cu^{+2} or H_2CrO_4. B is tightly attached to the metal ion and together with the metal ion, they occur complex species. These complex species take a task in the transfer process of charge.

"n" is the net quantity of electrons transferred during the electroplating process. It should be positive. "z" is the electric charge of the electroactive species in electron. It can be zero, negative or positive.

Electrodeposition method takes place according to Faraday's law. In his work on electrodeposition, Michael Faraday proved that the metal amount coated on the cathode and the amount solved on the anode are directly proportional to the quantity of electricity passed – in other words to the time and current of electroplating [24].

Faraday's Law equation is shown in Eq. 2.2

$$m = QA/nF \quad (2.2)$$

For this equation;

"F" is the Faraday constant (F = 96485 C/mol). "A" is the atomic weight of the metal. "m" is the deposited metal mass in gram. "n" is the valance electron of metal. "Q" is the net charge passes through the system, current multiply with time.

2.2.4.2 Parameters Affecting Quality of Coating

The parameters affecting the coating quality are given below.

- Additives
- Current density
- Concentration and mixing
- Temperature
- Impurity
- Nature of basic metal and electrolytic
- pH

a) Additives: Additives are often added to the solutions so that the coating can have the desired properties. In spite of the dissolution of some of the inorganic compounds, the additives are generally organic and colloidal. Additives reduce surface roughness and internal stresses [42].

b) Current density: The current density is the current intensity that corresponds to the unit surface. The increase in current density has two opposite effects on the structure of the coating. As the current density increases, the rate of formation of the crystals increases and the grain structure is examined. However, if the current density is too high, the metal ions that are discharged around the cathode cannot be sufficiently absorbed by the solution, so that a depletion occurs in the cathode, which results in inhomogeneity in the resultant coating and degrades the coating quality and leads to black and spongy coverings. Excess hydrogen output at the cathode indicates that the current density has increased excessively [43].

c) Concentration and mixing: The effect of concentration on the structure of the coating is great. Since the rate of formation of crystals is great, a thin coating with good adhesion to the base metal is obtained. It is useful to move the material to be covered in the bath with the aim of meeting the partial impoverishment of the cathode. It is also very useful to filter the coating solution at periodic intervals. Electrolyte can be supplied in air (low pressure) mixture, but there is a possibility that the sediments will stick to the parts to be coated because it will circulate continuously in the electrolyte [34]. In some cases, ultrasonic mixers are used to mix the electrolyte. Some advantages of using ultrasonic mixer in electrolytic coatings are as follows:

i. It allows to work at high current density which allows the coating to be fast.

ii. Adhesion develops.

iii. Reduce the porosity.

iv. Increases brightness.

vi. Increase hardness [43].

d) Temperature: There are two opposite effects of temperature. As it increases diffusion from one side, it increases the rate of formation of crystals and thus small crystalline structures are obtained. On the other hand, it reduces the polarization of the cathode and thus causes the formation of large crystals and their growth. In addition, since the hydrogen overvoltage is reduced, hydrogen will be released easily and the coating will be spongy [42].

e) Impurity: Organic impurities are usually caused by poor adhesion, a more fragile tensile structure and darker coatings. Metallic impurities, however, may result in poor shot power, poor adhesion, low cathode yield, brittle structure, burnt and pale patchy coatings. Poor impurities in the electrolyte lead to the formation of deposits in undesirable properties. Ions outside the metal to be coated may either accumulate in the cathode or remain in the solution depending on the charge release potential. Even the cathodic accumulators are influential in the quality of my accumulation. Insoluble impurities such as dust and metal particles physically act on the catheter and cause pits and holes to form in the coating. This is especially the case when the electrolyte is mixed and the insoluble materials are not allowed to collapse at the bottom.

f) Nature of basic metal and electrolytic: The effect of base metal on the quality of the coating is great. Particularly the coating of the casting parts of the zamak requires much attention. The quality and composition of the raw material is very important, and when the structure is "porous" spongy in a cold and careless cast, bubbles form after a while as a result of the coating. This is not the worst of the coating, but the basic metal is broken. As to the nature of electrolytes, it has long been known that the coatings obtained by electrolysis of complex salts are superior to those obtained with normal salts. Especially in cadmium, zinc, copper, gold and silver coatings, "electrolytes" are prepared by dissolving the double salts of these metals. Coatings made with such complex salts contain smaller grain-size crystal structures than simple salts.

g) pH: If the electrolytes are above or below the specified pH values, the coating quality is immediately affected. If the pH is high, precipitates (hydrates, etc.) are formed which go into the cathode and form defective areas (low hardness, abrasion resistance, etc.) in the coating layer. In continuous coatings, when passing through acidic coatings from alkaline baths during intermittent washing, care must be taken

that the factors that affect the pH value, such as neutralization. Soda caustic and hydrochloric acid should not be used when adjusting the pH [33].

2.2.4.3 Influence of Bath Types on Electroplating

There are 2 different nickel baths which are used the most. These baths have different compounds in different ways. They have different pH, temperature and cathode current densities. And also, the mechanical properties such as internal stress, hardness, etc. obtained at the end of the coating are different**.**

2.2.4.3.1 Nickel Watts Bath

The nickel watts bath, which known as the sulphate bath, is the one of most common nickel plating baths. Nickel watts plating baths are largely used for functional industrial applications. Watts solutions contain nickel sulphate, nickel chloride and boric acid. As the composition of the compounds varies depending on the application area, the typical chemical composition of the nickel watt bath is shown in Table 2.4 [25].

Table 2.4 Compound and operating conditions for nickel watts electroplating baths.

Nickel Sulphate ($NiSO_4.6H_2O$)	240 - 300 g/L
Nickel Chloride ($NiCl_2.6H_20$)	30 - 90 g/L
Boric Acid (H_3BO_3)	30 - 45 g/L
Temperature	40 - 60 ℃
pH	3.5 - 5
Cathode Current Density	2 - 7 A/dm^2
Deposition Rate	25 - 85 µm/h

In the nickel watts bath, nickel sulfate supplies nickel ions to the bath and is the source of most of the nickel ions. It is the not expensive nickel salt and can also be applied at the end of process for very bright industrial areas where uniform thickness is not a major consideration. Nickel chloride is basic for good anode corrosion and incrases the conductivity of the coating bath solution. The typical operating range is 30–90 g/L. Generally, minimum for anode corrosion is necessary 30 g/L nickel chloride in the

coating bath , unless special forms of anode material that involve nickel sulfide or nickel oxide are used as depolarizers. In some cases, however, the addition of nickel chloride may result in pitting on the coating surface. Boric acid pH buffer of the bath solution and it arranges the hydrogen ion concentration in the cathode film. If this buffering action had not taken place, the pH of cathode film in the higher-current-density regions would very quickly exceed 6.0, and nickel hydroxide would be precipitated and codeposited along with hydrogen, ending up with burned deposit and green nodulation [44].

Watts baths have four major advantages:

1. High speed plating is possible
2. Plating bath composition is simple, so control is easy.
3. Solubility to water is large. Use by high concentration and high current is possible.
4. Influence of impurities is slight [25].

2.2.4.3.2 Nickel Sulphamate Bath

Nickel sulphamate solutions are primarily used for the deposition of practical coatings or for electroforming. For such applications the low stress which might be achieved without the utilization of addition agents, the high deposition rates and desirable deposit properties offset their higher price. Chloride contains a significant impact on stress and additionally influences anode behavior. A low chloride concentration is fascinating to attain a low stress level. It is potential to control with zero chloride if Sulphur activated nickel anodes are used under appropriate operational conditions. But, a low concentration of nickel chloride (about 5 g/L) is usually suggested to supply some insurance of satisfactory anode performance. As an alternative, nickel bromide could also be substituted and doesn’t increase stress as much as chloride. One of the benefits of sulphamate solutions is the higher solubility of nickel sulphamate compared with nickel sulfate. it's thus attainable to use higher nickel concentrations and to control at very high current densities [25]. Table 2.5 shows compound and operating conditions for nickel sulphamate electroplating baths.

Table 2.5 Compound and operating conditions for nickel sulphamate electroplating baths [25].

Nickel Sulphamate ($Ni(NH_2SO_3)_2.4H_2O$)	300 - 450 g/L
Nickel Chloride ($NiCl_2.6\ H_20$)	0 - 30 g/L
Boric Acid (H_3BO_3)	30 g/L
Temperature	40 - 60 °C
pH	3.5 - 5
Cathode Current Density	2 - 15 A/dm^2
Deposition Rate	25 - 180 µm/h

2.2.4.3.3 Other Nickel Plating Baths

Fluoborate Bath: This bath may be operated at very high current densities. Mechanical characteristics are almost like the nickel watts deposits. This bath is high expensive and it extremely has corrosive electrolytes.

All-Chloride Bath: This bath type is an alternative method where high current densities are needed. Furthermore, these bath types are much more corrosive than watts baths and thus equipment for plating must be carefully chosen. Coating has fine-grained structure and usually harder than nickel watts coatings.

All-Sulphate Bath: The main use for this bath type is in area of usage including the use of insolvable anodes. The absence of chlorides removes the problem of harmful chlorine gas being releasing at the anode. Graphite or lead anodes are widely used. It is necessary to refill the nickel ions and to manage the hydrogen ion concentration through regular additions of nickel carbonate.

High Sulphate Bath: The essential property of these solutions is their good throwing power. They have found restricted use as a strike solution over zincate pre-treated aluminum.

Hard Nickel Bath: This solution supplies harder deposits and outstanding wear resistance without using of organic ingredients. The higher stiffness is obtained through the addition of ammonium ions. Close control of pH, current density and temperature are critical for consistent performance.

Black Nickel Bath: Except for some restricted use on optical equipment or for solar collectors, this bath type has primarily been practiced for decorative aims. The coating has thin structure. Thus, black nickel is generally carried out over textile application or bright nickel and plated with a lacquer or other organic finish [25]. Table 2.6 shows compound and operating conditions for other nickel electroplating baths.

Table 2.6 Compound and operating conditions for other nickel electroplating baths [25].

Type	Composition (g/L)	pH	Temp. (^{o}C)	Current Density A/dm^2
Fluoborate	Nickel Fluoborate, 225-300 Nickel Chloride, 0-15 Boric acid, 15-30	2.5- 4.0	38-70	3-30
All-chloride	Nickel Chloride, 225-300 Boric acid, 30-35	1.0-4.0	50-70	2.5-10
All-sulphate	Nickel Sulphate, 225-410 Boric acid, 30-45	1.5-4.0	38-70	1-10
High sulphate	Nickel Sulfate, 75-100 Boric acid, 15 Sodium Sulphate, 75-100 Ammonium chloride, 15-35	5.3-5.8	20-32	0.5-2.5
Hard nickel	Nickel Sulfate, 180 Boric acid, 30 Ammonium chloride, 25	5.6-5.9	43-60	2-10
Black nickel	Nickel Sulfate, 100 Ammonium chloride, 15 Zinc Sulphate, 22 Sodium thiocyanate, 15	5.5-6.0	26-32	0.2

2.2.4.3.4 Comparison of Nickel Watts and Nickel Sulphamate baths

Watts bath is relatively inexpensive and easier to control than Sulphamate bath. Sulphamate solution has distinct advantages. Nickel sulphamate solutions are commonly used for electroforming due to low internal stress, high deposition rates, and superior throwing power of the precipitates. The throwing power is the relationship between geometric factors and the uniformity of current distribution and coating thickness, which are influenced by the electrochemical characteristics of the solution. The throwing power is a measure of how much the uniformity of the cathode polarization and cathode efficiency can be produced than in the absence of the effects produced. Due to the very high solubility of the nickel sulphamate, there is a higher nickel metal concentration and allows for lower operating temperatures and higher

coating speeds. A small amount of nickel chloride is added to the nickel sulphamate solutions to minimize the anode passivity at high current densities. Nickel sulphamate solubles are soluble so that they cannot easily be recrystallized from the solution. Commercially, it is present as a concentrated solution prepared by reacting high purity nickel with sulfur sulphamic acid under controlled conditions. Nickel sulphamate coating solutions are more expensive than commercial nickel sulphate and nickel chloride grades. Long term use of sulfamate solutions at temperatures above 700 ° C (1400 ° F) or below a pH of 3 may result in nickel hydrolysis. Ammonium and sulphate ions produced by hydrolysis increase the internal stress and hardness of the deposits. Sulphamate nickel plating baths are particularly useful for applications requiring low residual stress in electrolytic nickel, such as electroforming, and coating of objects susceptible to fatigue cracking [44]. Table 2.7 shows comparison of nickel watts and nickel sulphamate solutions.

Table 2.7 Comparison of nickel watts and nickel sulphamate solutions [44].

Electrolyte Composition (g/L)		
	Nickel Watts	Nickel Sulphamate
Nickel Sulfate ($NiSO_4.6H_2O$)	240-300	-
Nickel Sulphamate $Ni(SO_3NH_2)_2.4H_2O$	-	30-45
Nickel Chloride $NiCl_2.6H2O$	30-90	300-450
Boric Acid (H_3BO_3)	30-45	0-30
	Operating Conditions	
Temperature (^oC)	40-60	40-60
Agitation	Air or Mechanical	Air or Mechanical
Cathode Current Density (A/dm^2)	2-7	2-15
Anodes	Nickel	Nickel
pH	3.5-5	3,5-5
	Mechanical Properties	
Tensile Strength (MPa)	345-435	415-610
Elongation (%)	10-30	5-30
Vickers Hardness (100 g load)	130-200	170-230
Internal Stress (MPa)	125-185 (tensile)	0-55 (tensile)

2.2.4.4 Influence of Current Types on Electroplating

Electrodeposition is an economical and simple method for producing metallic coatings of alloy coatings and dense nano-crystals. Electrodeposition methods are used under direct current (DC), pulse current (PC) and pulse reverse current (PRC) in metallic coating production. Qu et al. found that the hardness of the PC-made coatings on the nickel coatings under DC and PC currents was significantly higher than the nickel plating on the DC coatings. Karslıoğlu et al. produced Ni-Co/CNT nanocomposite coatings by direct current, pulse current and pulse revert current on copper substrate. PC and PRC coatings showed considerable improvement in microhardness and abrasion resistance. Tao et al. Produced nanocrystalline copper coatings with the aim of investigating mechanical and tribological properties. Copper coatings produced via PC current have been found to exhibit higher hardness and better wear resistance than coatings produced via DC. It is stated in the literature that pure nickel coatings produced using by PC and PRC technique show better mechanical properties than pure nickel coatings produced by DC. In the conventional DC electrodeposition system, current density can only be changed. The cycle in the DC electrodeposition system (ratio of current to total accumulated time) is 100%. Therefore, the average current density and the peak current density are equal to each other.

A new period has begun with the electrodeposition method of metals, alloys and metal matrix composites in electrodeposition. Compared to conventional direct current (DC), the Pulse Electrodeposition technique is much more sensitive in controlling basic electrodeposition parameters. The combination of the microstructure, components and combination of the coating layer can be better controlled by the unique combination of pulse current on-time (current time, T_{on}) and off (off-time, current cutoff, T_{off}) time. The average current density ($I_{average}$) is obtained from the combination of different current densities in the open and closed pulse currents [45]. DC and PC types were found to be inadequate for some applications, and studies on pulse reverse (PRC) current type were concentrated in recent years by adding reverse current to the PC method. Table 2.8 shows possible effects of current type on deposit structures.

Table 2.8 Possible effects of current type on deposit structures [46].

Time Interval	Conditions that differ from DC plating	Phenomena affected
On-time	Double layer charging Overvoltage Concentration profile near the electrode Adsorption (ions, additives, hydrogen)	Nucleation rate Growth mechanism Electrode reaction mechanism Codeposition rate Additive reaction
Off-time	Double layer discharge Potential relaxation Desorption (ions, additives, hydrogen)	Surface diffusion Surface recrystallization Corrosion, displacement reactions Passivation Hydrogen diffusion
Pulse-reverse time	Anodic potential Sign change of double layer charge Concentration profile near electrode Desorption / adsorption (additives, ions)	(selective) Metal dissolution Hydrogen reoxidation Additive oxidation Passivation

Chang et al. used a Pulse Reverse electrodeposition process to produce a composite coating layer. When reverse current is applied in the PRC process, the reverse transport (transformation) against the current direction take place. As a result of reverse transport increasing the electrochemical polarization of the cathode, it has been shown that the nucleation energy of the particles decreases on the electrode surface and that as a result of this decrease the nucleation rate is increased, so that a more compact structure and a smoother surface property can be obtained [46]. Chokkakula et al. published in Nature magazine in 2014 covered copper graphene on copper foil by using DC and PRC electrodeposition method. As a result of the study, they reported that the graphene coating added to the structure in the PRC type increased the hardness by about 90% and the elastic modulus by about 30% [47].

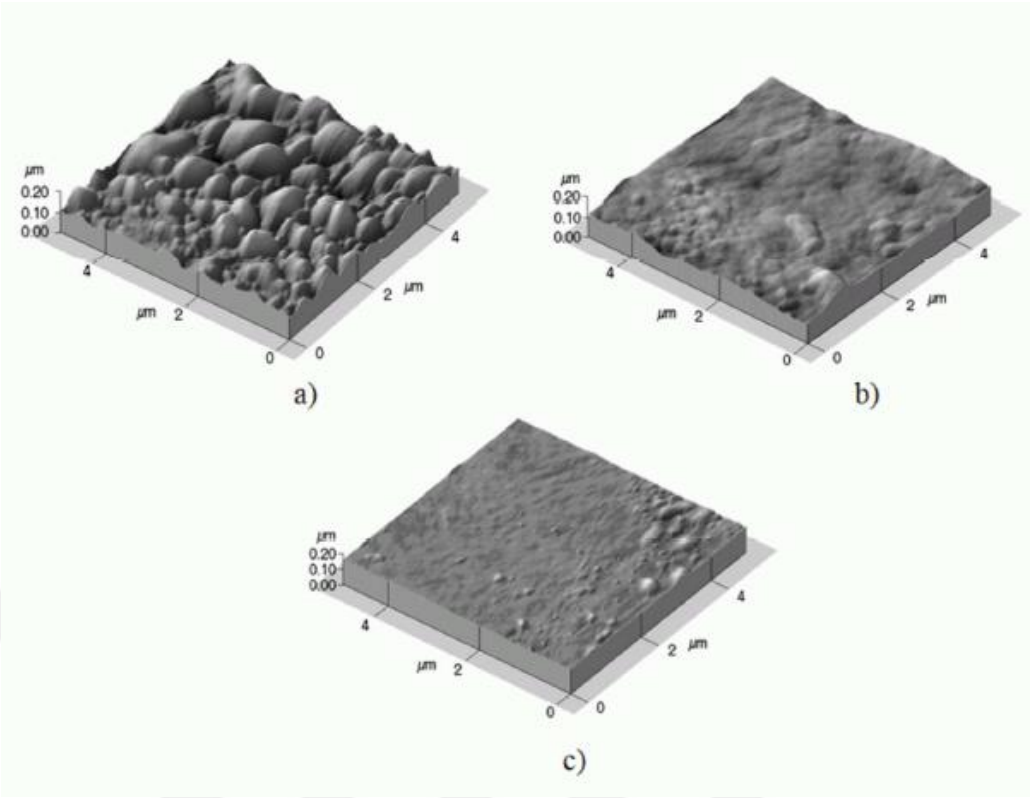


Figure 2.8 Topographic image of the Ni coating layer produced by using a) DC, b) PC, c) PRC electrodeposition method [48].

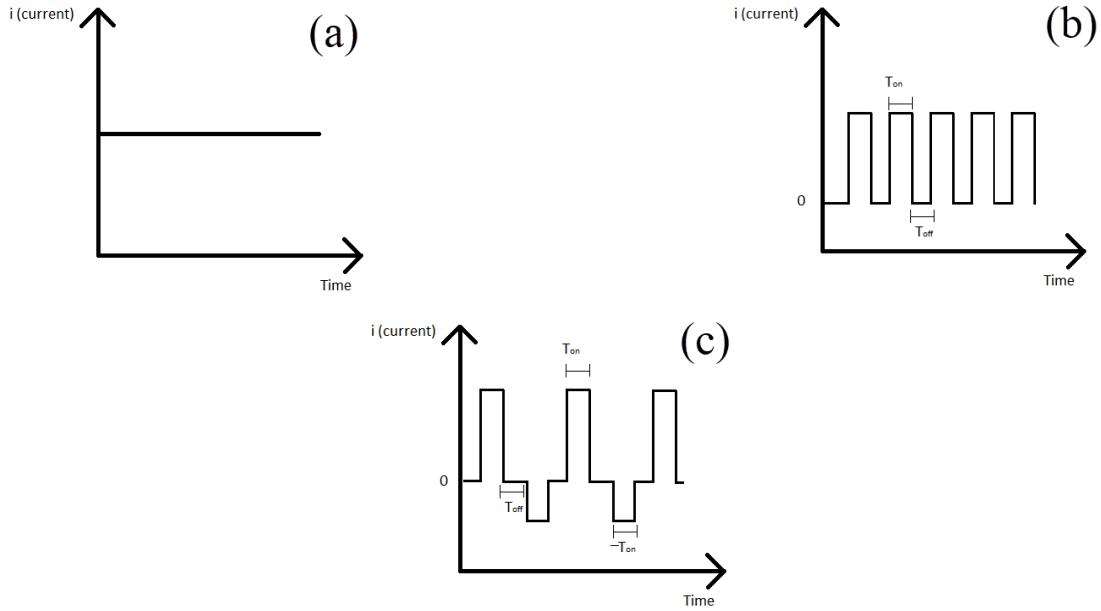


Figure 2.9 Types of current: a) DC, b) PC, c) PRC [49,50].

2.3 Review of Related Works

Ni-B coatings are noted for their high hardness, high abrasion resistance and good corrosion resistance. Furthermore, Ni-B coatings are also known for their price effectiveness, antibacterial properties, lubricity, thickness uniformity, excellent solderability, good electrical properties, extraordinary electro-magnetic properties, low porosity and high adhesion. Ni-B coatings have applications in a variety of industries, such as petrochemical, automotive, textile, food, aerospace, plastics, electronics, nuclear, computer and printing [51].

Krishnaveni et al.[52] reported that dimethylamine borane (DMAB) can also be used as a boron source in electrodeposited Ni–B alloy coatings and they results showed that the amount of boron, hardness and microstructure of Ni-B alloy coatings were considerably influenced from the sort of boron sources and other electrodeposited circumstances.

Chang et al. [1] examined that trimethylamine borane (TMAB) can also be used as a boron source in Ni-B alloy coating produced by DC and they results demonstrated that amount of boron and current density significantly influenced deposition rate, microhardness, microstructure and corrosion resistance.

Ogihara et al.[11] produced electrodeposited Ni–B coatings by using a traditional nickel coating bath including TMAB or DMAB which are boron sources and reported that in TMAB solution, the microstructure of Ni–B alloy coatings were controlled by the amount of co-deposited boron atoms; but in DMAB solution, explicit relationship between coating boron content and hardness was not verified.

Liang et al. [53]produced Ni-B alloy coatings with different amount of boron by DC by using DMAB as boron source from a sulphamate solution including DMAB and their results proved that increased microhardness of Ni-B alloy coatings is mainly caused by a decrease in grain size rather than boron content. So, they produced Ni-B alloy coatings with high hardness with a comparatively low boron content.

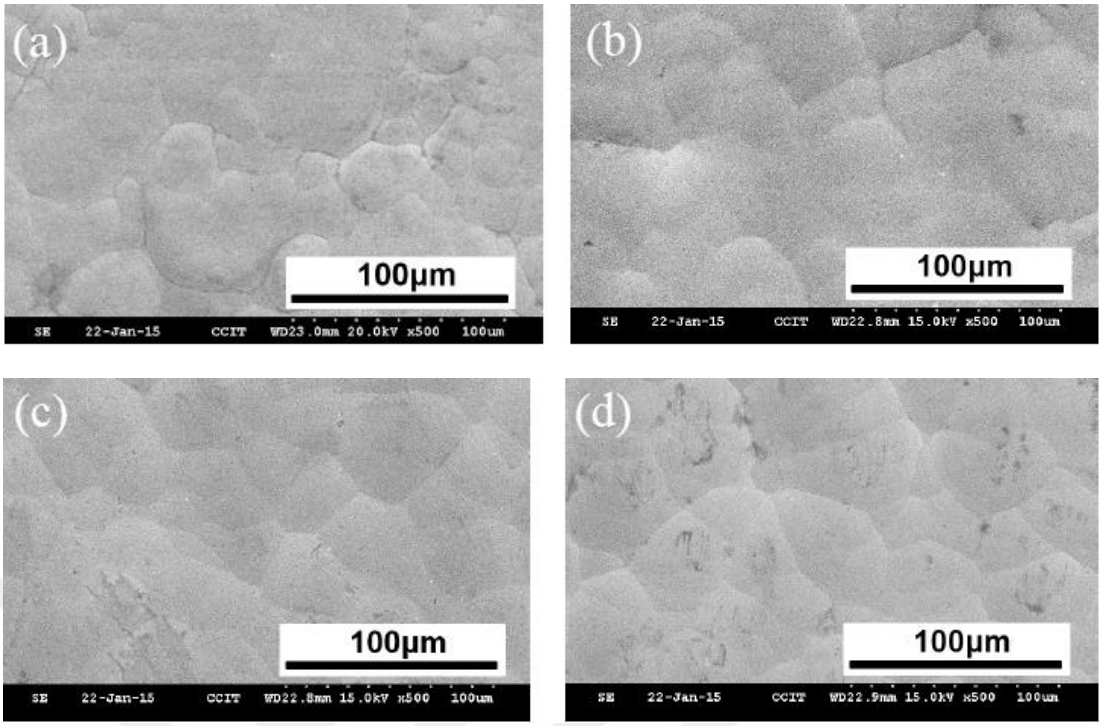


Figure 2.10 Surface morphology of Ni–B coatings electrodeposited at different current densities: (a) 1, (b) 3, (c) 5, and (d) 10 A/dm^2 [1].

Nickel-based alloys find a wide range of applications in space, aerospace, power generation, corrosion protection, high temperature applications, and high temperature oxidation. The Ni-Co alloy has a great popularity among these alloys due to its excellent functional properties, corrosion resistance and other properties. Examples of such properties include the combination of hardness and high corrosion resistance, magnetic materials, electrocatalysts used in hydrometallurgy [54]. Nickel-cobalt alloys and combinations can be produced very simply using the electrodeposition process from aqueous solutions. By adding 30 to 70% of cobalt in Ni, the highest hardness values of Ni-Co alloy are obtained [55]. By producing the same composites in pulse or pulse reverse current types, higher hardnesses are obtained compared to the coatings produced in direct current type [56]. Many studies indicate that Ni-Co alloy deposition is abnormal during electrodeposition [57-60]. The reason of this, the absorption of Co (OH) of Ni-Co alloy is higher than Ni (OH). For these reasons, the cobalt-rich coating is abnormally obtained after electrodeposition. This abnormal situation has only one logical explanation; hydrogen generated during electrolysis increases the formation of metal hydroxyl during coating [59]. Modern

electrochemical systems improve the properties of deposited metal layer using pulse reverse technique. Theoretically, when an anodic pulse is applied, it is necessary to redissolve the deposited layer. However, the deposited layer is passive depending on the canyon type and its electrochemical properties [61-63]. In addition, pulse reverse current is used to produce a more uniform and homogeneous coating layer, but it has been written by some researchers to reduce the internal tension of the pulse current. Especially in technological applications, homogeneous and high coating thickness is required, and in such cases, internal stress has a vital preventive effect [54].

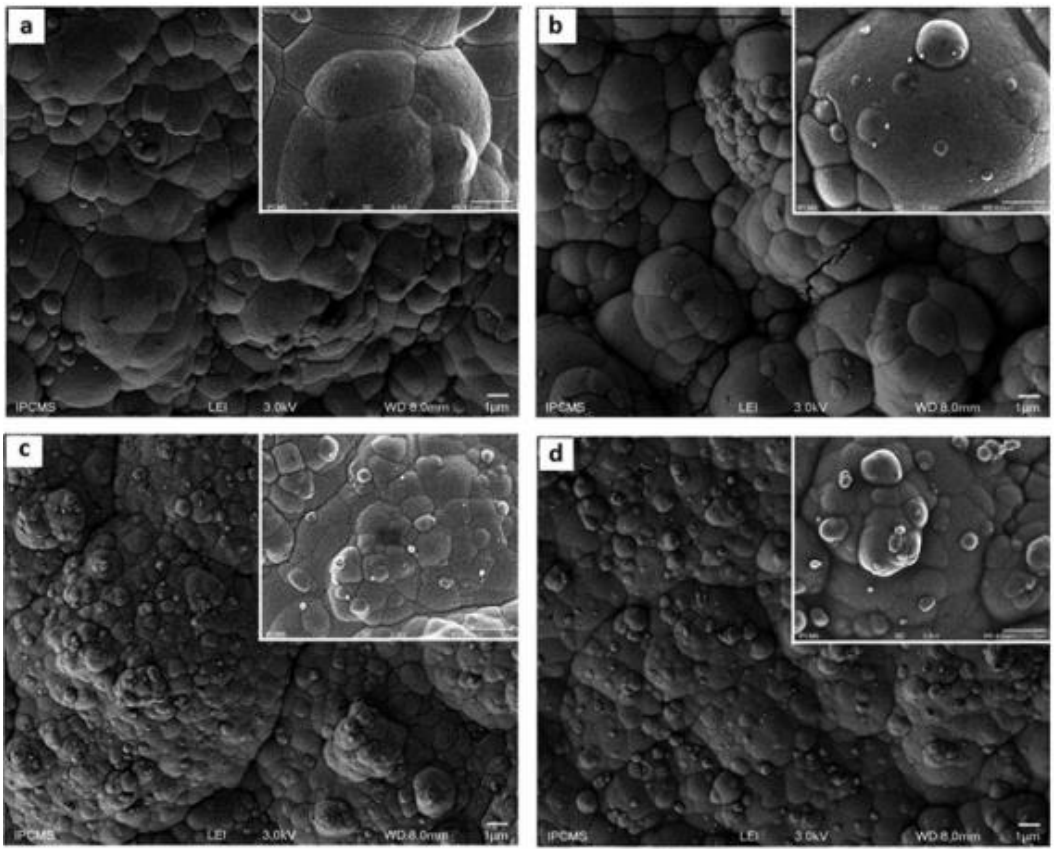


Figure 2.11 SEM surface micrographs of Co-Ni coatings at different current densities: a) A/dm^2 , b) 2 A/dm^2 , c) 3 A/dm^2 , d) 4 A/dm^2 [62].

Bouzit et al. [62] examined Ni-Co thin films were produced by electrodeposition on Cu substrate from chloride-sulfate bath containing thiourea as additive. The effects of applied current density (1, 2, 3 and 4 A/dm^2) on the composition, morphology,

microstructure and formation mechanism of deposited films were investigated by EDX, SEM and XRD techniques, respectively. The SEM images demonstrate that the deposits are well adherent and show a compact surface with a cauliflower-like appearance (see Figure 2.11) and changes from rough to smooth surface with the increase of current density. The structural investigation was occurred through the Rietveld refinement of XRD patterns by using MAUD program. The results reveal the formation of both HCP Co phase, FCC Co(Ni), HCP Co(Ni) and HCP Co(S) solid solutions (SS). The HCP SS formation mechanism is described by the diffusion of Ni and S atoms along c axis of HCP Co crystal lattice. The increase of current density causes a lattice distortion revealed by an increase of the lattice parameters of different SS.

Srivastava et al. [63] studied microhardness and corrosion resistance of Ni-Co alloys coating. They clarified that when cobalt content increases up to 50 wt.%, hardness increases, however as the content of cobalt continues to increase, microhardness decreases since the crystallographic morphology changes from spherical crystal to polyhedral crystal. When cobalt content reaches up to 80 wt.%, crystallographic morphology changes to acicular shape. Their study shows that 80% Ni – 20% Co alloy shows better corrosion resistance than plain nickel or cobalt coating and then other mixing percentages. This is correlated with FCC structure of alloy. Their results show that corrosion currents of mild steel, cobalt coating, nickel coating, Ni-20% Co and Ni-50% Co are 2.994, 2.602, 0.527, 0.455 and 0.894 $\mu A/cm^2$, respectively.

Karslioglu et al. [64] examined the effects of current type on Ni-Co alloys. Nickel–cobalt (Ni–Co) alloys were produced via direct current (DC), pulse current (PC) and pulse reverse current (PRC) methods. The influence of different deposition currents on the surface microstructure, crystallographic structure, microhardness and reciprocating sliding wear behavior were investigated. When compared according to current types, the highest microhardness was obtained with PRC and the lowest was obtained with DC. The crystallographic grain growth orientation changed and it effected microhardness. The results show that DC type cause bigger grain size (see Figure 2.12). They also examined the effect of $NiCl_2.6H_2O$, which is thought to be primarily used in the coating bath during coating, for the optimization of bath

parameters in addition to the added and selected coating conditions [33]. The effect of $NiCl_2.6H_2O$ on the microstructure is given in Figure 2.13. It is understood from this that, under the conditions selected in the production of coatings, pores and inhomogeneities are found on the $NiCl_2.6H_2O$ coating surface. As can be understood from Figures 2.13 (a-c), it has been found that the pore and stains on the surface are reduced as the amount of $NiCl_2.6H_2O$ decreases. Also, better results were obtained in coatings produced from non-$NiCl_2.6H_2O$-added baths. On the other hand, when $NiCl_2.6H_2O$ was not added, it was observed that the structure was quite homogeneous (Figure 2.13 d).

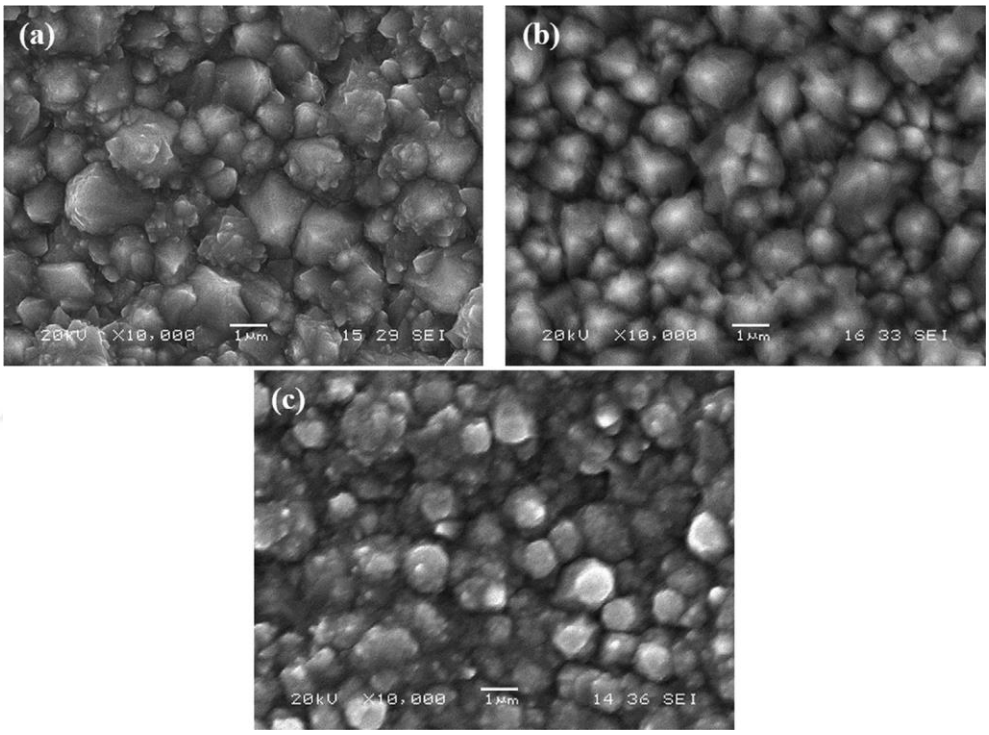


Figure 2.12 Ni–Co alloy coatings at 50°C for 30 min at 5 A/dm^2 current density; a) DC, b) PC and c) PRC methods [64].

Furthermore, they examined that the effects of $NiSO_4.6H_2O$ and $CoSO_4.7H_2O$ ratios on the coating layer in the bath composition were investigated. The effects on the coating layer of 4 different compositions were investigated such that the ratio of $NiSO_4.6H_2O/CoSO_4.7H_2O$ was 250/50 g/L, 200/100 g/L, 100/200 g/L and 50/250 g/L respectively. The results are given in Figure 2.14 a-d. Figure 2.14 (a) shows that the granules are in the form of polyhedron near the spherical form. However, there is a

distinct size difference between grain sizes, but the structure seems to be homogeneous. The increase of the ratio of $CoSO_4.7H_2O$ in the bath changed the surface morphology of the coating in the structure. With the increase of the amount of $CoSO_4.7H_2O$, the polyhedron-shaped grains in the structure first appeared to be rough and the appearance of some flakes in addition to the polyhedron-like grains was apparent from Figure 2.14 (b). With the increase in the amount of $CoSO_4.7H_2O$, it is understood that the ratio of the particles in the shape of the flake increases but there is not a large change in their dimensions, the particles of the polyhedron particles are reduced and the number of grains decreases per unit area (Figure 2.14 c). When 250 g/L of $CoSO_4.7H_2O$ was added to the bath, the proportion of the flakes in the structure increased and the polyhedron granules appeared to be located in the gaps among the particles in the shape of flake. However, while there is no significant change in the size of the particles in the shape of the flake, it is clear that the size of the particles in the form of polyhedrons is smaller (Figure 2.14 d).

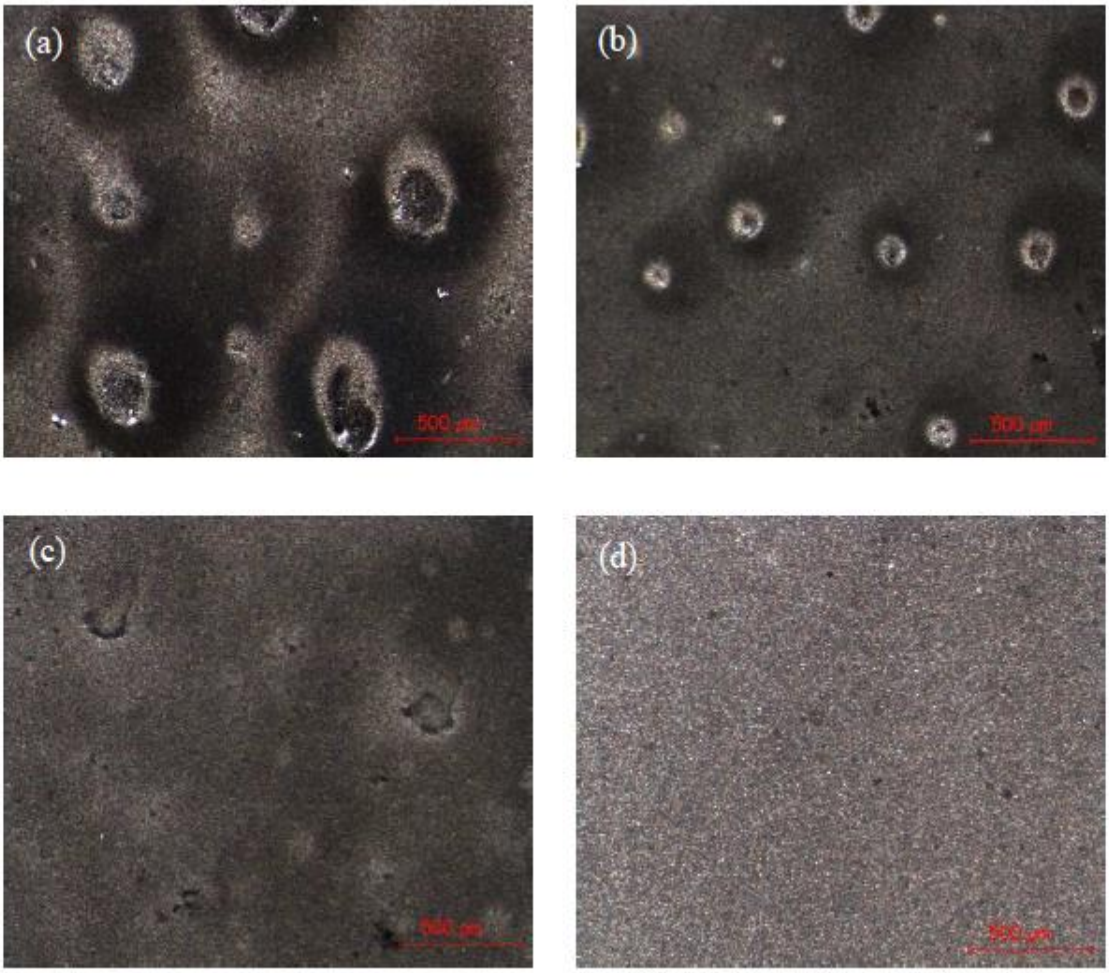


Figure 2.13 The micrographs of samples produced from coating bath with addition of a) 30 g/L, b) 20 g/L, c) 10 g/L, d) 0 g/L $Ni_2Cl.6H_2O$ for 30 min. at 50 °C by DC during optimization of bath parameters [33].

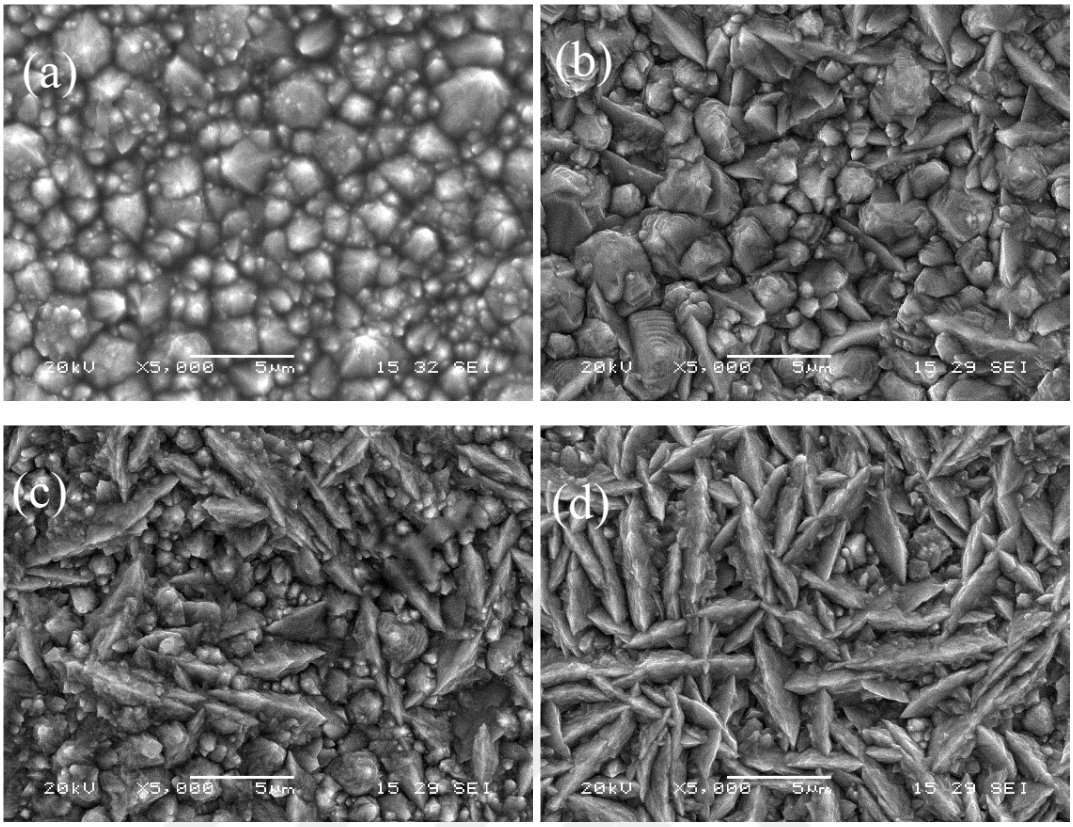


Figure 2.14 The SEM images of effect of $NiSO_4.6H_2O$ / $CoSO4.7H_2O$ (g/L) ratios on the coating layer 250/50, b) 200/100, c) 100/200 and d) 5/25 [33].

Mukhopadhyay et. al [65] examined that effect of heat treatment on the properties of electroless Ni-B, Ni-B-W and Ni-B-Mo Coatings. Ni-B and Ni-B-W coatings present a dense nodular surface morphology while Ni-B-Mo coatings show a cauliflower like morphology with aggregated clusters of nickel nodules and apparent surface cracks. At the end of heat treatment, grain growth and visible grain boundaries occurred in event of all the three electroless coatings. Also, the highest microhardness was occurred in Ni-B-W coatings among the all coatings in as-deposited condition and up to heat treatment temperature of 400°C. The nodular surface morphology similar that of broccoli and occurred in electroless Ni-B coating and flawless and without porosities surface occurred in electroless Ni-B coating (Figure 2.15). The nodular surface morphology similar that of broccoli and occurred in electroless Ni-B coating and flawless and without porosities surface occurred in electroless Ni-B coating (Figure 2.15 (a)). The coatings structure heat treated at 350°C for 1h is shown in Figure 2.15 (b) and in this situation, surface structure resembling cauliflower performed. This

can indicate a phase transformation from amorphous to crystalline structure. When the deposits are farther heat treated at 400°C for 1 hour, the deposites turn blueish which can be owing to generation of nickel oxides and further grain growth in shown in Figure 2.17 (c). As seen from Figure 2.17 (d), as these deposits are heat treated at 450°C for 1 h, coarse grain structure was obtained.

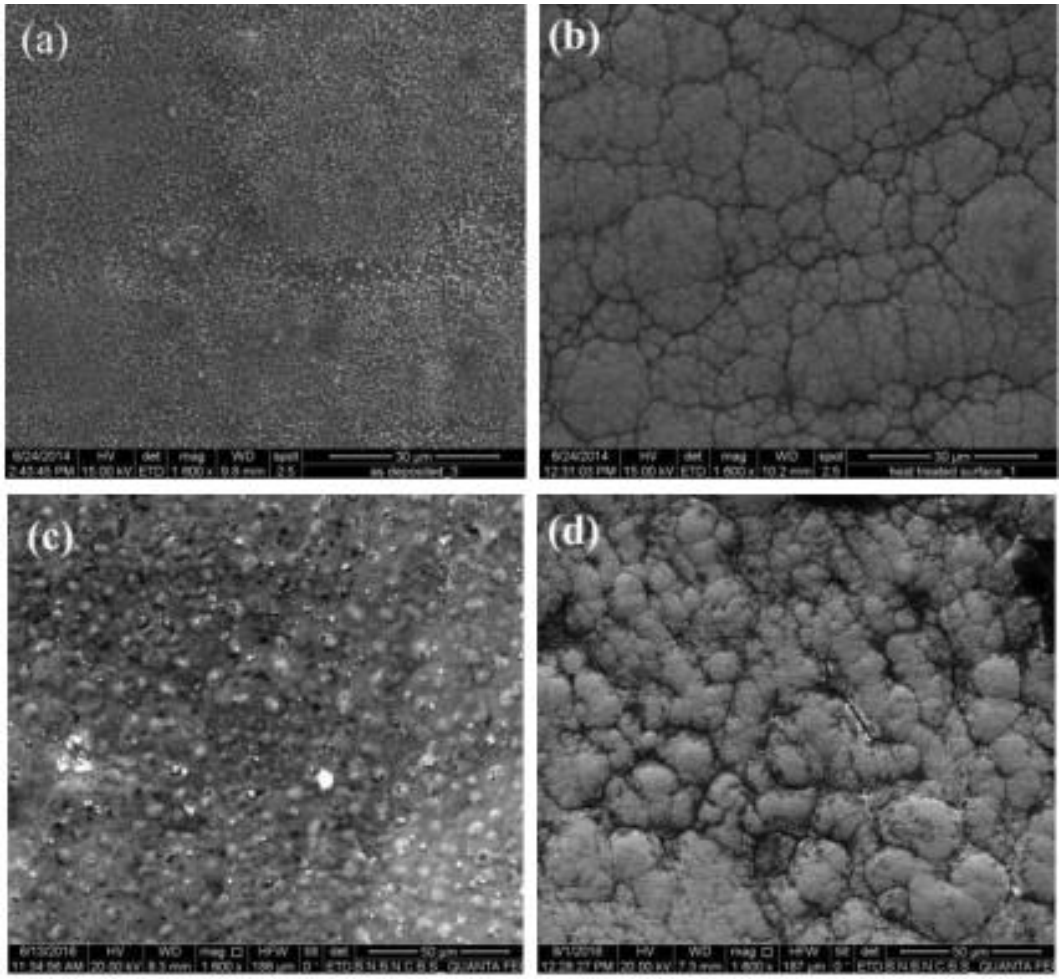


Figure 2.15 Electroless Ni-B coatings (a) as-deposited; and heat treated at (b) 350°C; (c) 400°C; (d) 450°C [65].

SEM micrograph of Ni-B-W coatings in its as-deposited and heat-treated condition is demonstrated in Fig. 2.16. Dense nodular surface is shown for Ni-B-W coatings in Figure 2.18a. From this image, it can observe that the size of nodules is partially higher than Ni-B plating (fig. 2.16a). Also, according to their results, higher corrosion resistance was obtained in this coating type. In fig.2.16b, it can be shown that there are

nodules which are inflated on heat treating deposits at 350ºC although grain boundaries are not exclusive compared to Ni-B coating heat treated at the same condition (fig. 2.15b). The morphology which is like typical cauliflower appears seem as Ni-B-W coating if farther heat treated at 400°C for 1 h in fig. 2.16c. The alloy coatings turn blueish at a heat treatment of 450°C for 1hour (Fig. 2.16d). So this is an indication of phase transformation occured similar to Ni-B coatings.

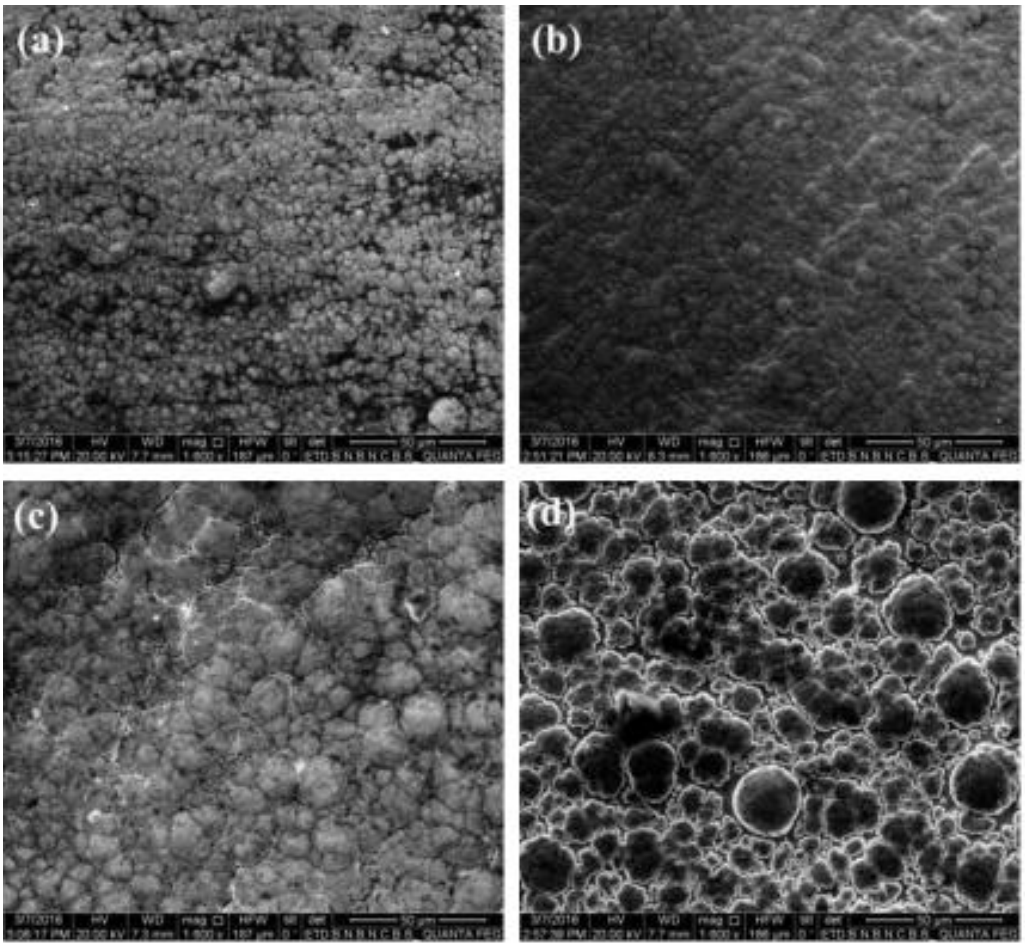


Figure 2.16 Electroless Ni-B-W coatings (a) as-deposited; and heat treated at (b) 350°C; (c) 400°C; (d) 450°C [65].

Lee et al. [66] investigated that effect of the amount of boron on the different properties of nanocrystalline Ni–B alloys produced by electrodeposition method. They found that significant decrease in grain size with the increasing amount of boron. Furthermore, they observed tensile stress which increased linearly with rising boron content. In

addition, the microhardness of Ni–B alloy coatings increased significantly owing to the intermetallic Ni_3B precipitation by the heat treatment and maximum microhardness of each coating rises with boron amount. Since the coatings which have high friction coefficient and brittle fracture, wear resistance decreased with increasing the boron amount.

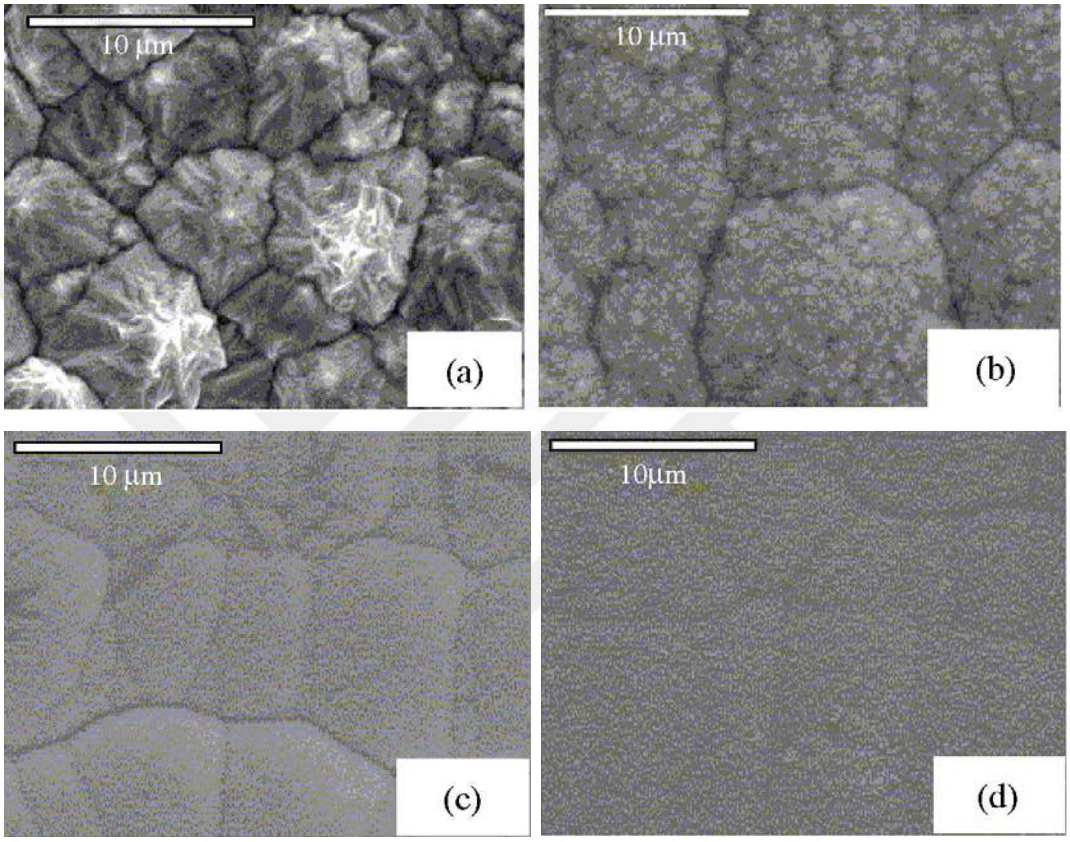


Figure 2.17 The change of surface morphology of Ni–B coatings with boron content. Scanning electron micrographs of (a) Pure Ni, (b) Ni-2 at.% B, (c) Ni-6 at.% B, (d) Ni-9 at.% B [66].

CHAPTER 3

EXPERIMENTAL PROCEDURE

All the experimental processes were conducted at Ankara Yıldırım Beyazıt University. Conventional watt type bath was used for electrodeposition process. Temperature for electrodeposition process was usually kept about 55ºC for watt type bath. Current density and pH are 5 A/dm^2 and 4-5, respectively. Electroplating device, BARAKUDA current source located at laboratories of Ankara Yıldırım Beyazıt University, was used as power supply. It can provide direct current, pulse current and pulse-reverse current. Coatings were carried out in 100 ml beaker with speed controlled magnetic stirrer (ISOTEX-SH 4C) in fume hood. Medium carbon steels were used with the dimensions of 20x40x1.5 mm as width, length and thickness, respectively. As anode material, pure nickel sheet was used with the dimensions of 30x40x3 mm as width, length and thickness, respectively. Coating baths contained high purity nickel sulphate ($NiSO_4.6H_2O$), trimethylamine borane (TMAB), cobalt sulphate ($CoSO_4.7H_2O$), boric acid (H_3BO_3) and distilled water.

In this study, influence of the addition of trimethylamine borane (TMAB) on nickel-boron coating and influence of cobalt sulphate and different current types on nickel-borane-cobalt coating containing fixed amount of TMAB were investigated on microstructure, hardness, wear resistance and corrosion behaviors.

3.1 Preparation of Experimental Setup and Testing

3.1.1 Preparation of Substrates

In this study, medium carbon steel plates were used as cathode with the dimensions of 20x40x1.5 mm as width, length and thickness, respectively. The substrates must be clean because the ions need to adhere well onto the substrate and thus homogeneous coatings are obtained**.** Medium carbon steels (40× 20× 1.5 mm) were grinded with grinding paper by using metal grinding device, respectively. After grinding, they were cleaned with acetone. And then, the medium carbon steels were degreased with pure

ethanol solution for 1 minute and cleaned with pure water before production of alloy coatings.

3.1.2 Preparation of Coating Bath

Three types of bath which are for pure nickel coating, Ni-B alloys coatings and Ni-B-Co alloys coatings were prepared. Electroplating processes were performed in nickel bath with the addition of trimethylamine borane and cobalt sulphate. The coating bath was poured into a 100 ml beaker and then it was mixed by a magnetic stirrer with mixing speed of 250 rpm to provide solution uniformly in the cathode-solution interface and heated to 55°C with a heat source. The pH of solution was between 4 and 5. During the coating, the pH and temperature of coating bath were maintained at ±0.5 units and ±3 °C, respectively. The medium carbon steel which is cathode and the pure nickel anode were vertically submersed in a 100 ml beaker separated by 2 cm from each other. Then coating systems were prepared in the fume hood. Pure nickel coating was prepared with direct current in the conventional nickel plating bath under constant current density (5 A/dm^2) for 30 minutes. Ni-B alloy coatings were produced with direct current in the different amount of trimethylamine borane and under constant current density (5 A/dm^2) for 30 minutes. Ni-B-Co alloy coatings were produced with both different amount of cobalt sulphate and different current types with constant TMAB amount. (DC, PC, PRC) and under constant current density (5 A/dm^2) for 30 minutes. After coating, pure nickel coating, Ni-B and Ni-B-Co alloy coatings were cleaned with pure water and dried in air at room temperature. Totally, fourteen specimens were coated. Test parameters are shown in Table 3.1, Table 3.2 and Table 3.3.

3.1.3 Electrodeposition Processes of Pure Ni coating and All Alloy Coatings

According to results of literature researches, it was decided to use conventional nickel watt type bath that contains nickel sulphate ($NiSO_4.6H_2O$), trimethylamine borane, cobalt sulphate ($CoSO_4.7H_2O$) and boric acid (H_3BO_3). The nickel sulfate ($NiSO_4.6H_2O$) was used as the essential salt of the bath solution, which supplies Ni ions to the bath and the content of nickel metal detects the limiting current density for producing good deposits, TMAB was used as the essential source of boron ions in the

plating bath, cobalt sulphate was used as the basic source of cobalt ions in the plating bath and also boric acid was used to stabilize the pH value of coating bath. pH is a substantial parameter for electrodeposition and it was between 4 and 5. Magnetic stirrer also functions as heat supply and has thermocouple. So, coating bath temperature could be kept constant at 55±3ºC.

According to results of literature researches, current density was used as 5 A/dm^2 in coatings. Also, DC, PC and PRC types were used at this current density. The effects of different amounts of boron and cobalt as well as different current types were investigated. One specimen were produced as pure nickel coating and this specimen was produced by DC method. Six specimens were produced as Ni-B alloy coatings by using DC. Five specimens were produced as Ni-B-Co alloy coatings by using DC and then two specimens were produced as Ni-B-Co alloy coatings by using PC and PRC methods. Current types are shown schematically in Figure 2.9.

Table 3.1 Bath composition and electrodeposition conditions of the coating bath.

	Pure Ni coating	**Ni-B alloy coatings**	**Ni-B-Co alloy coatings**
$NiSO_4.6H_2O$ **(Nickel source)**	250 g/L	250 g/L	250 g/L
TMAB **(Boron source)**	-	5, 2.5, 1.5, 1.0, 0.5, 0.25 g/L	1.5 g/L
$CoSO_4.7H_2O$ **(Cobalt source)**	-	-	50, 5, 2.5, 1.0, 0.5 g/L
H_3BO_3 **(pH regulator)**	40 g/L	40 g/L	40 g/L
Current density	Average 5 A/dm^2	Average 5 A/dm^2	Average 5 A/dm^2
Current type	DC	DC	DC, PC, PRC (for addition of 1g/L $CoSO_4$)
pH	4-5	4-5	4-5
Temperature	55±3ºC	55±3ºC	50±3ºC
Magnetic stirring	During deposition: 30 Minutes	During deposition: 30 Minutes	During deposition: 30 Minutes
Cathode	Medium Carbon Steel	Medium Carbon Steel	Medium Carbon Steel

Table 3.2 Bath parameters are given for pure nickel coating, Ni-B and Ni-B-Co alloy coatings.

Type of Coating	Specimen No:	Current	NiSO4.6H2O/ TMAB $CoSO_4.7H_2O$/ H_3BO_3 (g/L)	T_{on} / T_{off} / $-T_{on}$ (ms)
Pure Ni coating	1	5 A/dm^2 Current density$_{max}$: 200 mA Cathode surface: 4 cm^2	250/-/-/40	∞/0/0
Ni-B alloy coating	2	5 A/dm^2 Current density$_{max}$: 200 mA Cathode surface: 4 cm^2	250/5/-/40	∞/0/0
Ni-B alloy coating	3	5 A/dm^2 Current density$_{max}$: 200 mA Cathode surface: 4 cm^2	250/2.5/-/40	∞/0/0
Ni-B alloy coating	4	5 A/dm^2 Current density$_{max}$: 200 mA Cathode surface: 4 cm^2	250/1.5/-/40	∞/0/0
Ni-B alloy coating	5	5 A/dm^2 Current density$_{max}$: 200 mA Cathode surface: 4 cm^2	250/1/-/40	∞/0/0
Ni-B alloy coating	6	5 A/dm^2 Current density$_{max}$: 200 mA Cathode surface: 4 cm^2	250/0.5/-/40	∞/0/0
Ni-B alloy coating	7	5 A/dm^2 Current density$_{max}$: 200 mA Cathode surface: 4 cm^2	250/0.25/-/40	∞/0/0
Ni-B-Co alloy coating	8	5 A/dm^2 Current density$_{max}$: 200 mA Cathode surface: 4 cm^2	250/1.5/50/40	∞/0/0

Table 3.3 Bath parameters are given for pure nickel coating, Ni-B and Ni-B-Co alloy coatings (continue).

Ni-B-Co alloy coating	**9**	**5 A/dm^2 Current density$_{max}$: 200 mA** Cathode surface: 4 cm^2	**250/1.5/5/40**	∞**/0/0**
Ni-B-Co alloy coating	10	5 A/dm^2 Current density$_{max}$: 200 mA Cathode surface: 4 cm^2	250/1.5/2.5/40	∞/0/0
Ni-B-Co alloy coating	11	5 A/dm^2 Current density$_{max}$: 200 mA Cathode surface: 4 cm^2	250/1.5/1/40	∞/0/0
Ni-B-Co alloy coating	12	5 A/dm^2 Current density$_{max}$: 400 mA Cathode surface: 4 cm^2 $I_{average=}$ 200 m/A	250/1.5/1/40	10/10/0
Ni-B-Co alloy coating	13	5 A/dm^2 Current density$_{max}$: 450 mA Cathode surface: 4 cm^2 $I_{average=}$ 200 m/A	250/1.5/1/40	10/0/10
Ni-B-Co alloy coating	14	5 A/dm^2 Current density$_{max}$: 200 mA Cathode surface: 4 cm^2	250/1.5/0.5/40	∞/0/0

3.2 Characterization of Deposited Layers

3.2.1 Scanning Electron Microscope Analysis

Images of scanning electron microscope were examined with HITACHI-TM4000Plus Tabletop Microscope (see Figure 3.1) for characterization process and results were compared with literature researches. How the grain structure changed under different conditions was examined. With the same device, EDS (energy dispersive spectroscopy) analysis was conducted and the elemental ratio was investigated.

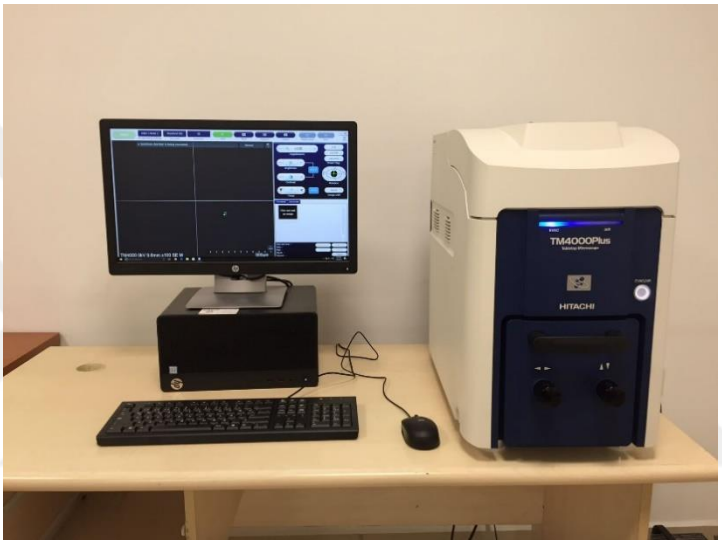


Figure 3.1 HITACHI TM4000Plus Tabletop Microscope.

3.2.2 XRD Analysis

In this study, the structural and phase analyses of the electrodeposited pure nickel coating, Ni-B and Ni-B-Co alloy coatings were determined via using a X-ray diffractometer (Rigaku-Miniflex 600) with a CuKα radiation 40 kV and 15 mA. The CuKα radiation value of wavelength is 1.54059 Å. The X-ray analysis was occured at 2°/min scan rate between 20° to 110° 2θ angles via using X-ray diffractometer (Rigaku MiniFlex 600, see Figure 3.2). The phase identification of the selected alloys was occurred by using a diffraction analysis program (PDXL). The full widths at half maximum (FWHM) values of X-ray diffractions were utilized to calculate grain sizes by using the Debye–Scherrer formula (Eq. 3.1) [67].

$$D = \frac{K\lambda}{\beta cos\theta} \quad (3.1)$$

In this equation, K is a Scherrer constant (K~0.9 in this case); λ is the wavelength of X-ray (λCuKα~1.54059 Å); θ is the diffraction angle, β is full width at half maximum (FWHM).



Figure 3.2 Rigaku-MiniFlex 600 X-ray diffractometer.

3.2.3 Microhardness Measurements

The microhardness of the pure Ni, Ni-B and Ni-B-Co electrodeposited films was calculated by using Vickers microhardness test device (Shimadzu-HMV-G 21S) carrying out load of 50 g for 10 seconds by diamond pyramid indenter. At least, ten measurements were applied and average values were taken as references. Figure 3.3 shows Shimadzu-HMV-G 21S Vickers microhardness tester.

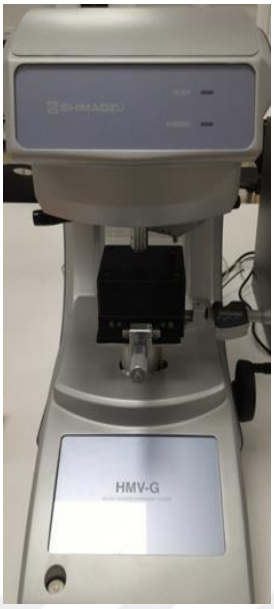


Figure 3.3 Shimadzu-HMV-G 21S Vickers microhardness test device.

3.2.4 Coating Thickness Measurements

Thicknesses of all alloy coatings are calculated by means of coating thickness gauge. The probe which is special produced for coating thickness measurement on ferrous substrate was used. Figure 3.4 shows coating thickness gauge and measurement probe.

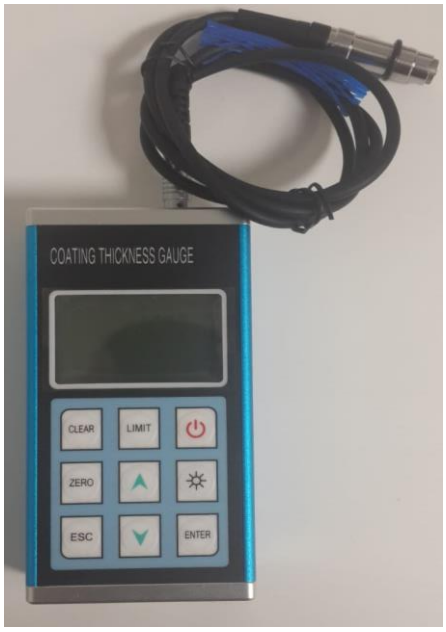


Figure 3.4 Coating thickness gauge.

3.2.5 Wear Tests

The wear resistance of pure nickel coating, Ni–B and Ni-B-Co alloy coatings was evaluated by using high-frequency reciprocating wear test machine. The reciprocating wear behaviours of the coatings sliding against an Al_2O_3 ball (Ø 10 mm) were investigated on a tribometer designed according to DIN 50324 and ASTM G 99-95a in a ball-on-disk configuration. The wear tests were operated at an ambient temperature and under non-lubricated conditions in air with relative humidity of 35±5%. The wear tests were carried out at sliding speeds of 75 mm/s with fixed applied load of 1.0 N. For each specimen, chosen total sliding distance is 250 meters, the reciprocating sliding motion was adjusted as 12 mm with a +6 mm and −6 mm. After wear tests finished, the average friction and wear results were taken from software. A complete microstructural characterization of worn surfaces was performed by scanning electron microscope (Hitachi-TM4000 Plus).

3.2.6 Corrosion Measurements

The corrosion resistance of pure nickel coating, Ni-B and Ni-B-Co alloy coatings were measured with potentiodynamic polarization test device (CH Instruments) with computer control at room temperature in 3 w.t % NaCl aqueous solution via a three-electrode cell system, in which pure nickel coating, Ni-B and Ni-B-Co alloy coatings were set as the working electrode, Ag/AgCl, graphite rod electrode were used as the reference and counter electrodes, respectively. Polarization curves of pure Ni, Ni-B and Ni-B-Co alloy coatings that attained with scan rate of 0.5 mV/s between -1.0 and 1.0 potential (V) in 3% aqueous NaCl solution. CH Instruments potentiodynamic polarization test device is shown in Figure 3.5.



Figure 3.5 CH Instruments potentiodynamic polarization test device.

CHAPTER 4

RESULTS AND DISCUSSION

4.1 Structural Analysis

4.1.1 Microstructural Analysis

By using the literature studies made on similar topics, a number of coating baths have been tried and the bath composition in which the most suitable surface properties are obtained has been used [1,16,70]. As a study of the structural, mechanical and tribological properties of Ni-B and Ni-B-Co coating layers, steel substrates were selected as cathode materials. In addition, preliminary studies and literature review showed that increasing the amount of B in the structure affects the mechanical and tribological properties well, while increasing the amount of Co affects the corrosion properties well. In accordance with the aims and information stated above, suitable parameters were selected to produce Ni-B-Co structure with maximum B and Co content. The literature and experimental results in this subject are given in detail in the following sections. Bath temperature during the coating is kept constant at about 55 ^{o}C. When the literature studies are taken into consideration, a current density of 5 A/dm^2 is generally used [69]. During the coating, high purity nickel was used as the anode material. Literature studies have shown that $NiCl_2$ compounds are added to the coating layer in some studies [46] and $NiCl_2$ compounds are not added in some studies [70]. Karslioglu [33] examined the effect of $NiCl_2.6H_2O$, which is thought to be primarily used in the coating bath during coating, for the optimization of bath parameters in addition to the added and selected coating conditions. The effect of $NiCl_2.6H_2O$ on the microstructure is given in Figure 2.13. It is understood from this Figure, under the conditions selected in the production of coatings, pores and inhomogeneities are found on the $NiCl_2.6H_2O$ coating surface. Figure 2.13 (d) shows that the structure was quite homogeneous when $NiCl_2.6H_2O$ was not added into the structure. As a result of this evaluation, it was decided that the bath composition consisted of $NiSO_4.6H_2O$, TMAB, $CoSO_4.7H_2O$, H_3BO_3 and pure water. So, it has

been decided to keep the bath parameters (pH, temperature, duration) and other additives, such as H_3BO_3, in the bath .

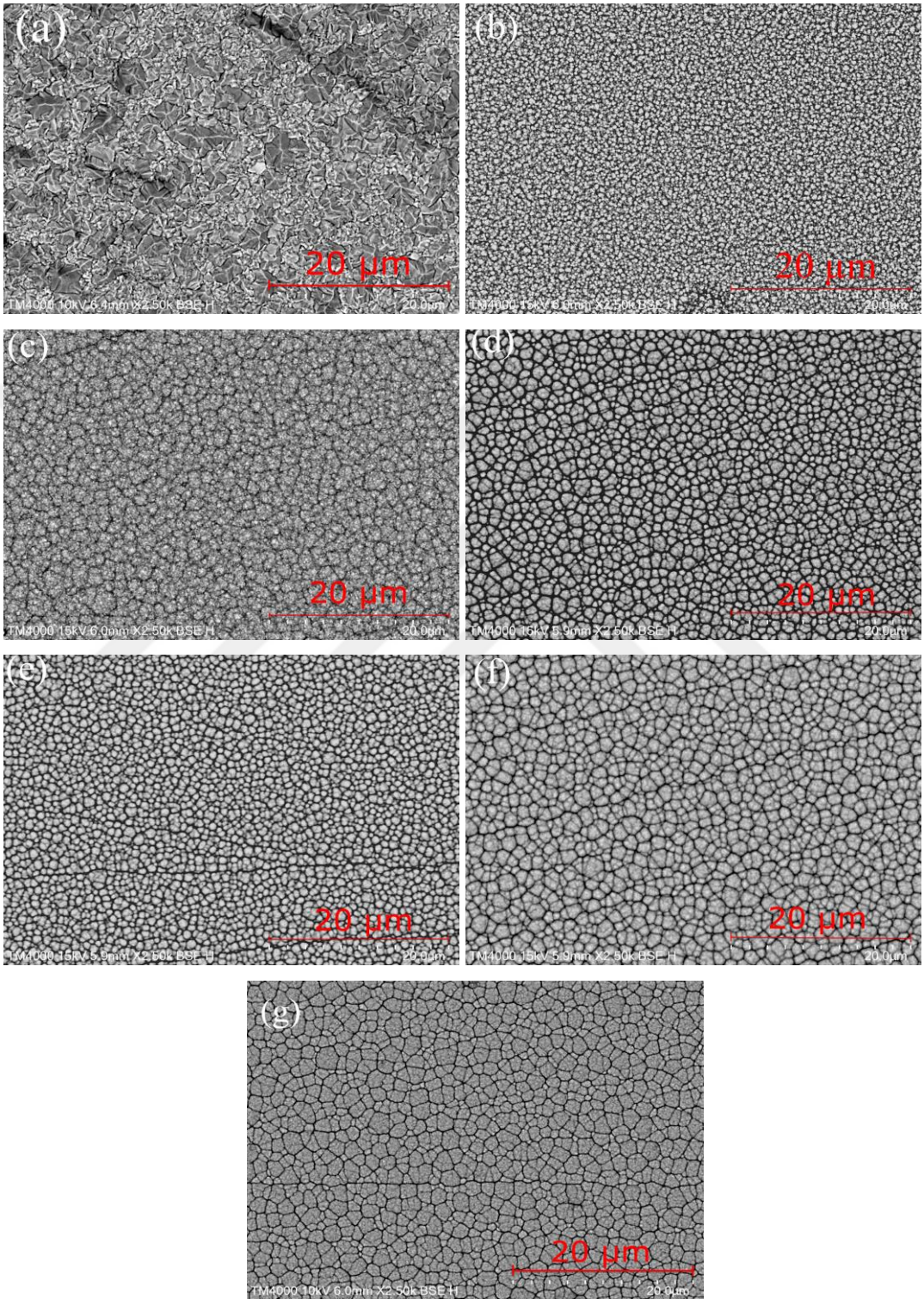


Figure 4.1 SEM surface images of pure nickel coating and Ni-B alloy coatings produced by DC according to amount of TMAB added to electrolytic bath (g/L) : a) pure nickel, b) 0.25, c) 0.5, d) 1, e) 1.5, f) 2.5, g) 5.

SEM surface images of pure nickel coating and Ni-B alloy coatings according to amount of TMAB (g/L) added to electrolytic bath are shown in Figure 4.1. It is understood that amount of TMAB is an important parameter on alloy coatings. When the microstructures of the coatings are compared according to the amount of TMAB, the coating prepared with 1.5 g/L TMAB has the lowest grain size whereas the pure nickel coating has the highest grain size. Grain size has an effect on the hardness value of specimen. Smaller grain size has higher hardness value than the bigger grain size [64]. This statement is consistent with the results we obtained. Furthermore, the microhardness and the XRD results in my thesis confirm the SEM images.

Chang et al. [1] investigate the influence of different amounts of TMAB on the Ni-B alloy coatings produced at different current densities and their results demonstrate their results showed that the best surface morphology coating was produced at 5 A/dm^2 and also, this value had the highest hardness value.

Liang et al. [53]produced Ni-B alloy coatings with different amount of boron by DC by using DMAB as boron source from a sulphamate solution including DMAB and their results proved that increased microhardness of Ni-B alloy coatings is mainly caused by a decrease in grain size rather than boron content. So, they produced Ni-B alloy coatings with high hardness with a comparatively low boron content.

Lee et al. [66] investigated that effect of the amount of boron on the different properties of nanocrystalline Ni–B alloys produced by electrodeposition method. They found that significant decrease in grain size with the increasing amount of boron.

The highest microhardness and the smallest grain size value was obtained by adding 1.5 g/L TMAB to the nickel sulphate bath and the SEM images of the coatings produced by DC by adding different amounts of $CoSO_4$ to this nickel bath which has constant 1.5 g/L TMAB are shown in Figure 4.2.

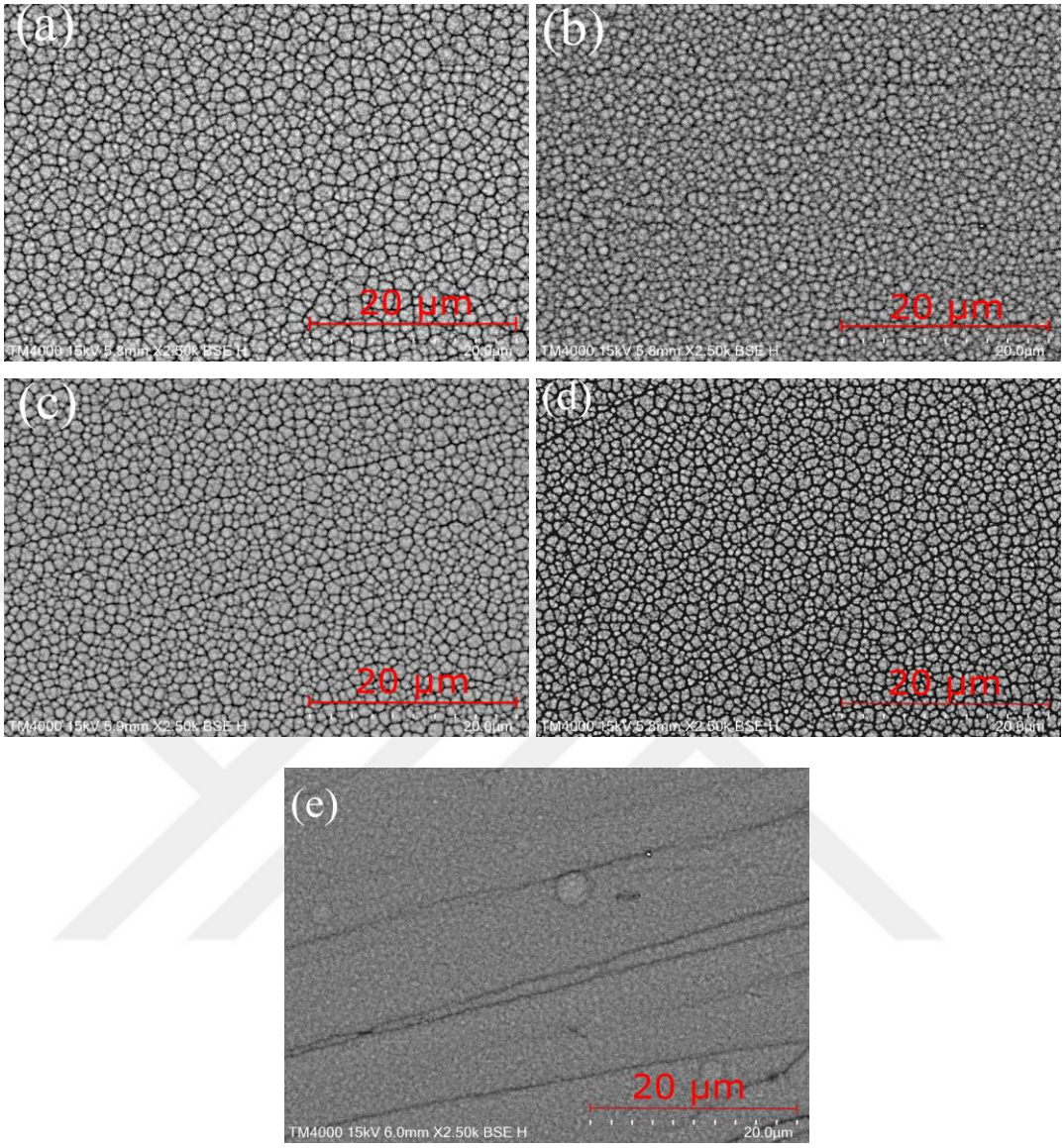


Figure 4.2 SEM surface images of Ni-B-Co alloy coatings containing fixed amount of TMAB (g/L) and different amount of $CoSO_4$ (g/L) in electrolytic bath produced by DC: a) 0.5, b) 1, c) 2.5, d) 5, e) 50.

It is understood that amount of $CoSO_4$ is an important parameter on Ni-B-Co alloy coatings. When the microstructures of the alloy coatings are compared according to the amount of $CoSO_4$, the coating prepared with 1 g/L $CoSO_4$ has the lowest grain size whereas the 50 g/L $CoSO_4$ produced with alloy coating has the highest grain size. The hardness of the Ni-B-Co alloy coatings decreases as the grain size decreases, as can be obtained from the relationship between microstructure and hardness of Ni-B alloy

coatings (Figure 4.1). In addition, the microhardness and the XRD results verify the SEM images of Ni-B-Co alloy coatings.

Srivastava et al. [63] studied microhardness and corrosion resistance of Ni-Co alloys coating. They clarified that when cobalt content increases up to 50 wt.%, hardness increases, however as the content of cobalt continues to increase, microhardness decreases since the crystallographic morphology changes from spherical crystal to polyhedral crystal. When cobalt content reaches up to 80 wt.%, crystallographic morphology changes to acicular shape. Our results are similar to the work they have done. Because the amount of $CoSO_4$ added to the coating bath was increased from 0.5 g/L to 1 g/L, the grain size decreased and the hardness value increased. When the amount of $CoSO_4$ was increased from 1 g/L to 50 g/L in the coating bath, a serious decrease in hardness occurred.

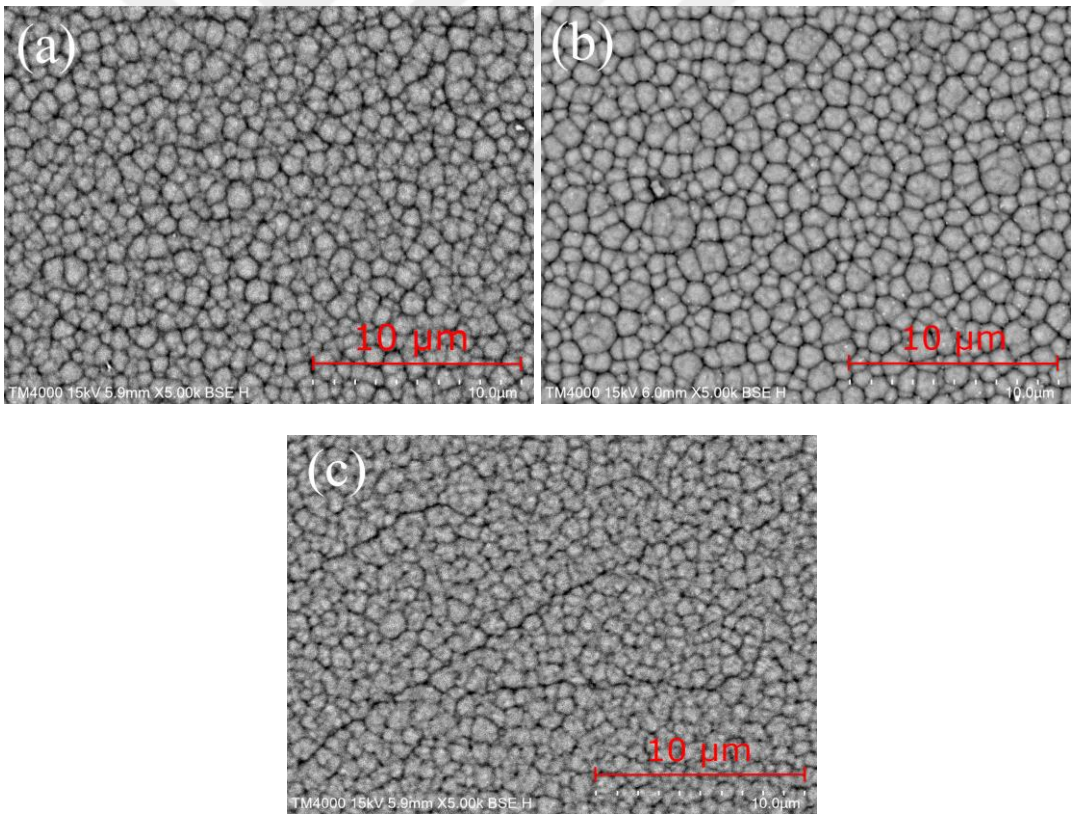


Figure 4.3 SEM surface images of Ni-B-Co alloy coatings produced by different current : a) DC, b) PC, c) PRC.

Ni-B-Co alloy coatings with the highest hardness in addition of 1.5 g/L TMAB and 1 g/L $CoSO_4$ achieved with DC were also produced with PC and PRC types to examine the relationship of the current types to coating quality. The SEM images of the alloy coatings produced by adding amounts of 1.5 g/L TMAB and 1 g/L $CoSO_4$ to nickel sulfate bath which has produced by DC, PC, PRC are shown in Figure 4.3.

It is understood that current type is an important electrodeposition parameter and it can change deposition properties as noticed in SEM images given in Figure 4.3. By comparison with the Ni-B-Co alloy coatings according to current type, DC type electrodeposition has smaller grain size than PC type and PC has smaller grain size than PRC. According to the hardness measurements, the highest hardness was measured in the DC coating and the lowest hardness was measured in the PRC coating. According to the results obtained from the EDS analysis, the amount of $CoSO_4$ entering the microstructure in the PRC coating is higher. The resulting as follows: the more cobalt sulphate has penetrated into the structure in PRC coating and the $CoSO_4$ has caused the decreasing of coating hardness.

Karslioglu et al. [64] examined the effects of current type on Ni-Co alloys. Nickel–cobalt (Ni–Co) alloys were produced via direct current (DC), pulse current (PC) and pulse reverse current (PRC) methods. When compared according to current types, the highest microhardness was obtained with PRC and the lowest was obtained with DC. Their results showed that Ni-Co alloy coatings produced by DC has relatively large grains size and exhibited irregular polyhedral crystals. There has been decrease in the grain size of Ni-Co alloy coating when applying PC. Also, by PRC method, alloy coatings have spherical cluster surface piled with a large number of equally sized grains with spherical-shape. The crystallographic grain growth orientation changed and it effected microhardness.

Landolt et al. [50] declares that pulse current type positively affects the microstructure, composition, mass transport and improves current distribution.

4.1.2 Energy Dispersive Spectrometer (EDS) analysis

The elements and their ratios in the alloys and composites were investigated by Energy Dispersive Spectrometer. Similarly, this technique is used in some studies [71]. EDS Map Sum Spectrum of pure Ni coating produced by DC is shown in fig. 4.4.

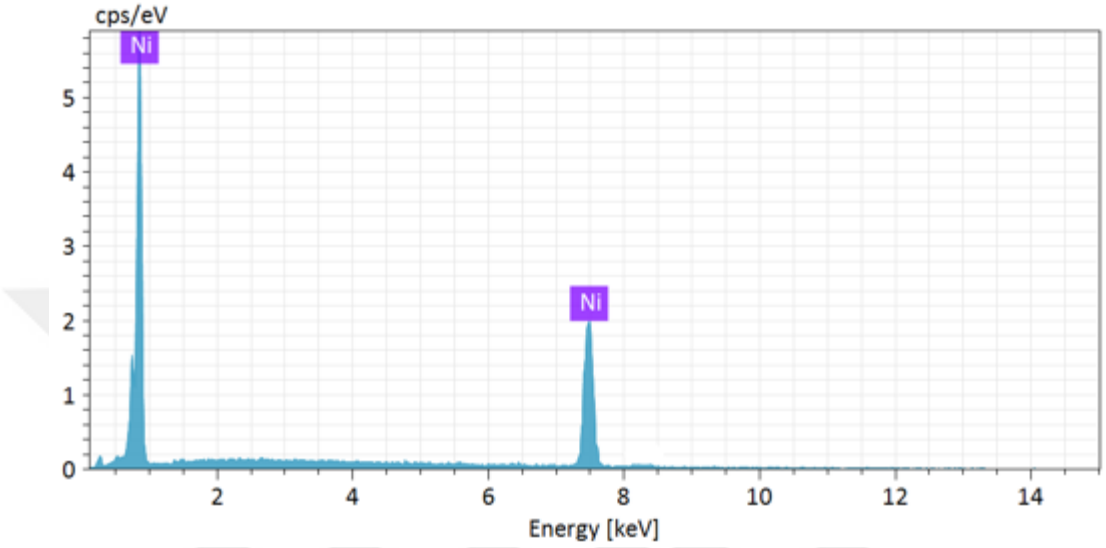


Figure 4.4 EDS Map Sum spectrum of pure nickel coating produced by DC.

The EDS results from the surface of the Ni-B coating layer containing different amounts of TMAB in electrolytic bath produced by DC type are graphically shown in Figure 4.5. It is seen that amounts of TMAB affects the elemental ratio of boron deposits. Boron ratio is the highest in the amount of 5 g/L TMAB produced by DC type electrodeposition. However, boron ratio is the smallest in the amount of 0.25 g/L TMAB produced via DC. The result is as follows: the amount of boron elemental content in the alloy coating increased as the amount of TMAB added to the coating was increased.

Also, the EDS results from the surface of Ni-B-Co coating layer containing constant amount of TMAB and different amount of $CoSO_4$ in electrolytic bath produced by DC type are graphically show in Figure 4.6. Cobalt ratio is the highest in the amount of 50 g/L $CoSO_4$ produced by DC type electrodeposition. But, boron ratio is the smallest in the amount of 50 g/L $CoSO_4$ produced via DC. Furthermore, boron ratio is the highest in the amount of 1 g/L $CoSO_4$ and cobalt ratio is the smallest in the amount of 1 g/L $CoSO_4$. The result is as follows: In the amount of 1g/L $CoSO_4$ added to the coating

bath, the lowest amount of cobalt in the coating structure and the highest amount of boron caused the highest hardness of the coating.

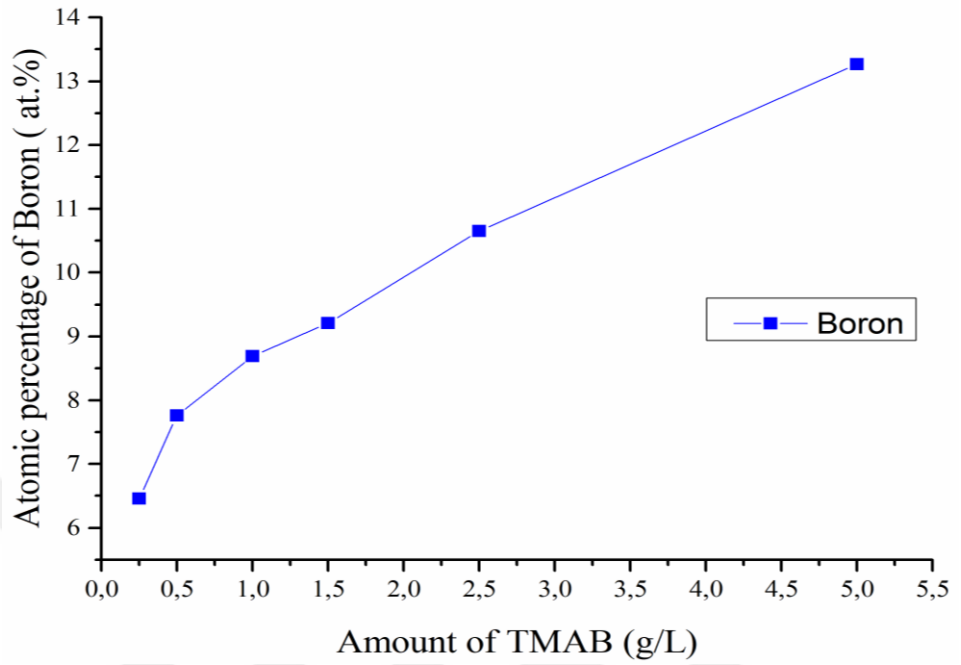


Figure 4.5 Atomic percentage of boron element in Ni-B alloy coatings containing different amount TMAB in electrolytic bath produced by DC according to result of EDS analysis.

The elements and their percentages in Ni-B-Co alloy coatings produced with different current type are given in Figure in 4.7. It is seen that current type affects the elemental ratio of deposits. Co ratio is the highest in alloy coating produced by PRC type electrodeposition. However, B ratio is the smallest in alloy coating produced via PRC. Furthermore, B ratio is highest in alloy coating produced via DC and Co ratio is the smallest in alloy coating produced DC. The result is as follows: while the DC type causes less cobalt to penetrate into the structure, the PRC type causes more cobalt to penetrate into the structure. This affected the mechanical properties of the coating and the lowest hardness was obtained in the PRC type.

Karslioglu et al. [64] examined the effects of current type on Ni-Co alloys. Nickel–cobalt (Ni–Co) alloys were produced via direct current (DC), pulse current (PC) and pulse reverse current (PRC) methods. Their results show that cobalt ratio penetrating

into the structure of coating produced by PRC type is more than that of the DC type and this result is similar to the result of my work.

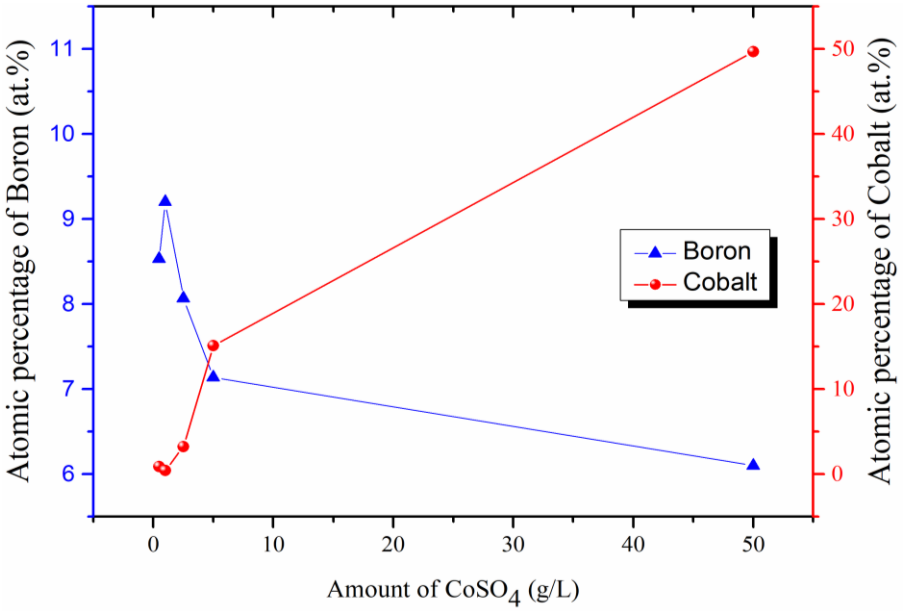


Figure 4.6 Atomic percentage of boron and cobalt element in Ni-B-Co coating layer containing constant amount of TMAB and different amount of $CoSO_4$ in electrolytic bath produced by DC according to result of EDS analysis.

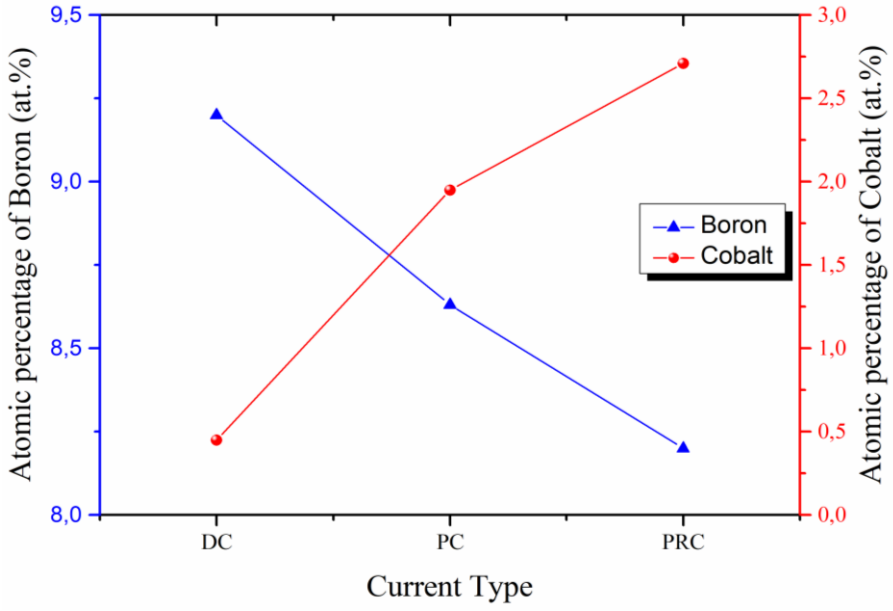


Figure 4.7 Atomic percentage of boron and cobalt element in Ni-B-Co alloy coatings produced by DC, PC and PRC type according to result of EDS analysis.

4.1.3 X-Ray Diffraction Analysis

Wavelength of X-ray beam is selected as 1.54059 Å in XRD analysis. Card number of JPDS used in the analysis is 00-004-0850 [33]. The structural analyses of pure nickel coating, Ni-B and Ni-B-Co alloy coatings were analyzed by X-ray diffraction (XRD) in this study. The patterns of XRD for electrodeposited pure nickel produced via DC method are shown in Figure 4.8. Five diffraction peaks located at 44.4597°, 51.8592°, 76.397°, 82.22°, 98.004° were determined for pure nickel coating which were detected the (1 1 1), (2 0 0), (2 2 0), (3 1 1), (2 2 2) reflection planes of nickel. For pure nickel coating, the highest intensity of peak was detected (2 0 0) plane. Also, I could detect some growing planes.

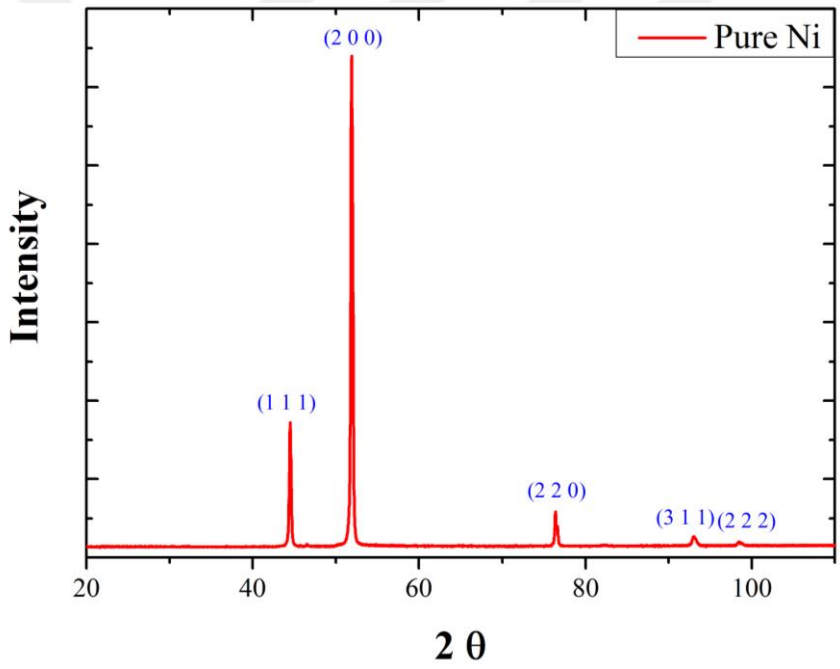


Figure 4.8 XRD patterns of pure nickel coating.

Influence of amount of TMAB added to electrolytic bath on phase structure in electrodeposited Ni-B coatings prepared by DC is shown Figure 4.9 (a). It can be clearly demonstrated that the microstructure of Ni-B alloy coatings is based on the amount of TMAB. Five diffraction peaks located at 44.589°, 52.32°, 76.981°, 82.24°, 98.95° for Ni-B alloy coating produced with addition of 0.25 g/L TMAB and five diffraction peaks located at 44.556°, 52.12°, 76.2°, 82.23°, 98.95° for Ni-B alloy coating produced with addition of 0.5 g/L TMAB and these peaks were determined for

Ni-B alloy coatings which were detected the (1 1 1), (2 0 0), (2 2 0), (3 1 1) and (2 2 2) reflection planes of nickel. For these Ni-B alloy coatings, the highest intensity of peak was detected (1 1 1) plane. When amount of TMAB was increased from 0.5 g/L to 5 g/L, the peaks in the (2 0 0), (2 2 0) and (3 1 1) planes have disappeared. Two diffraction peaks located at about 44° and 99° for Ni-B alloy coating produced with addition of 1, 1.5, 2.5, 5 g/L TMAB. Also, for these alloy coatings, the highest intensity of peak was detected (1 1 1) plane. Also, I could detect some (2 2 2) growing planes. The highest and the sharpest peak was obtained with addition of 5 g/L TMAB. When amount of TMAB was decreased from 5 g/L to 1.5 g/L, it was observed decrease in the (1 1 1) plane which is the dominant growth direction.

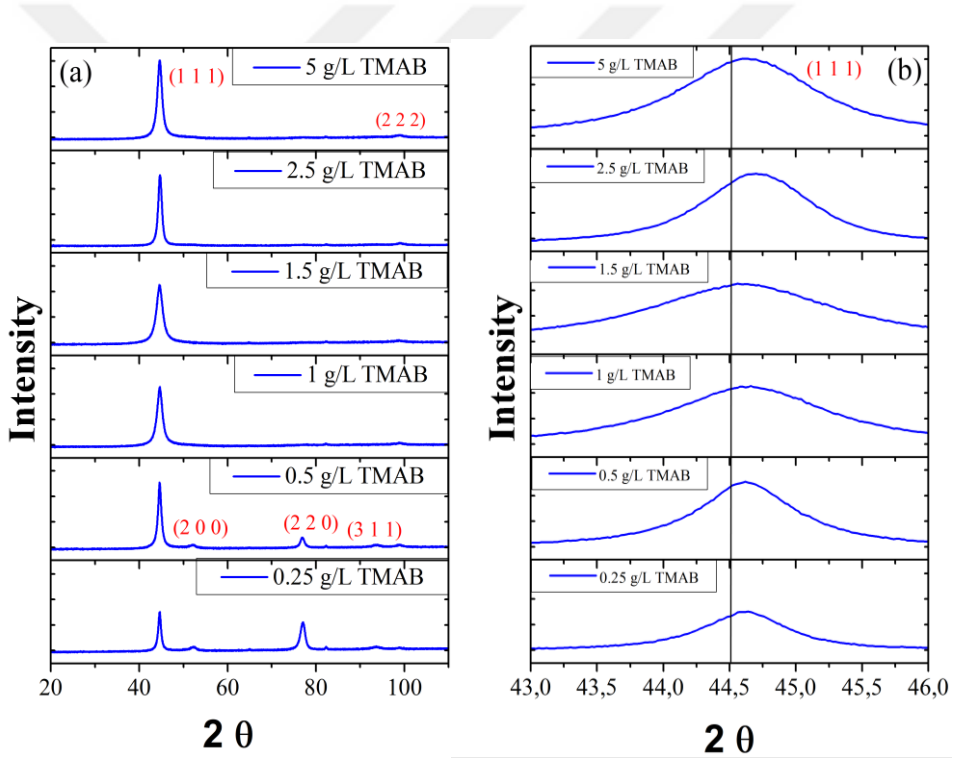


Figure 4.9 (a) Influence of amount of TMAB added to electrolytic bath on phase structure in electrodeposited Ni-B coatings prepared by DC, (b) detailed analysis of XRD patterns of the Ni-B alloy coatings deposited at different amount of TMAB added to electrolytic bath.

By addition of 1.5 g/L TMAB to electrolytic bath, the largest peak range were obtained. This is the indication to me that I have the smallest grain size in the addition of 1.5 g/L TMAB. Also, the highest grain size was obtained with addition of 5 g/L TMAB. The similar results were reported in Ni-Co alloy coatings by Karslioglu et al.

[64]. Also, there is no peak associated with B or Ni-B, it refers that boron atoms were finely deposited in crystalline lattice of Ni. The similar results were presented by Chang et al. [1] , Ogihara et al. [11] and Lopez[72] et al., respectively.

The crystallite sizes of the electrodeposited Ni-B films were measured from the width of the Ni (1 1 1) peak observed in the X-ray diffractograms using Debye-Scherrer method. According to results obtained from Debye-Scherrer method, the crystallite size of Ni decrease from 5 to 1.5 g/L in the Ni-B coatings. Grain sizes of the alloy coatings produced with addition of 5,2.5,1.5,1 g/L TMAB are 10.29, 9.36, 5.16 and 6.27 nm., respectively. The highest grain size of Ni-B alloy coatings was achieved with addition of 0.25 g/L TMAB type. The Ni-B alloy coating prepared with addition of 1.5 g/L TMAB revealed the finest grain size at almost 5,16 nm.

Detailed analysis of XRD patterns of the Ni-B alloy coatings deposited at different amount of TMAB added to electrolytic bath are shown in Figure 4.9 (b). According to JPDS card no : 00-004-0850 for pure nickel, the highest peak value is 44.51º. In the coatings prepared with addition of 5,2.5,1.5,1,0.5,0.25 g/L TMAB, the value of (2θ) angle shifted from 44.51 to 44.609, 44.674, 44.577, 44.633, 44.583, 44.589 which resulted in distortion during electroplating. With the addition of 1.5 g/L TMAB, the 2θ angle corresponding to the (1 1 1) direction is closer than the other Ni-B alloy coatings in the original JPDS card, as a result of re-decomposing the high energetic directions with the applied current. This shows that internal stresses and lattice distortion for Ni-B coating which has 1.5 g/L TMAB method are less than others.

Influence of amount of $CoSO_4$ added to electrolytic bath on phase structure in electrodeposited Ni-B-Co coatings prepared by DC are shown in Figure 4.10 (a). It can be clearly demonstrated that the microstructure of Ni-B-Co alloy coatings is based on the amount of $CoSO_4$. Two diffraction peaks were occurred at (1 1 1) and (2 2 2) planes for all Ni-B-Co coatings. As in the case of nickel-boron alloy coatings, there is no peak associated with B or Ni-B, it refers that boron atoms were finely deposited in crystalline lattice of Ni. For these Ni-B-Co alloy coatings, the highest intensity of peak was detected (1 1 1) plane. When amount of $CoSO_4$ was increased from 0.5 g/L to 50 g/L, it was observed increase in the (1 1 1) plane which is the dominant growth direction. The highest and the sharpest peak was obtained with

addition of 50 g/L $CoSO_4$. According to the EDS results given above for Ni-B-Co alloy coatings, the addition of 50 g/L of $CoSO_4$ resulted in the highest amount of cobalt and at least boron in the composition. The EDS and XRD results verify each other.

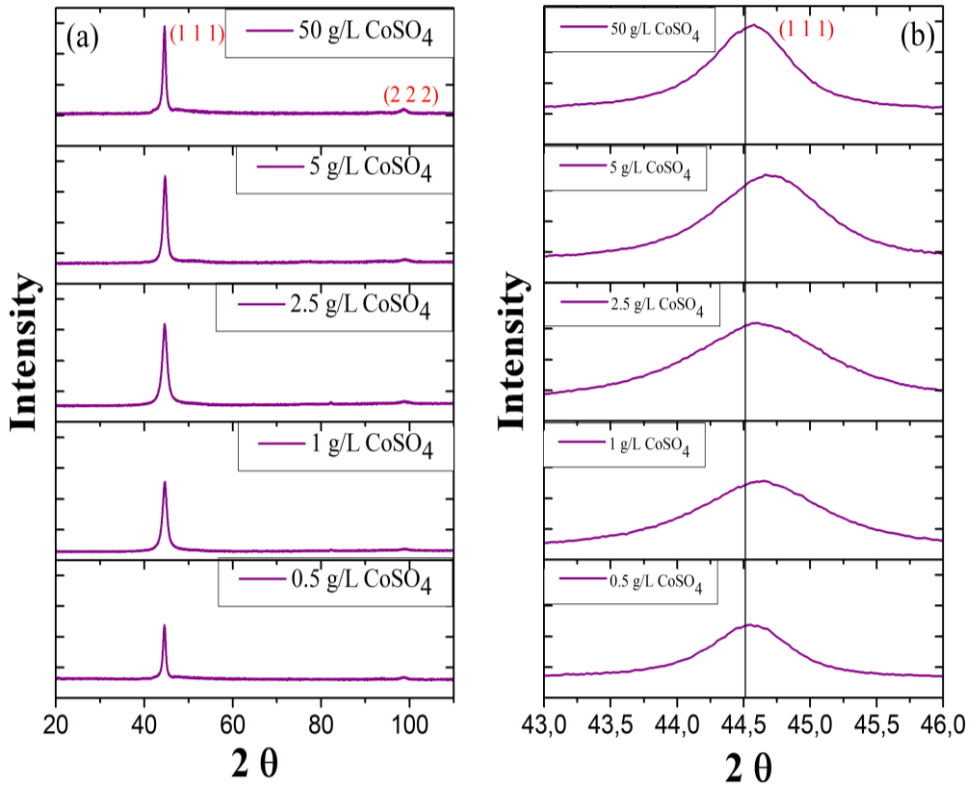


Figure 4.10 (a) Influence of amount of $CoSO_4$ added to electrolytic bath on phase structure in electrodeposited Ni-B-Co coatings prepared by DC, (b) detailed analysis of XRD patterns of the Ni-B-Co alloy coatings deposited at different amount of TMAB added to electrolytic bath.

The crystallite sizes of the electrodeposited Ni-B-Co films were measured from the width of the Ni (1 1 1) peak observed in the X-ray diffractograms using Debye-Scherrer method. According to results obtained from Debye-Scherrer method, the crystallite size of Ni decrease from 50 to 1 g/L in the Ni-B-Co coatings. Grain sizes of the alloy coatings produced with addition of 50,5,2.5,1,0.5 g/L TMAB are 12.91, 9.28, 7.33, 7.01 and 7.66 nm., respectively. The highest grain size of Ni-B-Co alloy coatings was achieved with addition of 50 g/L TMAB.

Detailed analysis of XRD patterns of the Ni-B-Co alloy coatings deposited at different amount of $CoSO_4$ are shown in Figure 4.10 (b). In the coatings prepared with addition of 0.5, 1, 2.5, 5, 50 g/L $CoSO_4$, the value of (2θ) angle shifted from 44.51 to 44.533,

44.665, 44.600, 44.606, 44.662. When the graph is examined in detail, the addition of $CoSO_4$ increases the peak intensities.

Cobalt is in hexagonal close packed structure. When the cobalt ratio in the structure exceeds a certain amount, it forms the hexagonal close packed which is own structure. At values lower than certain amount, the cobalt is placed in the nickel lattice which has face-centered cubic structure. With the addition of $CoSO_4$ to the bath composition above 5 g/L, the shift of the peak in the (1 1 1) plane is reduced. The reason for this is that high amounts of $CoSO_4$ form hexagonal structures in the coating structure. Phases below 3% can not be detected by XRD analysis. Therefore, cobalt peaks in hexagonal structure are not seen in XRD results [33].

Yang et al. [73] found two sharp peaks at 2θ 44.46 ° and 51.8 ° when they studied Ni-Co structure containing 37% and 35.6% cobalt, respectively, by XRD, in order to study Ni-Co alloys by electrodeposition method. They reported that the detected peaks show the (1 1 1) and (2 0 0) planes, respectively. In the same study, they stated that the formation of (111) direction increases with the rise of Co ratio from 35.6% to 37%, and the grain size decreases. Furthermore, it is stated that cobalt atoms are face-centered cubic because they form solid solution by entering into Nickel structure.

Wang et al. [74] studied the tribological and microstructural properties of the Ni-Co alloys produced by electrodeposition method. In the study, they added cobalt sulphate (between 0 and 80 gr) into the bath at various ratios and analyzed by using XRD. They studied XRD peaks between 35º and 75º at 2θ in their work. They indicated that the 100% Ni face-centered cubic (FCC) and (2 0 0) growth direction is dominant and the Co additions were dependent on the Co content and that the Ni-rich structures had face-centered cubic structure of the crystal system. In the same study, the peak of the Co lattice in a hexagonal close packed (HCP) structure was detected in the direction of (1 0 0), with the Co content in the structure exceeding 66% by weight. However, it has been reported that the main phase in the structure is Ni in the FCC structure, the secondary phase of the Co phase in the HCP structure.

The patterns of XRD of Ni-B-Co alloy coatings produced by different current types are shown in Figure 4.11 (a). It can be clearly demonstrated that the microstructure

of Ni-B-Co alloy coatings is based on the effect of current type. Two diffraction peaks were occurred at (1 1 1) and (2 2 2) planes for all Ni-B-Co coatings. As in the case of nickel-boron alloy coatings, there is no peak associated with B or Ni-B. For these Ni-B-Co alloy coatings, the highest intensity of peak was detected (1 1 1) plane. When the current type was changed from DC to PRC, it was observed increase in the (1 1 1) plane which is the dominant growth direction. The highest and the sharpest peak was obtained with PRC. According to the EDS results given above for Ni-B-Co alloy coatings produced via different current types, coating by DC resulted in the at least amount of cobalt and at highest amount of boron in the composition. The EDS and XRD results verify each other.

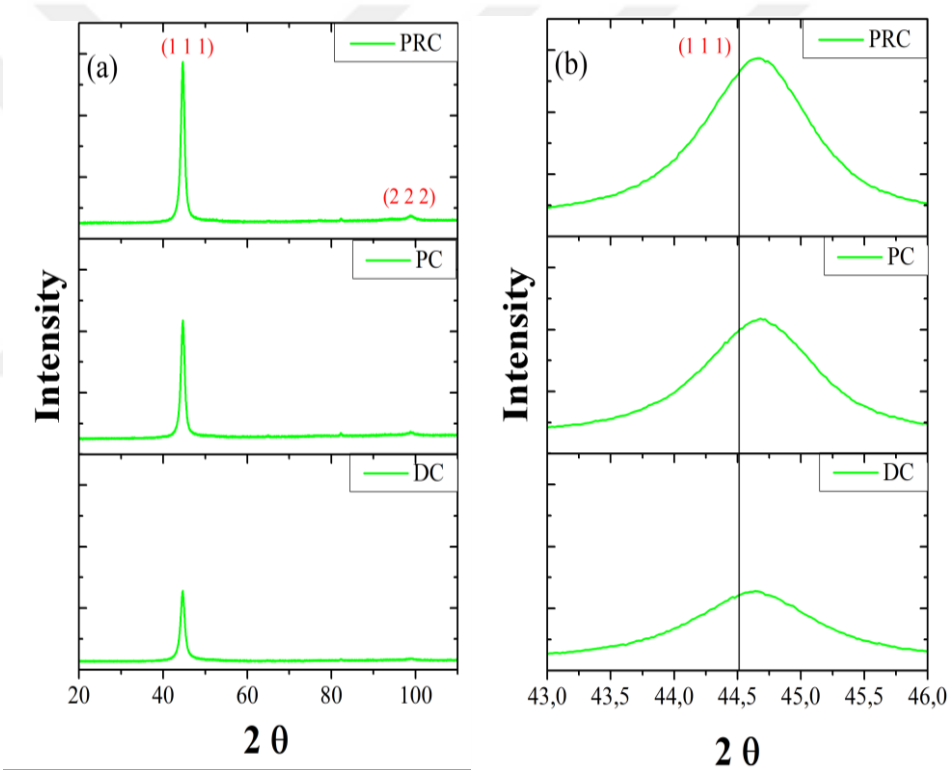


Figure 4.11 (a) Effect of current type on phase structure in Ni-B-Co alloy coatings, (b)detailed analysis of XRD patterns of the Ni-B-Co alloy coatings deposited by different current types.

The crystallite sizes of the electrodeposited Ni-B-Co films produced by different current types were measured from the width of the Ni (1 1 1) peak observed in the X-ray diffractograms using Debye-Scherrer method. According to results obtained from Debye-Scherrer method, the crystallite size of Ni decrease, when current type changes

from PRC to DC in the Ni-B-Co coatings. Grain sizes of the alloy coatings produced by DC, PC, PRC are 7.01, 8.38 and 8.89 nm., respectively. The highest grain size of Ni-B-Co alloy coatings was obtained by PRC method.

Detailed analysis of XRD patterns of the Ni-B-Co alloy coatings deposited at different current types are shown in Figure 4.11 (b). In the coatings produced by DC, PC, PRC, the value of (2θ) angle shifted from 44.51 to 44.606, 44.637 and 44.634, respectively. When current type changed from DC to PRC, the peak intensities in (1 1 1) plane increased and this results in distortion during coating to shift the peaks to the right.

4.2 Hardness of Coatings

The hardness values of the alloy coatings were measured by using the Vickers microhardness method**.** The hardness values of Ni-B and Ni-B-Co alloy coatings produced by DC and Ni-B-Co alloy coatings produced by different current types are shown in Figure 4.12,4.13 and 4.14, respectively. The hardness of the pure nickel coating is 313 HV and the addition of TMAB to the coating bath has greatly increased the hardness values. When Figure 4.12 is examined, TMAB was added in different amounts to the coatings under the same conditions and the highest hardness was obtained by the addition of 1.5 g/L TMAB. When XRD results are examined, it can be said that the reason of this situation is reached with the addition of 1.5 g/ L TMAB to the smallest grain size value. An increase in hardness was obtained until addition of 1.5 g/L TMAB to the coating bath and a TMAB amount more than 1.5 g/L resulted in a decrease in hardness.

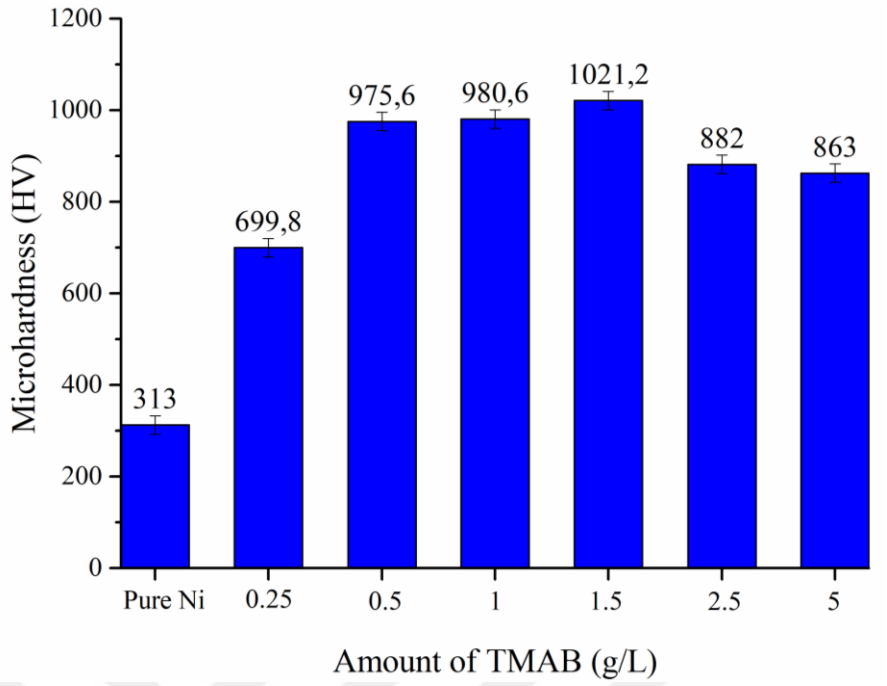


Figure 4.12 The microhardness of Ni-B alloy coatings produced by DC according to amount of TMAB added to electrolytic bath.

Chang et al. [1] also produced Ni-B alloy coatings with different amounts of TMAB addition. A significant increase in microhardness occurred when the TMAB amount increased from 1.85% to 4.38%. When the TMAB amount was increased from 4.38% to 18.63%, there was a sharp decrease in microhardness.

The highest microhardness value for Ni-B alloys was obtained with the addition of 1.5 g/L TMAB. Ni-B-Co alloy coatings were obtained by adding cobalt sulfate in different amounts to the coating bath containing 1.5 g/L TMAB. Microhardness values of Ni-B-Co alloy coatings are shown in Figure 4.13. When Figure 4.13 is examined, the highest microhardness value was achieved with the addition of 1 g/L cobalt sulphate, and when the amount of cobalt sulphate is increased from 1 g/L to 50 g/L, a significant decrease in microhardness value occurred. According to the EDS analysis results, it is understood that when the amount of cobalt sulphate is more than 1 g/L, the amount of cobalt penetrating into the structure increases. In addition, compared to Ni-B alloy coatings, less hardness values were obtained with the addition of cobalt sulphate. As a result, the penetration of cobalt into the microstructure resulted in a decrease in microhardness compared to Ni-B alloys.

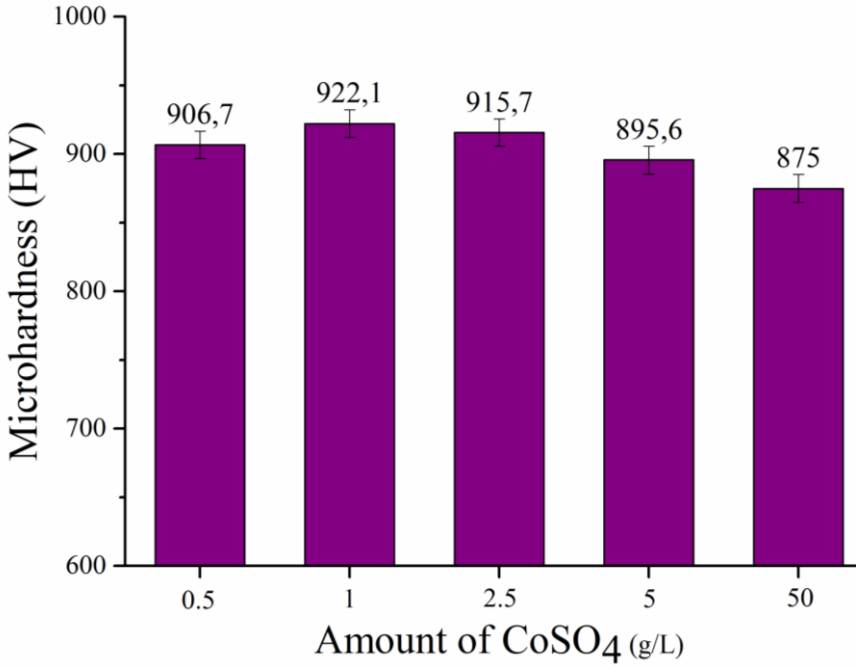


Figure 4.13 The microhardness of Ni-B-Co alloy coatings containing fixed amount of TMAB (g/L) and different amount of $CoSO_4$ (g/L) in electrolytic bath produced by DC.

The highest hardness value for Ni-B-Co alloy coatings produced by DC was obtained by the addition of 1 g/L cobalt sulphate. Furthermore, Ni-B-Co alloy coatings was produced by PC and PRC type and the microhardness values of Ni-B-Co alloys produced by DC, PC and PRC are shown in Figure 4.14. Figure 4.14 shows that the microhardness values for coatings decrease from DC to PRC. It can be seen that the cobalt penetrating into the structure is the most in the coating produced by PRC from the results of EDS analysis. The result of this is that the increase in the amount of cobalt in the structure led to a decrease in microhardness. Also, according to XRD results, the largest grain structure was obtained in PRC type. The results of XRD and EDS analysis verify each other.

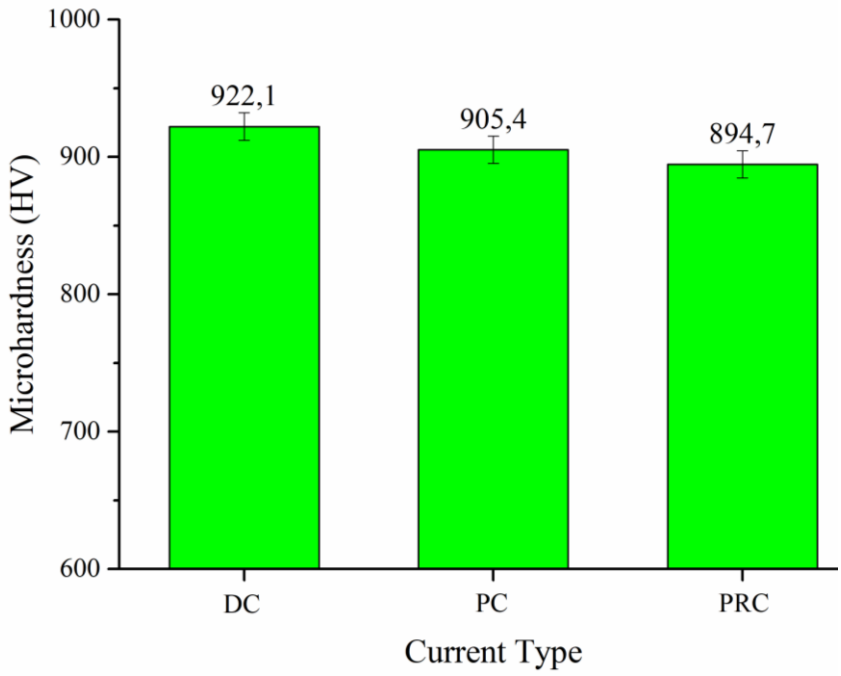


Figure 4.14 The microhardness of Ni-B-Co alloy coatings produced by DC.

4.3 Coating Thicknesses

Thicknesses of all alloy coatings are calculated by means of coating thickness gauge.

According to the measurement results, the thicknesses of all alloy coatings are similar and this value is between 6.5 and 10.2 micrometers.

4.4 Tribological Properties

4.4.1 Wear Behavior

Wear tests were conducted by handmade wear machine and the results were obtained by computer program that belongs to this machine. The wear tests were carried out at sliding speeds of 75 mm/s with fixed applied load of 1.0 N. For each specimen, chosen total sliding distance is 250 meters, the reciprocating sliding motion was adjusted as 12 mm with a +6 mm and −6 mm. As an abrasive material, an Al_2O_3 ball (Ø 10 mm) was used. As a result of abrasion, wear trace occurred on the coating surface and tribological properties were examined by using this trace. Wear trace widths were taken by NIKON Eclipse MA100 inverted optical microscope with 100X

magnification. Trace widths of pure nickel coating, some Ni-B and Ni-B-Co alloy coatings produced by DC and Ni-B-Co alloy coating produced by DC, PC and PRC types are given in Figure 4.15.

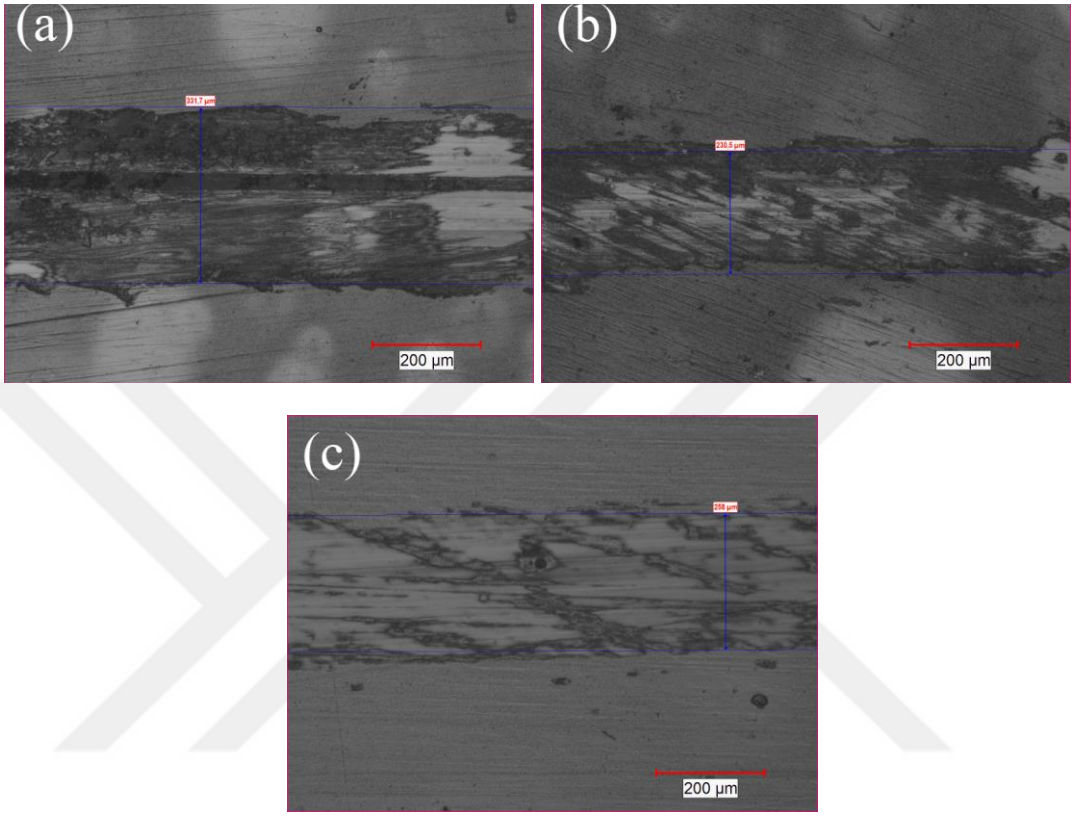


Figure 4.15 Wear trace width of pure nickel coating (a), Ni-B alloy coating which contains 1.5 g/L TMAB (b) and Ni-B-Co alloy coating which contains 1 g/L $CoSO_4$ in the electrolytic bath.

After wear tracks of all samples were measured, wear volume was calculated for all samples. Wear volume values of Ni-B and Ni-B-Co alloy coating produced by DC and Ni-B-Co alloy coating produced by different current types are shown in figure 4.16, 4.17 and 4.18, respectively.

Figure 4.15 shows that the largest trace of wear was found in pure nickel and the smallest trace of wear in Ni-B alloy containing 1.5 g/L TMAB.

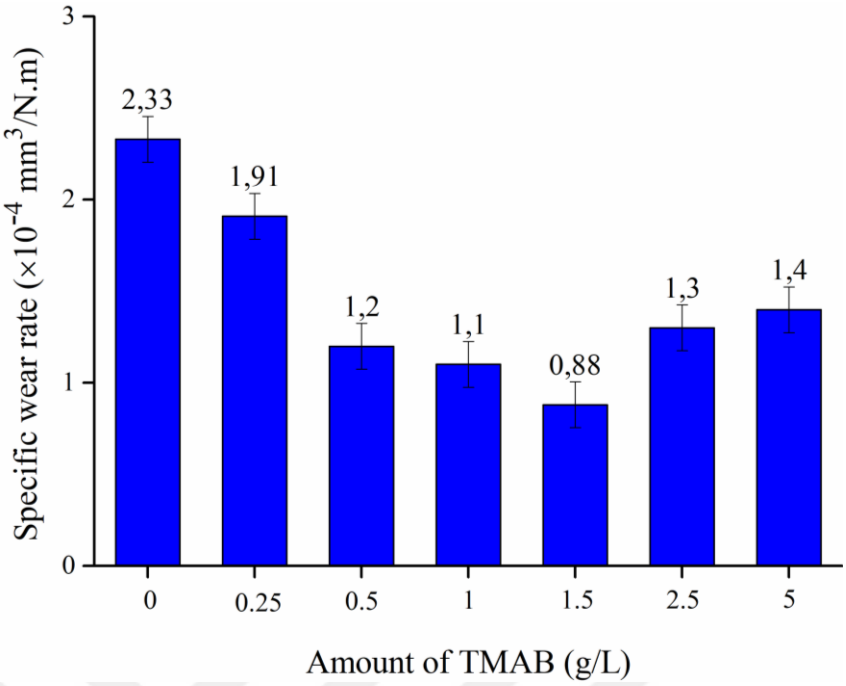


Figure 4.16 Specific wear rate of pure nickel coating and Ni-B alloy coatings coatings produced by DC according to amount of TMAB added to electrolytic bath.

It can be understood from Figure 4.16 that the increase in the width of the wear trace leads to an increase in specific wear rate. That is, the lowest specific wear rate was obtained with the addition of 1.5 g/L TMAB, which has the highest hardness. As a result, the increase in hardness reduces the wear rate and wear loss. The specific wear rate of pure nickel is about 2,6 times much than that of coating by addition of 1.5 g/L TMAB. These results are in accordance with Archard's equation that the wear of a material is inversely proportional to its hardness. Chang et al. [1] studied the influence of different density of deposition current on the different amounts of boron in Ni-B films prepared from bath including TMAB and informed that the specific wear rate was significantly decreased as microhardness of coating increased and this is compatible with my present results.

Figure 4.17 shows the specific wear rate of Ni-B-Co alloy coatings containing fixed amount of 1.5 g/L TMAB and 1 g/L $CoSO_4$ in the electrolytic bath. Figure 4.15 shows that the wear width of a Ni-B alloy containing 1.5 g/L of TMAB is narrower than that of a Ni-B-Co alloy containing 1 g/L of cobalt sulphate. So, $CoSO_4$ added to the coating bath reduces the hardness, which leads to increased specific wear rate. Since the lowest

hardness value is obtained by the addition of 50 g/L cobalt sulphate, the specific wear rate in this coating is the largest.

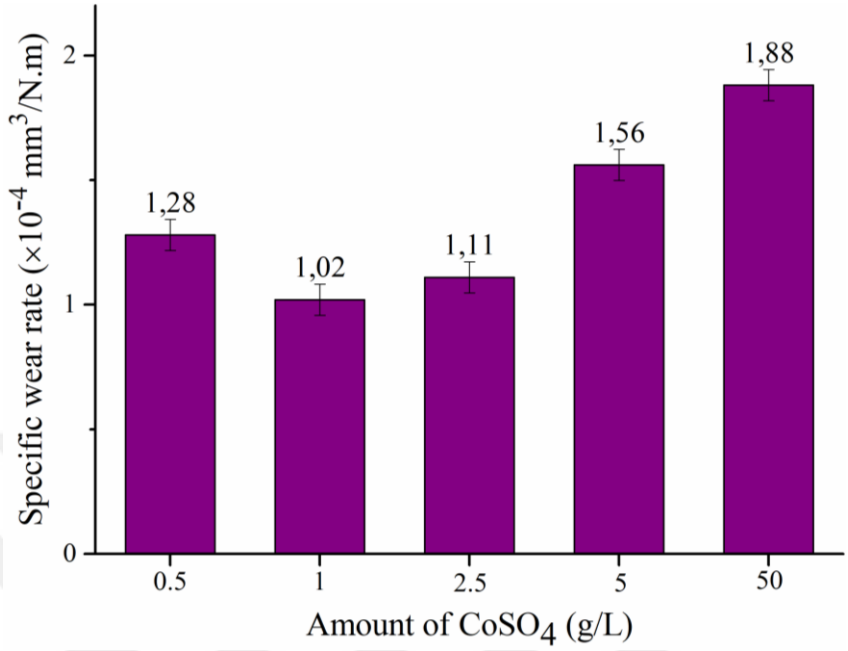


Figure 4.17 Specific wear rate of Ni-B-Co alloy coatings containing fixed amount of TMAB (g/L) and different amount of $CoSO_4$ (g/L) in electrolytic bath produced by DC.

Figure 4.18 shows specific wear rate of Ni-B-Co alloy coatings produced by different current types. Fig. 4.18 shows that the specific wear rate is the most for the coating obtained with PRC. Because the current type has affected grain growth and the lowest hardness was achieved in the coating produced by PRC. This caused the specific wear rate to be mostly in the coating produced by PRC. Therefore, it can be deduced that controlling the electroplating current type lets for accurate control of microhardness. The results obtained for all alloy coatings are consistent with the XRD results.

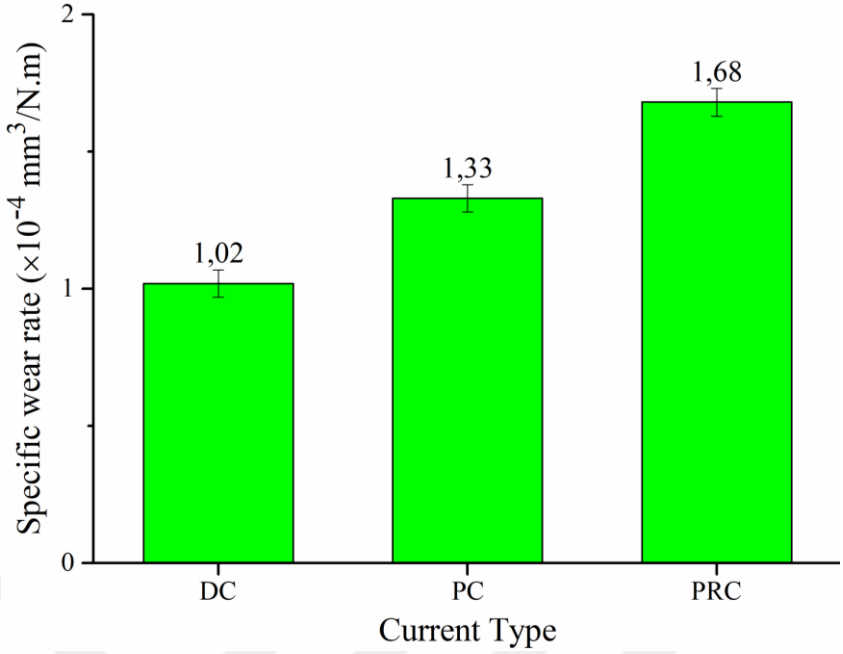


Figure 4.18 Specific wear rate of Ni-B-Co alloy coatings produced by DC,PC and PRC.

4.4.2 Wear Mechanisms

Figure 4.19 shows wear traces of pure nickel coating and Ni-B alloy coatings. When examined in detail in Figure 4.19, very severe wear deformation is observed in the pure nickel coating. But, the dominant wear mechanism is the type of adhesive wear. In some adhesive wear zones, traces of abrasive wear was observed. In addition, delamination cracks are observed between the adhesive deformation zones. With the addition of 0.25 g / L TMAB, it is seen in Figure 4.19 (b) that although partial adhesive zones are observed, the delamination cracks are quite large. It is seen that there is a very critical decrease in the deformation caused by the wear when compared with the wear trace on pure nickel. It can be seen from Figure 4.19 (c) that the size of delamination cracks became smaller than wear traces of pure nickel coating and alloy coating with addition of 0.25 g/L TMAB. It can also be seen that the traces of adhesive wear removed and partial abrasive wear traces occurred. When compared with the alloy coating produced with 0.5 g/L TMAB addition, it is seen that delamination cracks are significantly reduced in Ni-B alloy coating prepared with 1 g/L TMAB (Fig. 4.19 (d)). When 1.5 g/L TMAB is added, it is seen that the cracks of the delamination occur only in certain places. In addition, better wear trace is obtained than the others and the

wear deformation is less than that of other alloy coatings (Fig. 4.19 (e)). Figure 4.19f shows that delamination cracks begun to grow again with the addition of 2.5 g/L TMAB and traces of adhesive wear began to appear. The addition of 5 g/L TMAB has resulted in a mixed type of wear, which involves very intensive adhesive wear and delamination. The distance between the delamination cracks is considerably higher than in other alloy coatings.

Figure 4.20 shows SEM images of wear traces of Ni-B-Co alloy coatings produced with $CoSO_4$ added in different amounts to Ni-B alloys containing 0.15 g/L TMAB. Delamination wear in the structure is clearly visible with the addition of 0.5 g/L cobalt sulphate. Some of torn patches as a result of the delamination penetrated into the interface and it was understood that these patches transformed the wear trace from two-body to three-body. It was determined that this wear trace causes excessive damage on the surface. With the addition of 1 g/L $CoSO_4$, it is observed from Figure 4.20 (b) that there is a significant reduction in deformation and the size of wear cracks are slightly lower than the 0.5 g/L $CoSO_4$ additive. The areas that are peeled from the surface due to delamination as well as delamination cracks are clearly visible with the addition of 2.5 g/L $CoSO_4$ in Fig. 4.20 (c). When the amount of cobalt sulphate is greater than 2.5 g/L, the wear type changed completely and the wear mechanism turned into a form that abrasive and adhesive wear is together (see Fig. 4.20 (d)). It is clear that there is more wear compared to those containing less than 5 g/L of $CoSO_4$. When 50 g/L $CoSO_4$ is added, very severe deformation is observed (see Fig.4.20 (e)). Adhesive damage as well as abrasive traces occurred with the addition of 50 g/L $CoSO_4$.

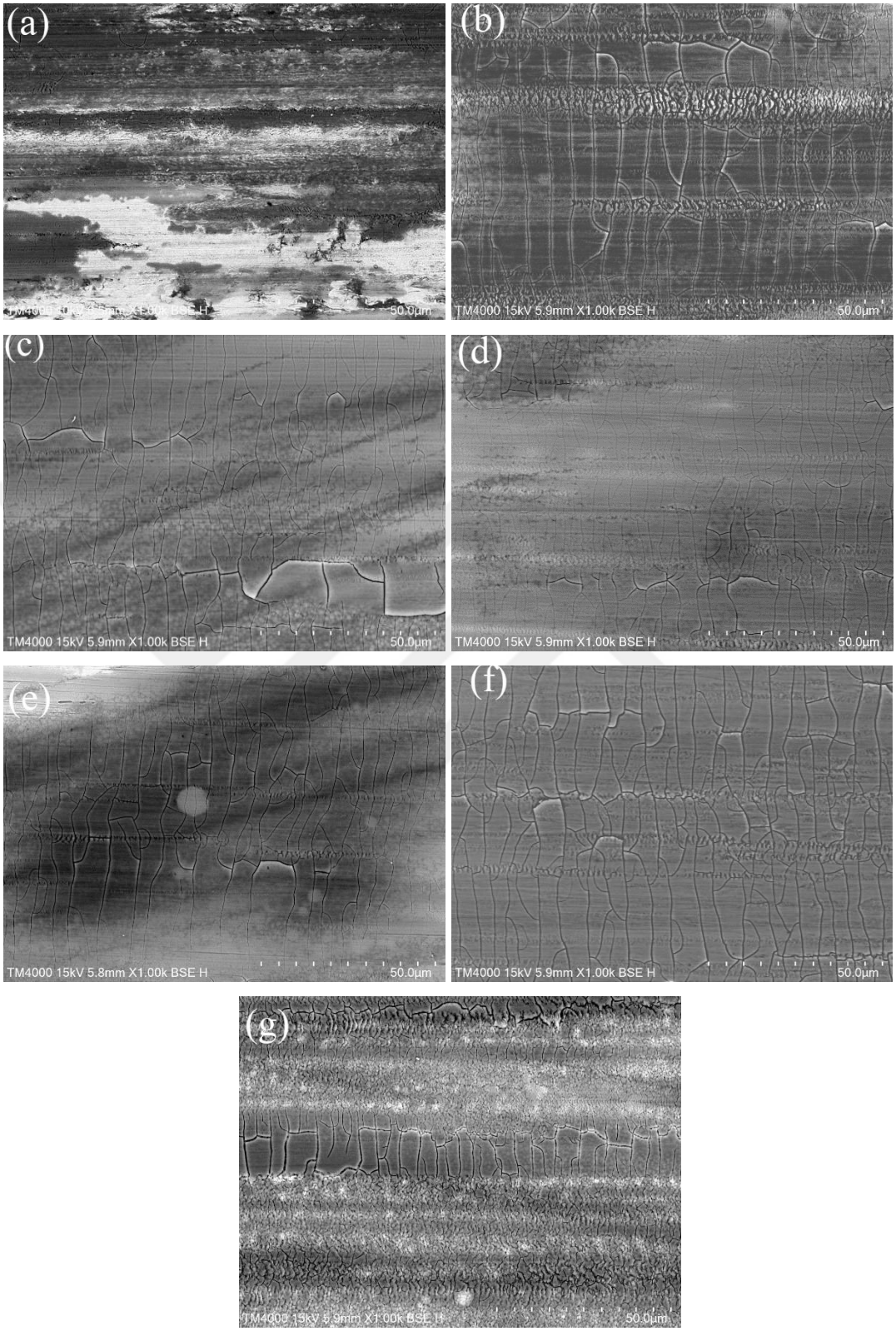


Figure 4.19 SEM images of wear traces of Ni-B alloy coatings produced by DC ; (a) pure Ni coating, addition of (b) 0.25, (c) 0.5, (d) 1, (e) 1.5, (f) 2.5, (g) 5 g/L TMAB to electrolytic bath.

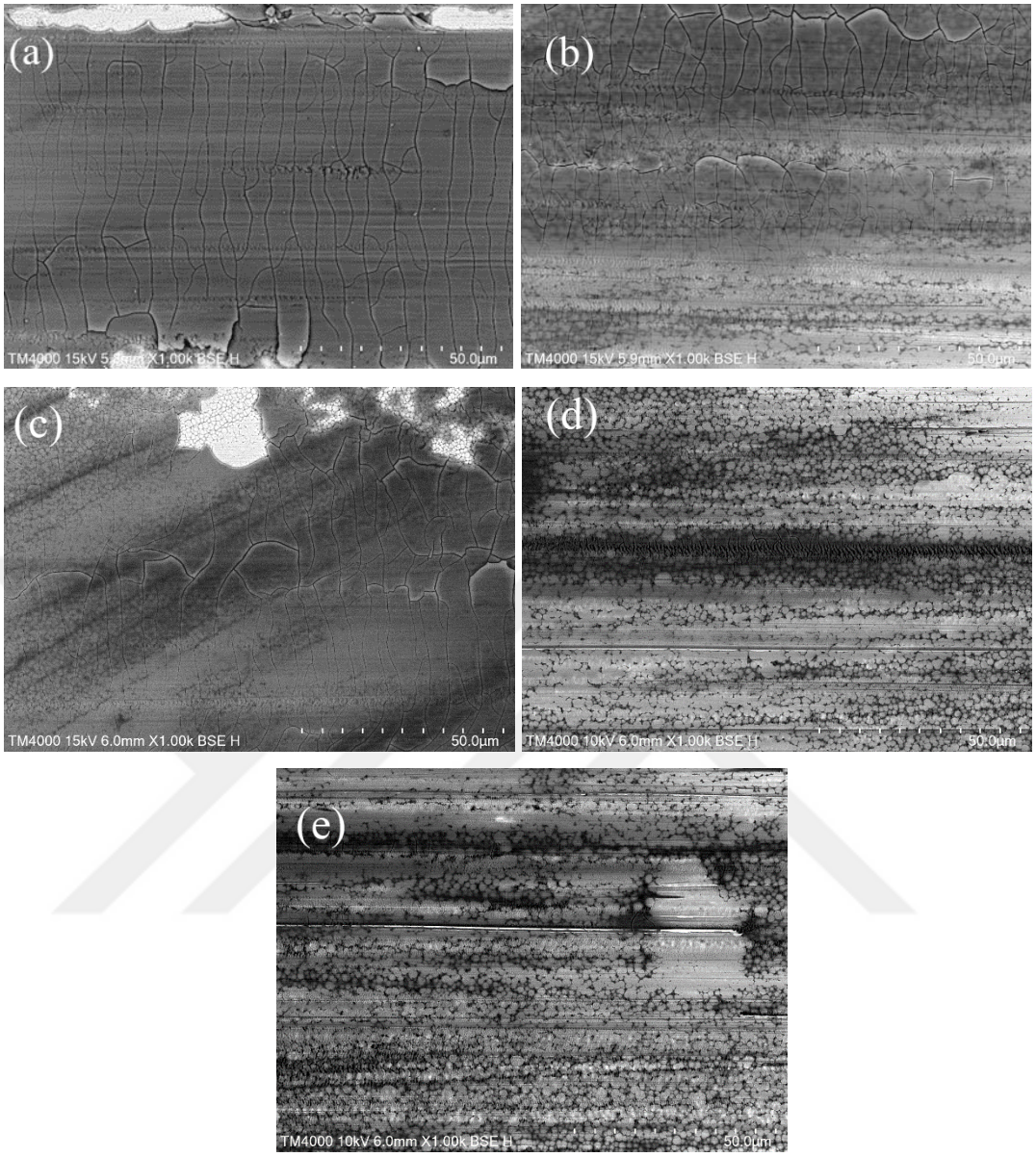


Figure 4.20 SEM images of wear traces of Ni-B-Co alloy coatings produced by DC; addition of (a) 0.5 (b) 1, (c) 2.5, (d) 5, (e) 50 g/L $CoSO_4$ to electrolytic bath.

Figure 4.21 shows SEM images of wear traces of Ni-B-Co alloy coatings produced by DC, PC and PRC. The mechanism of the wear trace of the coating produced by DC has been mentioned above. A very significant increase in abrasive traces was observed in the coatings produced by PC. As a result of the delamination, a large amount of detachment of coating occurred on the surface coating and this caused torn patches. In the PRC type, it was seen that the detachment of coating and deformation increased. The type of wear of the torn patches, has been turned into from two bodies to three

bodies. It is also seen that there is a serious increase in wear deformation. Torn patches at different locations as a result of wear are clearly visible in wear images.

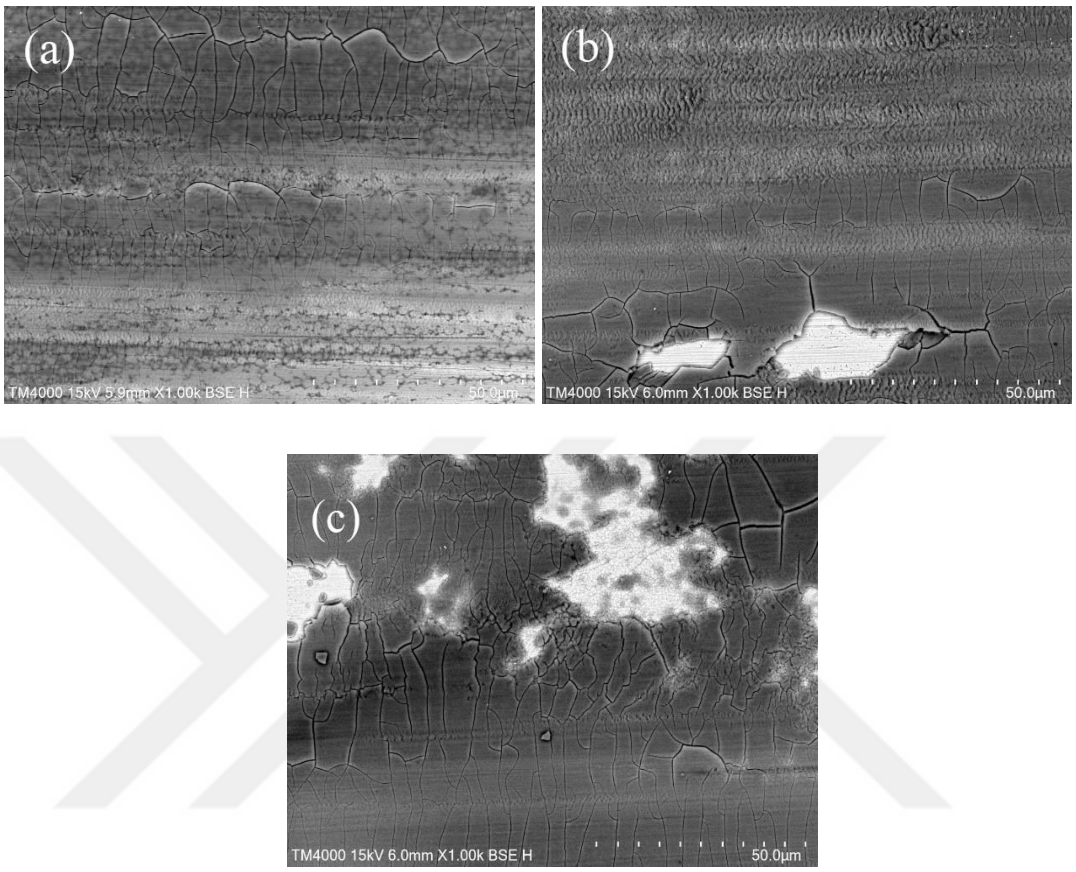


Figure 4.21 SEM images of wear traces of Ni-B-Co alloy coatings produced by (a) DC, (b) PC, (c) PRC.

4.5 Evaluation of Corrosion Resistance

The polarization curves of attained for Ni-B alloy coatings produced with different amount of TMAB, Ni-B-Co alloy coatings produced with different amount of $CoSO_4$ and Ni-B-Co alloy coatings produced with different current types are shown in Fig. 4.22,Fig. 4.23 and Fig. 4.24, respectively. At the beginning of corrosion test, in the polarization curves of all alloy coatings, passive film formation was observed on the surface of samples.

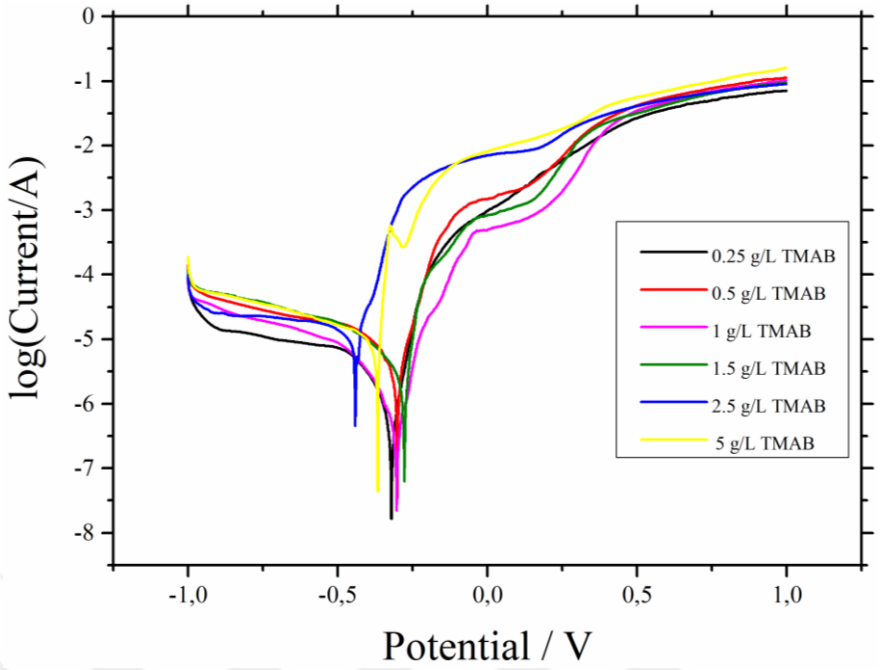


Figure 4.22 Polarization curves of Ni-B alloy coatings produced by different amount of TMAB that obtained with scan rate of 0.5 mV/s in 3% aqueous solution.

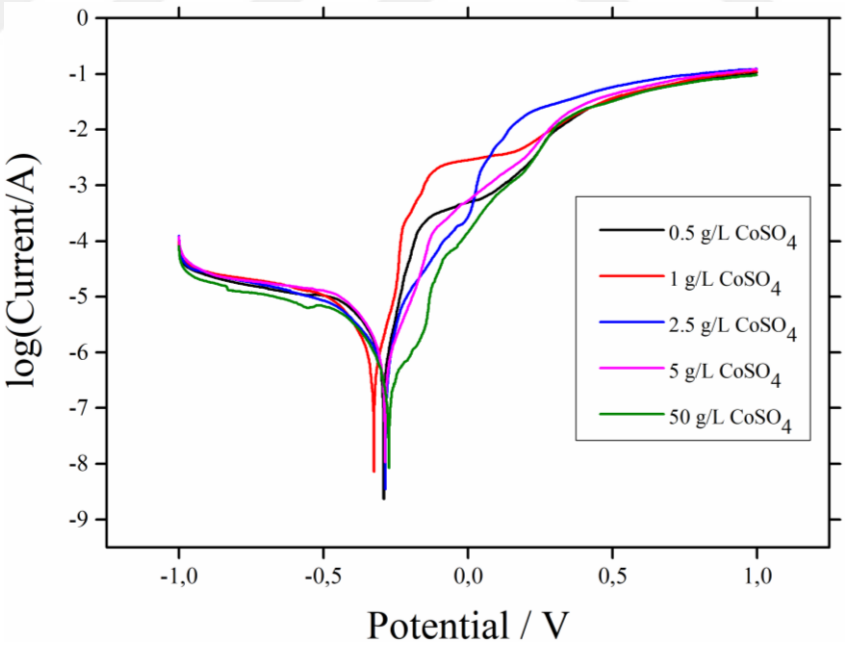


Figure 4.23 Polarization curves of Ni-B-Co alloy coatings produced by different amount of $CoSO_4$ that obtained with scan rate of 0.5 mV/s in 3% aqueous solution.

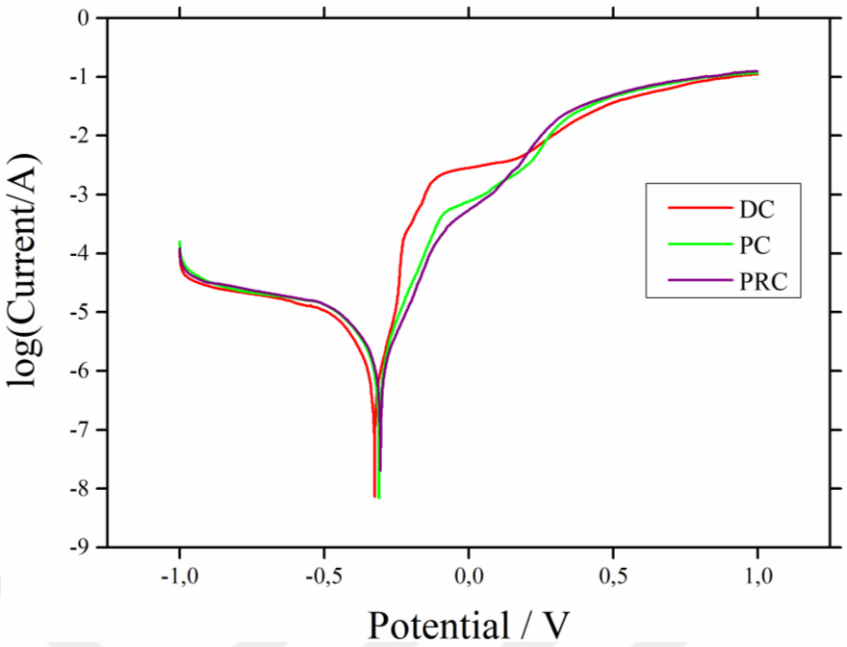


Figure 4.24 Polarization curves of Ni-B-Co alloy coatings produced by different current types that obtained with scan rate of 0.5 mV/s in 3% aqueous solution.

The corrosion rate formula is shown in Eq. 4.1 [75].

$$CR = I_{corr}\, K\, EW / d\, A \qquad (4.1)$$

In this equation, CR is the corrosion rate; I_{corr} is the corrosion current in amperes; K is a constant that defines the units for the corrosion rate; EW is the equivalent weight in grams/equivalent; d is the density in grams/cm^3 and A is area of the sample in cm^2.

As can be understood from Eq. 4.1, as the corrosion current (I_{corr}) increases, the corrosion rate increases. The increase in the corrosion rate also means the decrease in the corrosion resistance. Because, the average of anodic reaction increases.

Figure 4.25 shows corrosion current and grain size of Ni-B alloy coatings prepared with different amount of TMAB added to electrolytic bath. Figure 4.26 Corrosion current and grain size of Ni-B-Co alloy coatings prepared with different amount of $CoSO_4$ added to electrolytic bath. Figure 4.27 Corrosion current and grain size of Ni-B-Co alloy coatings prepared with different current type.

It was clearly shown from Fig. 4.25, Fig. 4.26 and Fig. 4.27 that the corrosion current (I_{corr}) of all alloy coatings decreased with increasing in grain size. The rise of the corrosion resistance with rising grain size can be clarified by the fact that there are more grain boundaries in small grains when compared to large grains. The grain boundaries are more easily affected by corrosion because of their low stability and high energies. Also, the corrosion solution can penetrate into all alloy coatings through grain boundaries and reach substrate, ending up with diminishing resistance of corrosion. Therefore, the decrease of grain size reduces the corrosion resistance. According to the results obtained from XRD, the highest grain size was obtained in amount of 0.25 g/L TMAB for Ni-B alloy coatings and obtained in the amount of 50 g/L $CoSO_4$ for Ni-B-Co coatings produced by different amount of $CoSO_4$ and obtained in PRC type for Ni-B-Co coatings produced by different current type method and the lowest grain size was obtained in amount of 1.5 g/L TMAB, 1 g/L $CoSO_4$ and DC type, respectively. According to these data, the XRD and the corrosion test results are consistent.

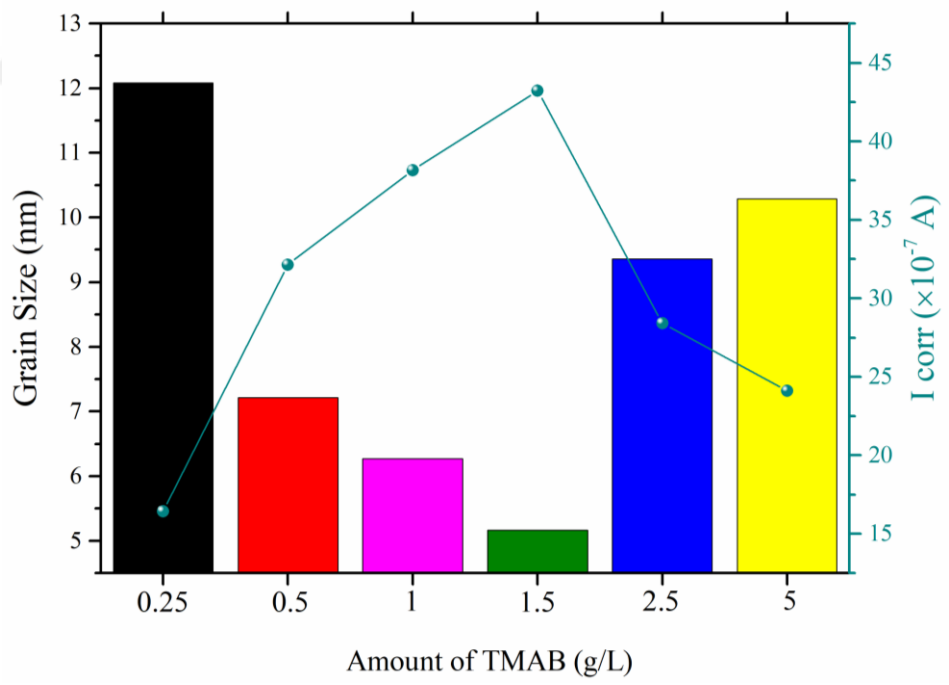


Figure 4.25 Corrosion current and grain size of Ni-B alloy coatings prepared with different amount of TMAB added to electrolytic bath.

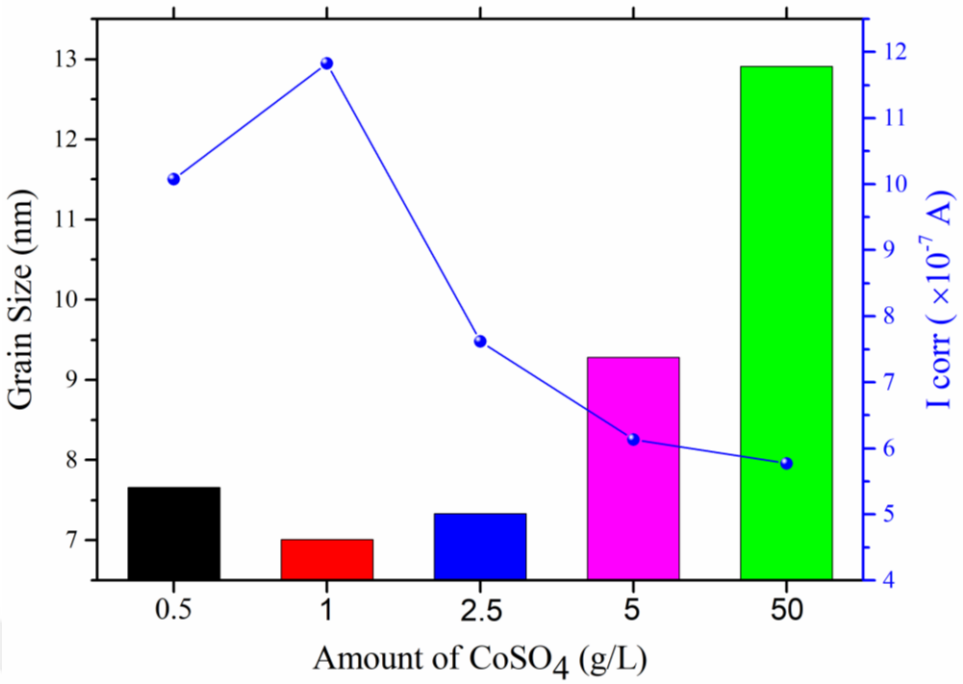


Figure 4.26 Corrosion current and grain size of Ni-B-Co alloy coatings prepared with different amount of $CoSO_4$ added to electrolytic bath.

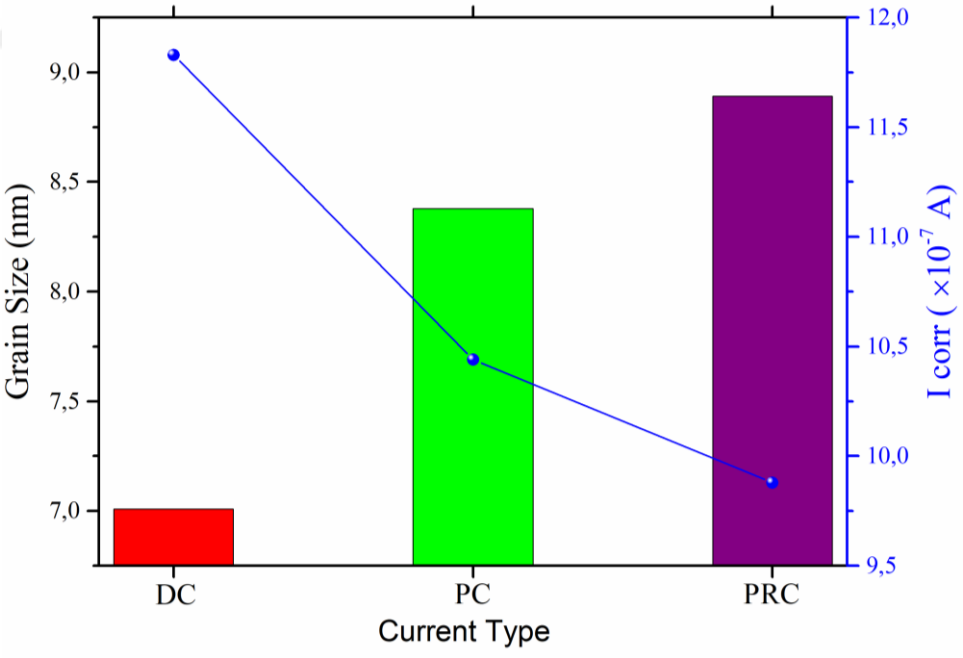


Figure 4.27 Corrosion current and grain size of Ni-B-Co alloy coatings prepared with different current type.

The results found by Chang et al. [1] are similar. They study electrodeposited Ni-B alloy coatings with different amounts of the boron prepared via direct current in a bath including trimethylamine borane at 0.06 M. They found that as the grain size increases, resistance of corrosion rises.

CHAPTER 5

CONCLUSIONS AND FUTURE WORK

5.1 Conclusions

In this work, the influence of mechanical properties, wear and corrosion resistance on electrodeposited Ni-B alloy coatings produced by different amount of TMAB, Ni-B-Co alloy coatings produced by different amount of $CoSO_4$ and Ni-B-Co alloy coatings produced by different current types were investigated. The our results we obtained are as follows:

1. Hardness and microstructure of the Ni-B, Ni-B-Co alloy coatings were considerably influenced by addition of TMAB and $CoSO_4$, respectively. The hardness of pure nickel produced with DC, which is 313 HV, reached up to 1021.2 HV with the addition of 1.5 g/L and also, the lowest grain size was obtained with the addition of 1.5 g/L TMAB.

While the hardness of Ni-B-Co alloy coating produced with addition of 50 g/L $CoSO_4$ is 875 HV, the hardness of Ni-B-Co alloy coating produced with addition of 1 g/L $CoSO_4$ is 922.1 and also the lowest grain size was obtained with addition of 1 g/L $CoSO_4$.

Furthermore, hardness and microstructure of Ni-B-Co alloy coatings produced with different current types were considerably influenced by current type. The hardness of Ni-B-Co coating produced with DC is 922.1 while the hardness of Ni-B-Co coating produced with PRC is 894.7 and the highest grain size produced with PRC type.

2. EDS analysis gives the values of elemental ratio. According to EDS analysis results for Ni-B coatings, it is understood that amounts of TMAB affects the elemental ratio of boron deposits. Boron ratio is the highest in the amount of 5 g/L TMAB produced by DC type electrodeposition. However, boron ratio is the smallest in the amount of 0.25 g/L TMAB produced via DC. The result is as follows: the amount of boron

elemental content in the alloy coating increased as the amount of TMAB added to the coating was increased.

According to EDS analysis results for Ni-B-Co alloy coating produced with DC, Cobalt ratio is the highest in the amount of 50 g/L $CoSO_4$ produced by DC type electrodeposition. But, boron ratio is the smallest in the amount of 50 g/L $CoSO_4$ produced via DC. Furthermore, boron ratio is the highest in the amount of 1 g/L $CoSO_4$ and cobalt ratio is the smallest in the amount of 1 g/L $CoSO_4$. The result is as follows: In the amount of 1g/L $CoSO_4$ added to the coating bath , the lowest amount of cobalt in the coating structure and the highest amount of boron caused the highest hardness of the coating.

According to EDS analysis results for Ni-B-Co alloy coating produced by different current types, Co ratio is the highest in alloy coating produced by PRC type electrodeposition. However, B ratio is the smallest in alloy coating produced via PRC. Furthermore, B ratio is highest in alloy coating produced via DC and Co ratio is the smallest in alloy coating produced DC. The result is as follows: while the DC type causes less cobalt to penetrate into the structure, the PRC type causes more cobalt to penetrate into the structure. This affected the mechanical properties of the coating and the lowest hardness was obtained in the PRC type.

3. All the Ni-B alloy coatings prepared with different amount of TMAB exhibited predominant growth in the (1 1 1) planes. The grain sizes were attained between 5.16 and 9.39 nm. With the addition of 1.5 g/L TMAB, the 2θ angle corresponding to the (1 1 1) direction is closer than the other Ni-B alloy coatings in the original JPDS card, as a result of re-decomposing the high energetic directions with the applied current. This shows that internal stresses and lattice distortion for Ni-B coating which has 1.5 g/L TMAB method are less than others.

All the Ni-B-Co alloy coatings prepared with different amount of $CoSO_4$ exhibited predominant growth in the (1 1 1) planes. The grain sizes were attained between 7.01 and 12.91 nm. The highest and the sharpest peak was obtained with addition of 50 g/L $CoSO_4$. The increase of addition of $CoSO_4$ increases the peak intensities and results in distortion during coating to shift the peaks to the right.

All the Ni-B-Co alloy coatings prepared with different current types exhibited predominant growth in the (1 1 1) planes. The grain sizes were obtained between 7.01 and 8.89 nm. When the current type was changed from DC to PRC, it was observed increase in the (1 1 1) plane which is the dominant growth direction and this results in distortion during coating to shift the peaks to the right.

4. Ni-B alloy coatings produced with different amount of TMAB demonstrated better wear resistance as compared to pure Ni coating. The highest wear resistance was achieved with 1.5 g/L TMAB addition. When 1.5 g/L TMAB was added, it was seen that the cracks of the delamination occur only in certain places. In addition, better wear trace is obtained than the others and the wear deformation is less than that of other alloy coatings.

With the addition of 1 g/L $CoSO_4$ for Ni-B-Co alloy coatings, there is a significant reduction in deformation and the size of wear cracks are slightly lower than that of other alloy coatings. When 50 g/L $CoSO_4$ was added, very severe deformation was observed. Adhesive damage as well as abrasive traces occurred with the addition of 50 g/L $CoSO_4$.

For Ni-B-Co alloy coatings produced by different current types, alloy coating produced by DC exhibited better resistance as compared to PC and PRC. A very significant increase in abrasive marks was observed in the coatings produced by PC when compared to DC. As a result of the delamination, a large amount of detachment of coating occurred on the surface coating and this caused torn patches. In the PRC type, it was seen that the detachment of coating and deformation increased. The wear type of the torn patches has been turned into from two bodies to three bodies. It was also seen that there is a serious increase in wear deformation. Torn patches at different locations as a result of wear are clearly visible in wear images.

5. According to the corrosion test results obtained from 3 w.t % NaCl solution for Ni-B alloy coatings produced by different amount of TMAB, the highest corrosion resistance was achieved with the addition of 0.25 g/L TMAB, the lowest corrosion resistance was achieved with the addition of 1.5 g/L TMAB.

According to the corrosion test results obtained from 3 w.t % NaCl solution for Ni-B-Co alloy coatings produced by different amount of $CoSO_4$, the highest corrosion resistance was obtained with addition of 50 g/L $CoSO_4$ and the lowest corrosion resistance was obtained with 1 g/L $CoSO_4$.

According to the corrosion test results obtained from 3 w.t % NaCl solution for Ni-B-Co alloy coatings produced by different current type, the highest corrosion resistance was obtained by PRC and the lowest corrosion resistance was obtained by DC. The following conclusion can be drawn for all alloy coatings:

Grain size is the main factor in the resistance of corrosion of alloy coatings. The resistance of corrosion increased with increasing in grain size of all alloy coatings.

Hard chrome platings have a hardness value of 850-1050 vickers [76]. In this study, 1021.2 vickers hardness values were obtained with addition of 1.5 g/L TMAB to the nickel watt bath. Addition of 1 g/L CoSO4 to nickel watt bath containing 1.5 g/L TMAB resulted in a hardness value of 922.1 vickers hardness. Addition of 1 g/L $CoSO_4$ to the nickel watt bath containing 1.5 g/L TMAB also increased the corrosion resistance of the coating.

As compared with the hardness of hard chrome plating, the desired hardness values were obtained with the produced Ni-B and Ni-B-Co coatings.

The cracked microstructures forming during the hard chrome plating were removed with Ni-B and Ni-B-Co alloy coatings. Thus, it is aimed to avoid the decrease of the fatigue resistance which is seen in hard chrome plating over time.

Nickel-based coatings also poses no threat to human health and the environment, as it avoids the formation of hexavalent chromium, which is very harmful to human health and the environment, which occurs during hard chromium plating production.

5.2 Future Work

- For all coatings, wear resistance can be examined at different sliding speeds.
- The magnetic properties of the produced alloy coatings can be examined.

- The electrical properties of the produced coatings can be examined and their electrical properties can be optimized.
- The strength of the coating structure should be measured by the scratch test.
- The surface roughness of the coatings should be measured.
- To analyze the growth morphology of the alloy coatings, TEM analysis should be applied from the cross sections of the alloy coatings.

REFERENCES

[1] Chang, C.-R., Hou, K.-H., Ger, M.-D., Wang, J.-R. "Characteristics of Nickel Boron Coatings prepared by Direct Current Electrodeposition Technique", *Int. J. Electrochem. Sci.*, 12, 2055-2069. 2017.

[2] Hena, S. "Removal of chromium hexavalent ion from aqueous solutions using biopolymer chitosan coated with poly 3-methyl thiophene polymer", *J. Hazard. Mater.*, 181, 474-479. 2010.

[3] Torresdey, J. L., Tiemann, K. J., Armendariz, V., Oberto, L., Chianelli, R., Rios, J., Parsons, J. G., Gamez G. "Characterization of Cr(VI) binding and reduction to Cr(III) by the agricultural byproducts of Avena monida (oat) biomass", *J. Hazard. Mater.*, 80, 175-188. 2000.

[4] Monteiro, O. R., Murugesan, S., Khabashesku, V. "Electroplated Ni–B films and Ni–B metal matrix diamond nanocomposite coatings", *Surf. Coat. Technol.*, 272, 291-297. 2015.

[5] Hou, K.-H., Jeng, M.-C., Ger, M.-D. "A study on the wear resistance characteristics of pulse electroforming Ni–P alloy coatings as plated", *Wear*, 262, 833-844. 2007.

[6] Srivastava, M., Grips, V. K. W., Rajam, K. S. "Electrochemical deposition and tribological behaviour of Ni and Ni–Co metal matrix composites with SiC nano-particles", *Appl. Surf. Sci.*, 253, 3814-3824. 2007.

[7] Vitry, V., Sens, A., Kanta, A.-F., Delaunois, F. "Experimental study on the formation and growth of electroless nickel–boron coatings from borohydride-reduced bath on mild steel", *Appl. Surf. Sci.*, 263, 640-647. 2012.

[8] Gaevskaya, T. V., Novotortseva, I. G., Tsybulskaya, L. S. "The effect of boron on the microstructure and properties of electrodeposited nickel films", *Met. Finish.*, 94, 100-103. 1996.

[9] Ng, P. K., Snyder, D. D., LaSala, J., Clemens, B., Fuerst, C. "Structure and Crystallization of Nickel-Phosphorus Alloys Prepared by High-Rate Electrodeposition", *J. Electrochem. Soc.*, 135,1376-1381. 1988.

[10] Peeters, P., Hoorn, G., Daenen, T., Kurowski, A., Staikov, G. "Properties of electroless and electroplated Ni–P and its application in microgalvanics", *Electrochimica Acta*, 47, 161-169. 2001.

[11] Ogihara, H., Udagawa, K., Saji, T. "Effect of boron content and crystalline structure on hardness in electrodeposited Ni–B alloy films", *Surf. Coat. Technol.*, 206, 2933-2940. 2012.

[12] Bekish, Y. N., Poznyak, S. K., Tsybulskaya, L. S., Gaevskaya, T. V. "Electrodeposited Ni–B alloy coatings: Structure, corrosion resistance and mechanical properties", *Electrochimica Acta*, 55, 2223-2231. 2010.

[13] Lee, K. H., Chang, D., Kwon, S. C. "Properties of electrodeposited nanocrystalline Ni–B alloy films", *Electrochimica Acta*, 50, 4538-4543. 2005.

[14] Krishnaveni, K., Narayanan, T. S. N., Seshadri, S. K. "Electroless Ni-B-Si_3N_4 Composite Coating: Deposition and Evaluation of Its Characteristic Properties", *Synth. React. Inorg. Met.-Org. Nano-Met. Chem.*, 42, 920-927. 2012.

[15] Tian, L., Xu, J., Qiang, C. "The electrodeposition behaviors and magnetic properties of Ni–Co films", *Appl. Surf. Sci.*, 257, 4689-4694. 2011.

[16] Shi, L., Sun, C. F., Gao, P., Zhou, F., Liu, W. M. "Electrodeposition and characterization of Ni–Co–carbon nanotubes composite coatings", *Surf. Coat. Technol.*, 200, 4870-4875. 2006.

[17] "Facts About Nickel". Retrieved June 2, 2018 from https://www.livescience.com/29327-nickel.html.

[18] Davis, J. R. ASM Specialty Handbook, Nickel, Cobalt, and Their Alloys. Materials Park, Ohio, 2000.

[19] “Technical data for the element Cobalt in the Periodic Table”. Retrieved June 2, 2018, from http://www.periodictable.com/Elements/027/data.html.

[20] “Broken Hill Prospecting”. Retrieved June 2, 2018, from https://www.bhpl.net.au/projects/cobalt-deposits/cobalt-research/.

[21] “Boron (B) - Chemical properties, Health and Environmental effects”. Retrieved June 2, 2018, from https://www.lenntech.com/periodic/elements/b.htm.

[22] “Technical data for the element Boron in the Periodic Table”. Retrieved June 2, 2018, from http://www.periodictable.com/Elements/005/data.html.

[23] Li, M., Fossey, J. S., James, T. D. Monographs in Supramolecular Chemistry, Cambridge: Royal Society of Chemistry, 2015.

[24] Reidenbach, F. ASM Metals Handbook Volume 5, Surface Engineering. ASM International, Ohio, 1994.

[25] “Nickel Plating Handbook”. Retrieved June 3, 2018, from https://www.nickelinstitute.org/~/media/Files/TechnicalLiterature/NPH_1410.

[26] “What Every Engineer Needs to Know”. Retrieved June 3, 2018, from https://www.engineering.com/AdvancedManufacturing/ArticleID/10797/Electroplating-What-Every-Engineer-Needs-to-Know.aspx.

[27] Parkinson, R. “Electroforming — a unique metal fabrication process”, Retrieved June 3, 2018, from https://www.nickelinstitute.org/~/Media/Files/TechnicalLiterature/Electroforming_AUniqueMetalFabricationProcess_10084_.pdf.

[28] Goddard, W. “Handbook of nanoscience, engineering, and technology”. Retrieved June 4, 2018, from http://cnqzu.com/library/Anarchy%20Folder/Nanotechnology/Handbook%20of%20Nanoscience,%20Engineering%20&%20Technology.pdf.

[29] Mallory, G.O, Hajdu, J.B. Electroless Plating - Fundamentals and Applications, Noyes Publications: New York. 1990.

[30] Estrada, M. E. Model-based framework for alloy electrodeposition processes. Louisiana State University. 2008.

[31] Dini, J. W. Electrodeposition: the materials science of coatings and substrates, Noyes Publications: New Jersey. 1993.

[32] T. Osaka, "Electrodeposition of highly functional thin films for magnetic recording devices of the next century", *Electrochimica Acta*, 45, 3311-3321, 2000.

[33] Karslıoğlu, R. "Karbon Nanotüp Takviyeli Nikel-Kobalt Kaplamaların Geliştirilmesi", M. Sc. Thesis, Sakarya University, Graduate School of Natural and Applied Sciences, Sakarya-Turkey, 2014.

[34] DEMİRKESEN, E., Kompozit Malzemeler. İTÜ: İstanbul. 1991.

[35] Guidry, D. J., Lian K., Jiang J.C., Meletis "E. *Tribological Behavior of Nanocrystalline Nickel*", *J. Nanosci. Nanotechnol.*, 9, 4156-4153. 2002.

[36] Gleiter, H. "Nanostructured materials: basic concepts and microstructure", *Acta Mater.*, 48, 1-29, 2000.

[37] Gleiter, H. "Nanostructured materials: state of the art and perspectives", *Nanostructured Mater.*, 6, 3-14, 1995.

[38] Zhang, B. "Amorphous and nano alloys electroless depositions: technology, composition, structure and theory", Elsevier: China. 2016.

[39] "Electroless Plating Method | Electroless Plating Techniques | SPC". Retrieved June 3, 2018, from https://www.sharrettsplating.com/plating-methods/electroless-plating.

[40] Rehman, A., Lee S.-H. "Crystalline Silicon Solar Cells with Nickel/Copper Contacts", Retrieved June 3, 2018, from https://www.researchgate.net/

publication/283980908_Crystalline_Silicon_Solar_Cells_with_NickelCopper_Contacts/figures?lo=1.

[41] Kay, D. “Electroless Nickel Plating as a Brazing Filler Metal”, Retrieved June 3, 2018 from https://vacaero.com/information-resources/vacuum-brazing-with-dan-kay/1493-electroless-nickel-plating-as-a-brazing-filler-metal.html.

[42] UYSAL, M., Elektrolitik kalay kaplama ve oksidasyonu, Yüksek Lisans Tezi, Sakarya Üniversitesi, Fen Bilimleri Enstitüsü, 2007.

[43] “BERK, V., Yüzey islem teknolojileri 1, Elektrokimya Sanayi, 4-42, 92 İstanbul, 2004.” .

[44] Di Bari, G. A. “Electrodeposition of Nickel”, *Modern Electroplating*, M. Schlesinger : NJ, USA. 2011.

[45] Borkar, T. “Electrodeposition of Nickel Composite Coatings”, Master thesis, Mumbai University. 2007.

[46] CHANG, L. M., AN, M. Z., S. Y. SHI, Microstructure and characterization of Ni-Co/Al_2O_3 composite coatings by pulse reversal electrodeposit. Materials Chemistry and Physics, 100(2–3), 395–399, 2006.” .

[47] Pavithra, C. L. P., Sarada, B. V., Rajulapati, K. V., Rao, T. N., Sundararajan, G. “A New Electrochemical Approach for the Synthesis of Copper-Graphene Nanocomposite Foils with High Hardness”, *Sci. Rep.*, 4, 4049. 2014.

[48] Chaparro, A., Arnulfo, W., Lopez, E. V. “Electrodeposition of nickel plates on copper substrates using PC y PRC”, *Matér. Rio Jan.*, 12, 583-588. 2007.

[49] Hu, F., Chan, K.C. “Electrocodeposition behavior of Ni–SiC composite under different shaped waveforms”, *Appl. Surf. Sci.*, 233, 163-171. 2004.

[50] Chandrasekar, M. S., Pushpavanam, M. “Pulse and pulse reverse plating—Conceptual, advantages and applications”, *Electrochimica Acta*, 53, 3313-3322. 2008.

[51] Shakoor, R. A., Kahraman, R., Waware, U. S., Wang, Y., Gao, W. "Synthesis and properties of electrodeposited Ni-B-Zn ternary alloy coatings", *Int. J. Electrochem. Sci.*, 9, 5520-5536. 2014.

[52] Krishnaveni, K., Narayanan, T. S. N., Seshadri, S. K. "Electrodeposited Ni–B coatings: Formation and evaluation of hardness and wear resistance", *Mater. Chem. Phys.*, 99, 300-308. 2006.

[53] Liang, Y., Li, Y. S., Yu, Q. Y., Zhang, Y. X., Zhao, W. J., Zeng, Z. X. "Structure and wear resistance of high hardness Ni-B coatings as alternative for Cr coatings", *Surf. Coat. Technol.,* 264 (2015) 80-86."

[54] "Hansal, E.G., Tury, B., Halmdienst, M., Varsanyi, M.L, Kautek, W. "Pulse reverse plating of Ni–Co alloys: Deposition kinetics of Watts, sulfamate and chloride electrolytes", *Electrochimica Acta,* 52, 1145-1151. 2006.

[55] Tang, P. T. "Pulse reversal plating of nickel and nickel alloys for microgalvanics", *Electrochimica Acta*, 47, 61-66. 2001.

[56] Chang, L. M., An, M. Z., Shi, S. Y. "Corrosion behavior of electrodeposited Ni–Co alloy coatings under the presence of NaCl deposit at 800°C", *Mater. Chem. Phys.*, 1, 125-130. 2005.

[57] Correia, A.N, Machado, S.A.S "Electrodeposition and characterisation of thin layers of Ni□Co alloys obtained from dilute chloride baths", *Electrochimica Acta,* 45, 1733-1740. 2000.

[58] Gómez, E., Pané, S., Vallés, E. "Electrodeposition of Co–Ni and Co–Ni–Cu systems in sulphate–citrate medium", *Electrochimica Acta,* 51, 146-153. 2005.

[59] Bai, A., Hu, C.C. " Effects of electroplating variables on the composition and morphology of nickel–cobalt deposits plated through means of cyclic voltammetry", *Electrochimica Acta*, 47, 2447-3456. 2002.

[60] Landolt, D., Marlot, A. "Microstructure and composition of pulse-plated metals and alloys", *Surf. Coat. Technol.*, 170, 8-13. 2003.

[61] Tury, B., Varsányi, M.L., Roy, S. “Ni–Co alloys plated by pulse currents”, *Surf. Coat. Technol.*, 200, 6713-6717. 2006.

[62] Bouzit, F. Z., Nemamcha, A., Moumeni, H., Rehspringer, J. L.“Morphology and Rietveld analysis of nanostructured Co-Ni electrodeposited thin films obtained at different current densities”, *Surf. Coat. Technol.*, c. 315, ss. 172-180, Nis. 2017.

[63] Srivastava, M., Selvi, V.E., Grips, V.K., Rajam, K.S. “Corrosion resistance and microstructure of electrodeposited nickel–cobalt alloy coatings”, *Surf. Coat. Technol.*,201, 3051-3060. 2006.

[64] Karslioglu, R., Akbulut, H. “Comparison microstructure and sliding wear properties of nickel–cobalt/CNT composite coatings by DC, PC and PRC current electrodeposition”, *Appl. Surf. Sci.*, 353, 615-627. 2015.

[65] Mukhopadhyay, A., Barman, T. K., Sahoo, P. “Effect of Heat Treatment on the Characteristics of Electroless Ni-B, Ni-B-W and Ni-B-Mo Coatings”, *Mater. Today Proc.*, 5, 3306-3315. 2018.

[66] Lee, K. H., Chang, D., Kwon, S. C. “Properties of electrodeposited nanocrystalline Ni–B alloy films”, *Electrochimica Acta*, 50, 4538-4543. 2005.

[67] Chen, C. C., Su, K. W., Chen, Y. F., Huang, K. F. “Various high-order modes in vertical-cavity surface-emitting lasers with equilateral triangular lateral confinement”, *Opt. Lett.*, 33, 509-511. 2008.

[68] Shi, L., Sun, C. F., Zhou, F., Liu, W. M. “Electrodeposited nickel–cobalt composite coating containing nano-sized Si_3N_4”, *Mater. Sci. Eng. A*, 397, 190-194. 2005.

[69] Gibson, R. F. “A review of recent research on mechanics of multifunctional composite materials and structures”, *Compos. Struct.*, 92, 2793-2810. 2010.

[70] Golodnitsky, D., Rosenberg, Y., Ulus, A. “The role of anion additives in the electrodeposition of nickel–cobalt alloys from sulfamate electrolyte”, *Electrochimica Acta*, 47, 2707-2714. 2002.

[71] Ranjith, B., Kalaignan, G.P. “Ni–Co–TiO_2 nanocomposite coating prepared by pulse and pulse reversal methods using acetate bath”, *Appl. Surf. Sci.*, 257, 42-47. 2010.

[72] López, J. R., Mendez, P.F., Bueno, J.J., Trejo, G., Stremsdoerfer, G., Meas, Y. “The Effect of Boron Content, Crystal Structure, Crystal Size on the Hardness and the Corrosion Resistance of Electrodeposited Ni-B Coatings”, *Int. J. Electrochem. Sci.*, 11, 4231-4244. 2016.

[73] Yang, Y.-Y, Deng, B. “Preparation of Ni-Co Alloy Foils by Electrodeposition”, *Adv. Chem. Eng. Sci.*, 01, 27-32. 2011.

[74] Wang, L., Gao, Y., Xue, Q., Liu, H., Xu, T. “Microstructure and tribological properties of electrodeposited Ni–Co alloy deposits”, *Appl. Surf. Sci.*, 242, 326–332. 2005.

[75] Bell, T. “How to Calculate the Rate of Metal Corrosion”, Retrieved June 6, 2018, from https://www.thebalance.com/corrosion-rate-calculator-2339697.

[76] “Hard Chrome Plating”. Retrieved July 13, 2018, from http://www.hardchrome.com.au/technologies/hardchrome-plating/.

CURRICULUM VITAE



PERSONAL INFORMATION

Name Surname : Uğur BARUT

Date of Birth : 1993

Phone : +90 554 2604533

E-mail : ubarut@ybu.edu.tr

EDUCATION

High School : M. Adnan Özçelik Anatolian High School / MERSİN (2007-2011)

Bachelor : Yıldız Technical University / İSTANBUL (2011-2015) (3.23/4.0)

Master Degree : Ankara Yıldırım Beyazıt University / (2017-continued)

WORK EXPERIENCE

Research Assist. : Ankara Yıldırım Beyazıt University / (2017-continued)

TOPICS OF INTEREST

- Electrodeposition
- Nickel Electrodeposition